

UNCLASSIFIED

AD NUMBER

AD889662

LIMITATION CHANGES

TO:

Approved for public release; distribution is unlimited.

FROM:

Distribution authorized to U.S. Gov't. agencies only; Test and Evaluation; DEC 1971. Other requests shall be referred to Air Force Armament Lab., Eglin AFB, FL.

AUTHORITY

AFATL ltr 24 Jun 1974

THIS PAGE IS UNCLASSIFIED

cy.2

**FREE-FLIGHT RANGE TESTS OF BLUNTED 4-,
4.5- AND 5-CALIBER BODIES OF REVOLUTION
WITH SECANT-OGIVE, TANGENT-OGIVE, AND
CONICAL NOSE SHAPES**



R. M. Watt and G. L. Winchenbach

ARO, Inc.

December 1971

This document has been approved for public release
its distribution is unlimited.

*Per AB 7417, 74
27 Aug, 74*

Distribution limited to U.S. Government agencies only;
this report contains information on test and evaluation
of military hardware; December 1971; other requests for
this document must be referred to Air Force Armament
Laboratory (DLRA), Eglin AFB, FL 32542.

**VON KÁRMÁN GAS DYNAMICS FACILITY
ARNOLD ENGINEERING DEVELOPMENT CENTER
AIR FORCE SYSTEMS COMMAND
ARNOLD AIR FORCE STATION, TENNESSEE**

NOTICES

When U. S. Government drawings specifications, or other data are used for any purpose other than a definitely related Government procurement operation, the Government thereby incurs no responsibility nor any obligation whatsoever, and the fact that the Government may have formulated, furnished, or in any way supplied the said drawings, specifications, or other data, is not to be regarded by implication or otherwise, or in any manner licensing the holder or any other person or corporation, or conveying any rights or permission to manufacture, use, or sell any patented invention that may in any way be related thereto.

Qualified users may obtain copies of this report from the Defense Documentation Center.

References to named commercial products in this report are not to be considered in any sense as an endorsement of the product by the United States Air Force or the Government.

**FREE-FLIGHT RANGE TESTS OF BLUNTED 4,
4.5- AND 5-CALIBER BODIES OF REVOLUTION
WITH SECANT-OGIVE, TANGENT-OGIVE, AND
CONICAL NOSE SHAPES**

**R. M. Watt and G. L. Winchenbach
ARO, Inc.**

This document has been approved for public release
its distribution is unlimited. *Per TAB 74-17
dt 16 Aug 74*

Distribution limited to U.S. Government agencies only;
this report contains information on test and evaluation
of military hardware, December 1971; other requests for
this document must be referred to Air Force Armament
Laboratory (DLRA), Eglin AFB, FL 32542.

FOREWORD

The work reported herein was done at the request of the Air Force Armament Laboratory (DLRA/K. K. Cobb), Armament Development and Test Center, Air Force Systems Command (AFSC), Eglin Air Force Base, Florida, under Program Element 63716F, System 670A.

The results presented were obtained by ARO, Inc. (a subsidiary of Sverdrup & Parcel and Associates, Inc.), contract operator of the Arnold Engineering Development Center (AEDC), AFSC, Arnold Air Force Station, Tennessee, under Contract F40600-72-C-0003. The tests were conducted from December 10, 1970, through March 4, 1971, under ARO Project VG0179. Data reduction was completed March 29, 1971, and the manuscript was submitted for publication on May 27, 1971.

The authors thank D. R. Dixon and R. B. Darden for their contribution in reducing the data.

This technical report has been reviewed and is approved.

Emmett A. Niblack, Jr.
Lt Colonel, USAF
AF Representative, VKF
Directorate of Test

Duncan W. Rabey, Jr.
Colonel, USAF
Director of Test

ABSTRACT

Results of free-flight range tests of spin stabilized, blunted 4-, 4.5-, and 5-cal bodies of revolution with secant-ogive, tangent-ogive, and conical nose shapes, and cylindrical afterbodies with and without boattails are presented. The tests were conducted over a Mach number range from approximately 1.5 to 3.5 and at simulated altitudes up to 60,000 ft. Measurements indicate that the drag coefficient decreased with increasing nose length and that the secant-ogive nose shape had the minimum drag coefficient. The drag coefficient could be further reduced by the addition of a boattail. Measurements also indicate that the static instability decreased significantly with an increase in the ogive radius of the nose. Nonlinear variations of force and moment coefficients with yaw angle were observed and treated using a cubic analysis.

This document has been approved for public release
its distribution is unlimited. Per TAB 74-12
dtd 16 Aug 74

Distribution limited to U.S. Government agencies only;
this report contains information on test and evaluation
of military hardware; December 1971, other requests for
this document must be referred to Air Force Armament
Laboratory (DLRA), Eglin AFB, FL 32542.

CONTENTS

	<u>Page</u>
ABSTRACT	iii
NOMENCLATURE	vii
I. INTRODUCTION	1
II. APPARATUS	
2.1 Range	1
2.2 Projectiles, Sabots, and Test Conditions	2
III. DATA REDUCTION	3
IV. TEST RESULTS	
4.1 Photographic Observations	4
4.2 Drag Measurements	4
4.3 Stability Measurements	5
V. CONCLUDING REMARKS	8
REFERENCES	8

APPENDIXES

I. ILLUSTRATIONS

Figure

1. Range G	13
2. Support System for the 20-mm Cannon	14
3. Sketches of the Projectiles	16
4. Photograph of Projectiles, Sabots, and Gas Seals	17
5. Photographic Observations of Typical Configurations	20
6. Drag Measurements for Secant-Ogive-Cylinder	
Configurations at Ground Level	22
7. Effect of Nose Length on the Drag Coefficient of Secant-Ogive-Cylinder	
Configurations at Ground Level	23
8. Effect of Bluntness on the Drag Coefficient of Secant-Ogive-Cylinder	
Configurations at Ground Level	24
9. Drag Measurements for Tangent-Ogive- and Cone-Cylinder	
Configurations at Ground Level	25
10. Comparison of Drag Levels for 3-cal Nose Configurations at Ground Level	26
11. Drag Measurements at $M \approx 2$ for Secant-Ogive-Cylinder	
Configurations with Boattail	27
12. Effect of Bluntness on the Drag Coefficient of Secant-Ogive-Cylinder	
Configurations with Boattail at $M = 2$	28
13. Representative Amplitude Effects on C_{m_α} for Typical Ogive- and	
Cone-Cylinder Configurations at Ground Level	29
14. Static Stability Derivatives at Zero Yaw Angle for Secant-Ogive-Cylinder	
Configurations at Ground Level	30

<u>Figure</u>	<u>Page</u>
15. Effect of Nose Length on $C_{m_{ao}}$ for Secant-Ogive-Cylinder Configurations at Ground Level	31
16. Effect of Nose Bluntness on $C_{m_{ao}}$ for Secant-Ogive-Cylinder Configurations at Ground Level	32
17. Static Stability Derivatives at Zero Yaw Angle for Tangent-Ogive- and Cone-Cylinder Configurations at Ground Level	33
18. Comparison of Levels of $C_{m_{ao}}$ for 3-cal Nose Configurations at Ground Level	34
19. Static Stability Derivatives at $M = 2$ and Zero Yaw Angle for Secant-Ogive-Cylinder Configurations with Boattail	35
20. Effect of Nose Bluntness on $C_{m_{ao}}$ at $M \approx 2$ for Secant-Ogive-Cylinder Configurations with Boattail	36
21. Representative Amplitude Effects on C_{N_a} for Typical Ogive- and Cone-Cylinder Configurations at Ground Level	37
22. Normal-Force Data at Zero Yaw Angle for Secant-Ogive-Cylinder Configurations at Ground Level	38
23. Effect of Nose Length on $C_{N_{ao}}$ for Secant-Ogive-Cylinder Configurations at Ground Level	39
24. Effect of Nose Bluntness on $C_{N_{ao}}$ for Secant-Ogive-Cylinder Configurations at Ground Level	40
25. Normal-Force Data at Zero Yaw Angle for Tangent-Ogive- and Cone-Cylinder Configurations at Ground Level	41
26. Comparison of Levels of $C_{N_{ao}}$ for 3-cal Nose Configurations at Ground Level	42
27. Normal-Force Data at $M = 2$ and Zero Yaw Angle for Secant-Ogive-Cylinder Configurations with Boattail	43
28. Effect of Nose Bluntness on $C_{N_{ao}}$ at $M = 2$ for Secant-Ogive-Cylinder Configurations with Boattail	44
29. Center-of-Pressure Data for Secant-Ogive-Cylinder Configurations at Ground Level (Zero Yaw Angle)	45
30. Effect of Nose Length on cp_o for Secant-Ogive-Cylinder Configurations at Ground Level	46
31. Effect of Nose Bluntness on cp_o for Secant-Ogive-Cylinder Configurations at Ground Level	47
32. Center-of-Pressure Data for Tangent-Ogive- and Cone-Cylinder Configurations at Ground Level (Zero Yaw Angle)	48
33. Comparison of Levels of cp_o for 3-cal Nose Configurations at Ground Level	49
34. Center-of-Pressure Data at $M \approx 2$ for Secant-Ogive-Cylinder Configurations with Boattail (Zero Yaw Angle)	50
35. Effect of Nose Bluntness on cp_o at $M = 2$ for Secant-Ogive-Cylinder Configurations with Boattail	51
36. Representative Amplitude Effects on Nutational and Precessional Damping Rates of Typical Ogive- and Cone-Cylinder Configurations at Ground Level . . .	52

<u>Figure</u>	<u>Page</u>
37. Damping-In-Pitch Derivatives for Ogive- and Cone-Cylinder Configurations at Ground Level (Zero Yaw Angle)	53
38. Effect of Altitude on Nutational and Precessional Damping Rates for Secant-Ogive-Cylinder Configurations with Boattail (Zero Yaw Angle)	55
39. Damping-in-Pitch Derivatives at $M = 2$ for Secant-Ogive-Cylinder Configurations with Boattail (Zero Yaw Angle)	56
40. Magnus-Moment Derivatives for Ogive- and Cone-Cylinder Configurations at Ground Level (Zero Yaw Angle)	57
41. Magnus-Moment Derivatives at $M = 2$ for Secant-Ogive-Cylinder Configurations with Boattail (Zero Yaw Angle)	58
42. Roll Damping for the Ogive- and Cone-Cylinder Configurations	59

II. TABLES

I. Nominal Physical Properties of the Projectiles	61
II. Aerodynamic Properties of the Projectiles	62

NOMENCLATURE

A_N, A_P	Nutational and precessional vector lengths, respectively. at midpoint of flight interval
C_1	Slope of C_D versus $\bar{\delta}^2$ curve, $1/\text{deg}^2$
C_2	Slope of C_{m_α} versus δ_{e1}^2 curve, $1/\text{deg}^2$
C_3	Slope of C_{N_α} versus $\delta_{e_s}^2$ curve, $1/\text{deg}^2$
C_4	Slope of μ_P versus δ_{e1}^2 curve, $(1/\text{ft}) (1/\text{deg}^2)$
C_5	Slope of μ_N versus δ_{e2}^2 curve, $(1/\text{ft}) (1/\text{deg}^2)$
C_D	Drag coefficient
C_{ℓ_p}	Damping-in-roll derivative, $\frac{\partial C_{\ell}}{\partial (pd/V)}$
$C_{m_{p\beta}}$	Magnus-moment derivative, $\frac{\partial C_m}{\partial (p\beta) \frac{d}{2V}}$, $1/\text{radian}^2$
$C_{m_q} + C_{m_{\dot{\alpha}}}$	Damping-in-pitch derivatives, $\frac{\partial C_m}{\partial \left(\frac{qd}{2V}\right)} + \frac{\partial C_m}{\partial \left(\frac{\dot{\alpha}d}{2V}\right)}$, $1/\text{radian}$
C_{m_α}	Pitching-moment derivative, $1/\text{radian}$

C_{N_α}	Normal-force derivative, 1/radian
cg	Position of the center of gravity, percentage of model length from the nose
cp	Position of the center of pressure, percentage of model length from the nose
d	Model diameter and moment reference length
I_x	Model moment of inertia (relative to a longitudinal axis)
I_y	Model moment of inertia (relative to a transverse axis)
K_N, K_P, K_T	Nutational, precessional, and trim vector lengths
k_a^2	$I_x/(md^2)$
k_p	Constant in Eq. (1)
ℓ	Model length
M	Mach number
m	Model mass
p	Model spin rate
r_B	$d/2$
Re ℓ	Reynolds number based on free-stream conditions and model length
r_N	Model nose radius
S	Reference area based on model diameter
s	Length of range interval used in reducing drag data
V	Model velocity
x	Distance along flight path
α, β	Components of the complex yaw angle
δ^2	$\alpha^2 + \beta^2$
$\overline{\delta}$	Root-mean-square value of δ , $\sqrt{\delta^2}$

$\overline{\delta^2}$	$(1/s) \int_0^s \delta^2 ds$	
δ_e^2	$A_p^2 + A_N^2 + \frac{\phi_p' A_p^2 - \phi_N' A_N^2}{\phi_p' - \phi_N'}$	Expressions Derived in Ref. 10
δ_{e1}^2	$A_p^2 + 2 A_N^2$	
δ_{e2}^2	$2 A_p^2 + A_N^2$	
$\delta_{e_s}^2$	$\frac{(\phi_N')^4 A_p^2 \delta_{e1}^2 + (\phi_p')^4 A_N^2 \delta_{e2}^2}{(\phi_N')^4 A_p^2 + (\phi_p')^4 A_N^2}$	
μ_N, μ_P	Damping rates of the nutational and precessional vectors	
ξ	Complex yaw angle, $\beta + ia$	
ρ	Mass density of range air	
ϕ	Roll angle	
ϕ_N', ϕ_P'	Rates of rotation of nutational and precessional vectors	
ψ	r_N/r_B	

SUBSCRIPTS

i	Initial values
o	Zero-angle-of-attack values

SECTION I INTRODUCTION

An aerodynamic design study program of projectiles for 20-, 25-, and 30-mm gun systems is presently being conducted. Projectile configurations being considered are, in general, basic cone-cylinder, secant-ogive-cylinder, and tangent-ogive-cylinder combinations with and without boattails. Such a design program requires not only accurate estimates of the aerodynamic parameters that influence the flight of a projectile but a determination of the combinations of forebody and afterbody geometries which tend to optimize the flight performance of the finalized projectile.

Over a period of years, numerous studies have been conducted on various aerodynamic characteristics of basic cone-cylinder, secant-ogive-cylinder, and tangent-ogive-cylinder configurations (Refs. 1 through 8). Much of the work performed has been of an uncoordinated nature resulting from the testing of specific configurations or isolated missile components. More recently, tests were conducted at AEDC on 2-cal secant-ogive nose shapes to determine the effects of afterbody length and boattails on the aerodynamics of the projectile. To supplement the existing data and provide design criteria for present and future projectile design work, the present parametric investigation of the effects of nose length, nose shape, bluntness, and boattails on 4-, 4.5-, and 5-cal projectiles was requested.

The tests were conducted in Hyperballistic Range (G) of the von Kármán Gas Dynamics Facility (VKF). Measurements were obtained over a nominal Mach number range from 1.5 to 3.5 and at simulated altitudes up to 60,000 ft.

SECTION II APPARATUS

2.1 RANGE

Range G consists of a 10-ft-diam, 1000-ft-long tank that is contained within an underground enclosure (Fig. 1, Appendix I). It is a variable density aerodynamic range and contains 53 dual-plane shadowgraph stations. Forty-three stations are positioned at nominal 20-ft intervals, yielding an 840-ft instrumented length. The other ten stations are located approximately 10 ft downrange of stations 5 through 10, 12, 13, 15, and 16. The angular orientation and position of most test configurations can be determined to within approximately ± 0.25 deg and ± 0.002 ft, respectively, at each station. A chronograph system measures intervals of flight time to within $\pm 2 \times 10^{-7}$ sec. The range vacuum pumping system provides range pressures from 1 atm down to about 20 μ Hg. The nominal operating temperature of the range is 76°F.

The launcher normally used with the range is a two-stage, light-gas gun having a 2.5-in.-diam launch tube. In the present tests, however, the projectiles were launched using a 20-mm cannon. The rifled cannon barrel had a twist rate of one turn in 30 cal and was approximately 10 ft in length. The cannon was positioned either in the blast tank section of the range or in the range proper, in contrast to the normal launcher position

shown in Fig. 1. A photograph of the cannon and its support system is shown in Fig. 2.

In order to launch the projectiles at the higher velocities, a powder chamber extension was utilized which permitted extra-large powder charges to be used.

2.2 PROJECTILES, SABOTS, AND TEST CONDITIONS

The 14 configurations that were tested are defined and numbered in Fig. 3, and photographs showing each type of projectile are presented in Fig. 4. The projectiles consisted of 2-cal cylindrical bodies with either 2.0-, 2.5-, or 3.0-cal nose lengths. Nose shapes employed were either conical, secant-ogive, or tangent-ogive and had bluntness ratios of 0.1, 0.2, and 0.3. Three configurations had a 7-deg boattail, 0.5 cal in length, aft of the cylindrical portion of the projectile. The projectiles were designed to have a maximum diameter about 0.003 in. less than the 20-mm launch tube diameter, and the projectile surface was smooth (no rifling bands were involved). Pins were inserted into the base of the projectile (Fig. 4a) parallel to and equidistant from the longitudinal axis of each projectile. The 0.06- and 0.04-in.-diam pins protruded from the base 0.1 in. These pins were used to obtain the projectile roll orientation as a function of the downrange distance traveled.

Length, diameter, and mass measurements were obtained for each projectile. Measurements of I_x , I_y , and cg were obtained on half of the projectiles of each type. The mean values of these measurements were used in reducing the data on projectiles for which individual measurements were not obtained. In order to obtain a longitudinal cg position of approximately 60 percent measured from the true nose, bimetal construction was employed on most of the rounds. The materials used in the construction were Viscount 44®, Fansteel 60®, Mallory 3000®, 4130 steel, aluminum, and a titanium alloy (90-percent titanium 8-percent aluminum, and 1-percent each of vanadium and molybdenum). A list of the nominal physical measurements and the materials used for each configuration is presented in Table I, Appendix II.

Because of the requirement that the projectiles be launched without rifling bands (smooth surface), a pusher-type sabot was used (Fig. 4a). The projectile-sabot combination (Fig. 4c) was loaded into the cannon such that the launch tube rifling engaged the grooves on the pusher sabot. The roll torque was transferred from the sabot to the projectile during launch by the square sabot key (Fig. 4a) that engaged a socket in the base of the projectile. For some launch conditions separation of the sabot from the projectile after launch was accomplished by a mechanical device mounted on the gun muzzle which allowed the projectile to pass but retarded the movement of the sabot sufficiently to ensure clean separation. In order to minimize interference between the pusher sabot and the gun barrel, the sabot was designed to fit loosely in the rifling of the barrel, hence, a gas seal was required to retain the gun gases behind the sabot during launch. Lexan® gas seals (Fig. 4a) were used initially; however, polyethylene gas seals (Fig. 4b) proved to be more effective and were used throughout the remainder of the test.

The use of a pusher-type sabot frequently results in large initial disturbances in the yawing motion at the higher Mach numbers. To restrict these disturbances at this condition to a magnitude that permits a reasonable stability analysis, a Lexan nose sabot was employed (Fig. 4c) which supported the forebody of the projectile during its travel inside the launch tube. This nose support significantly reduced launch disturbances to the projectiles. Nose sabots and mechanical pusher-sabot strippers were not required at the same conditions.

The tests were conducted in a nominal Mach number range from 1.5 to 3.5 at ground level conditions for all configurations. In addition, measurements were obtained on the boattail configurations at $M = 2$ for simulated altitudes up to 60,000 ft. Yawing amplitudes experienced ranged up to about 12 deg. The test conditions and the measurements obtained are presented in Table II.

SECTION III DATA REDUCTION

Most of the aerodynamic data were derived from the measured motion histories of the projectiles in free flight by means of the data reduction procedures outlined in Ref. 9. The methods of Ref. 9 assume linear variations of force and moment with yaw angle; hence, any nonlinearities in the force and moment data result in "effective" derivatives being obtained for the observed amplitude variations. To aid in examining amplitude effects and resolving effective measurements back to zero-angle-of-attack values, some of the nonlinear methods of Ref. 10 were utilized. In using the analysis procedures of Ref. 10, a cubic variation of force and moment data with yaw angle has been assumed adequate for the present data. For some of the test shots, the drag coefficient, C_D , was evaluated by fitting a cubic equation, by the least-squares method, to the time-position data, as discussed in Ref. 11. This procedure is useful when the velocity drop of the projectile over the range interval is greater than about 5 percent of the initial velocity.

The damping-in-roll derivative, $C_{\dot{\phi}_p}$, was obtained by first fitting the equation

$$\phi = \phi_i + p_i x - \left(\frac{p_i k_p}{2} \right) x^2 + \left(\frac{p_i k_p^2}{6} \right) x^3 \quad (1)$$

to the measured roll history of the projectile, also using a least-squares curve-fitting procedure. Once the coefficients of Eq. (1) were determined, the damping-in-roll derivative was computed from the equation

$$C_{\dot{\phi}_p} = k_a^2 [-k_p (2m/\rho s) - C_D] \quad (2)$$

This method of determining $C_{\dot{\phi}_p}$ is convenient for finless configurations which have small damping-in-roll derivatives. For a more complete treatment concerning methods of measuring $C_{\dot{\phi}_p}$, see Ref. 11.

The experimental errors of concern in ballistic range aerodynamic measurements are, in general, of a random nature. Part of the spread experienced in aerodynamic

measurements of projectiles is related to using nominal values for certain physical measurements of the rounds. The extent of variations in the physical parameters of the rounds of the present tests is noted in Table I. It is believed that the spread in the measured aerodynamic parameters provides a reasonable estimate of errors in these measurements. It should be noted that larger errors can be expected in tests of statically unstable configurations than in tests involving statically stable configurations.

SECTION IV TEST RESULTS

4.1 PHOTOGRAPHIC OBSERVATIONS

Photographs of the projectiles were obtained for most tests using a pulsed laser light source. These photographs are useful since they reveal the condition of the projectile after launch. The example shown in Fig. 5a indicates that the interaction between the projectile and the lands of the rifled barrel was not severe. An examination of several projectiles recovered after launch verified that the scoring shown in the laser photograph was, in most cases, merely a surface abrasion and should result in negligible effects on the aerodynamic parameters.

Schlieren photographs were obtained for a portion of the tests, and typical examples are shown in Figs. 5b through d for the 5-cal cone-cylinder configuration at ground level. The photographs indicate that the flow on the body at $M = 1.5$ was largely laminar (Fig. 5b) whereas at $M = 2.5$ (Fig. 5c) the flow had become turbulent on a portion of the cylindrical afterbody. At $M = 3.5$ (Fig. 5d) the flow appeared turbulent over most of the body. Figure 5e indicates that transition was on the boattail at $M = 2$. Hence, it appears that turbulent flow moved onto the body of the 5-cal projectiles near $M = 2$ at ground level which corresponds to a Reynolds number (based on free-stream conditions and model axial length) of 4 million.

4.2 DRAG MEASUREMENTS

The drag measurements obtained are presented in Figs. 6 through 12 and are tabulated in Table II. Zero-angle-of-attack drag values, C_{D_0} , were obtained from an analysis of C_D as a function of the amplitude parameter, $\bar{\delta}^2$, by the method described in Ref. 14. Slope values of C_D versus $\bar{\delta}^2$ (C_1) are also listed in Table II.

Measurements for the secant-ogive-cylinder configurations indicate that C_{D_0} decreased systematically with increasing Mach number (Fig. 6) and increasing nose length (Fig. 7). Notice, in Fig. 8, that C_{D_0} varied only slightly with nose bluntness in the range $0 < \psi < 0.2$, and the magnitude and direction of the variations were dependent on Mach number and nose length. Of significance, however, is the fairly large increase in C_{D_0} at the higher Mach numbers when ψ was increased to 0.3.

Figure 9 shows the zero yaw angle drag measurements for the tangent-ogive-cylinder and cone-cylinder configurations, and Fig. 10 presents a comparison of the data obtained

for the three nose shapes. It is apparent in Fig. 10 that the secant-ogive nose shape in general produced the minimum drag throughout the Mach number range.

The boattail was tested only at $M = 2$ with the 2.5-cal secant-ogive nose, and these data are presented in Figs. 11 and 12. The data in Fig. 11 show no significant effects of altitude on C_{D_o} . In contrast to the trends in Fig. 8, Fig. 12 shows a systematic increase in C_{D_o} over the range of ψ from 0.1 to 0.3 for the boattail configuration. In fact, the increase in C_{D_o} caused by increasing ψ from 0.1 to 0.2 averaged eight percent over the altitude range. Thus, it appears that a sharper nose may offer more advantage in conjunction with a boattail than in the case of a cylindrical afterbody (Fig. 6b). However, this comparison is restricted to the $M = 2$ and ground-level condition at which the effect of nose bluntness on C_{D_o} for the 2.5-cal secant-ogive nose was shown to be a minimum (Fig. 6b).

Two comparisons are made in Fig. 12a. The boattail configuration (5-cal overall length) may be compared with the 2.5-cal nose configuration (4.5-cal overall length) to illustrate the boattail effect. The boattail resulted in lower C_{D_o} values at both bluntness ratios. The decreased C_{D_o} level for the boattail configuration is believed to result almost entirely from the boattail effect since it has been shown in previous testing that C_{D_o} was not sensitive to changes of this magnitude in the length of a cylindrical afterbody. The second comparison, of the boattail configuration to the 3-cal nose configuration (5-cal overall length), illustrates the relative merits of increasing the nose length of the 4.5-cal body by 0.5 cal versus adding the 0.5-cal boattail. As may be seen in Fig. 12a, the boattail resulted in slightly lower C_{D_o} .

4.3 STABILITY MEASUREMENTS

Shown in Fig. 13 are some representative measurements of the effective static stability derivative, C_{m_α} , plotted as a function of the effective amplitude parameter, δ_e^2 . It was shown in the analysis of Ref. 10 that for the case of a cubic variation of the moment with yaw angle, the C_{m_α} versus δ_e^2 variation is linear and that the C_2 value in Fig. 13 corresponds to the coefficient ($C_{m_{\alpha 2}}$) in the nonlinear relationship

$$C_m = (C_{m_{\alpha 0}} + C_{m_{\alpha 2}} \delta_e^2) \xi$$

The linear variations in Fig. 13 indicate that the assumption of a cubic variation of the pitching-moment coefficient, C_m , with yaw angle is quite reasonable, and that C_{m_α} tends to decrease with increasing amplitude. Most of the amplitude variations were reasonably well defined in the amplitude range experienced in these tests, and the slope parameters are listed in Table II. It should be noted that in some cases the C_2 values were obtained from quite small yawing amplitudes. The $C_{m_{\alpha 0}}$ values are believed to be well defined, regardless of the C_2 values determined. However, in using the C_2 values to generate general amplitude variations of C_{m_α} , care should be exercised to ensure that the amplitude variations were in fact determined in the amplitude range desired (see Table II). This comment also holds for amplitude variations presented later in the normal-force and damping measurements.

Using the C_2 values determined, individual C_{m_a} measurements were resolved to zero-angle-of-attack values and are presented in Figs. 14 through 20. All moment measurements have been adjusted to a common reference position of 0.6ℓ (measured from the projectile nose) by using the measured C_{N_a} values presented in later figures. Since all projectiles were designed to have a 60-percent cg location (relative to the nose), the moment adjustments involved were small.

Figure 18 presents a comparison of the $C_{m_{a0}}$ measurements for the three nose shapes. Nose shape had a large effect upon the static stability derivative, with the conical nose shape displaying the least amount of static instability and the tangent-ogive shape the largest over the Mach number range.

One of the comparisons of Fig. 12a, the relative merits of increasing nose length by 0.5 cal versus adding the 0.5-cal boattail, is continued in Fig. 20a. As may be seen, the boattail configuration resulted in larger static instability. A precautionary note should be added here, inasmuch as this comparison does not illustrate a true boattail effect. Rather, a combination of geometry changes contribute to the differences: the addition of afterbody length, boattailing, and increasing nose length.

Measurements of the normal-force derivative are presented in Figs. 21 through 28. Again the linearity of C_{N_a} with δ_{es}^2 (Fig. 21) indicates that the assumption of a cubic variation of the normal-force coefficient, C_N , with yaw angle is justified and that the slopes (C_3) are reasonably well defined. Using C_3 , the corresponding C_{N_a} was reduced to its zero-angle-of-attack value.

Measurements for the secant-ogive-cylinder configurations indicate that $C_{N_{a0}}$ was mildly sensitive to nose length (Fig. 23) and nose bluntness (Fig. 24). The comparison of $C_{N_{a0}}$ for the three nose shapes (Fig. 26) shows that $C_{N_{a0}}$ was quite sensitive to nose shape and Mach number for $\psi = 0.1$ but much less sensitive for $\psi = 0.2$.

A comparison of data for the 2.5-cal nose, boattail configuration and the 3-cal nose, nonboattail configuration in Fig. 28 indicates that the levels differ only slightly for the two 5-cal configurations.

Although the levels are believed to be well defined, it should be noted that the difficulty of measuring $C_{N_{a0}}$ for a given body increases with increasing altitude and is related to the reduced dynamic pressure at the altitude conditions. In addition, some of the test shots experienced only small yawing amplitudes at launch which also contributes to the difficulty of determining C_{N_a} .

The center-of-pressure measurements for zero angle of attack, cp_0 , are shown in Figs. 29 through 35. The cp_0 values were computed using measured $C_{m_{a0}}$ and for the most part measured $C_{N_{a0}}$. For some tests in which $C_{N_{a0}}$ could not be measured accurately, mean values of $C_{N_{a0}}$ were obtained from Figs. 22 through 28. A comparison of the levels of cp_0 for the different nose shapes tested (Fig. 33) indicates that the center of pressure is more sensitive to nose shape than to nose length (Fig. 30) or to nose bluntness (Fig. 31). The levels of data of Fig. 33 indicate that as the radius of the ogive nose

decreases from the limiting case of the conical nose, cp_o moves forward on the body of the projectile. The large shift in cp_o as a function of nose shape is consistent with shifts in the levels of $C_{m_{\alpha o}}$ observed for the same configurations in Fig. 18.

A comparison of the cp_o data for the 2.5-cal nose, boattail configuration and the 3-cal nose, nonboattail configuration in Fig. 35a indicates that the center of pressure was farther aft in the case of the nonboattail configuration. This backward shift of cp_o is also consistent with the decreased static instability of the projectile shown in Fig. 20. Note again that the comparison does not illustrate a true boattail effect, but a combined effect of boattail, afterbody length, and nose geometry.

An examination of the amplitude effect on the damping-in-pitch derivatives was made by analyzing separately the precessional and nutational damping rates as functions of the effective amplitude parameters, δ_{e1}^2 and δ_{e2}^2 . Representative plots shown in Fig. 36 indicate that measurable amplitude effects did occur at some conditions. Since amplitude effects on the damping rates generally are in opposite directions, the net amplitude effect on $C_{m_q} + C_{m_{\dot{\alpha}}}$ is usually less than that determined for the individual damping rates.

Using the slope parameters, C_4 and C_5 , μ_{P_o} and μ_{N_o} were determined for individual tests and were used in conjunction with measured C_{D_o} and $C_{N_{\alpha o}}$ values to compute the damping-in-pitch derivatives shown in Fig. 37. The measurements shown in Fig. 37 for the secant-ogive nose configurations indicate that $(C_{m_q} + C_{m_{\dot{\alpha}}})_o$ generally decreased with increasing Mach number; however, the configurations remain dynamically stable throughout the Mach number range. A comparison of the levels of the faired curves indicates that nose length does not affect $(C_{m_q} + C_{m_{\dot{\alpha}}})_o$ appreciably, and any effect of bluntness appears to be within the scatter of the measurements. In contrast, the measurement for the tangent-ogive and conical nose configurations (Figs. 37d and e) reveal significant bluntness effects.

The $(C_{m_q} + C_{m_{\dot{\alpha}}})_o$ values for the boattail configurations shown in Fig. 39 were computed using values from fairings of μ_{N_o} and μ_{P_o} (Fig. 38), C_{D_o} (Fig. 11), and $C_{N_{\alpha o}}$ (Fig. 27) as a function of simulated altitude. Faired values were used since they are better defined than individual measurements. The results in Fig. 39 show that the configurations were dynamically stable throughout the altitude range. Also, there is no notable difference from the comparison of the compromise between the boattail configuration and the longer nose configuration of Fig. 37c.

Magnus moment and roll damping derivatives are presented in Figs. 40 through 42. Within the scatter of these measurements there are no discernible effects of nose length, nose bluntness, or boattailing. Notice, however, that $C_{m_{p\beta o}}$ measurements for the conical nose shape configurations were measurably smaller than those for other configurations.

The sample comparison called to attention throughout Section IV may now be summarized. Compared were the relative merits of increasing the overall length of a projectile from 4.5 to 5 cal by adding 0.5 cal of boattail versus adding 0.5 cal of nose length. The comparison was restricted to the secant-ogive nose shape, ground level, $M = 2$, and $0.1 < \psi < 0.3$. Electing to add the boattail results in a small decrease in C_{D_o} ,

averaging 3 percent over the bluntness range. The boattail also increased the static instability, primarily by a forward shift of cp_o averaging 0.5 cal over the bluntness range. Effects on the dynamic stability coefficients were negligible. Further analysis of the trade-offs in terms of projectile time of flight, production complexity, and dispersion appears warranted but is beyond the scope of this report.

SECTION V CONCLUDING REMARKS

Free-flight range tests of spin stabilized, blunted 4-, 4.5-, and 5-cal ogive-cylinder and cone-cylinder configurations were conducted over a nominal Mach number range from 1.5 to 3.5 and at simulated altitudes up to 60 kft. All configurations had a cylindrical section of 2-cal length. Results show that:

1. The secant-ogive nose shape yielded the lowest drag coefficient of the configurations tested. The drag coefficient was further reduced by an increase in the nose length and with the addition of a boattail even though projectile length was increased.
2. The effect of nose bluntness on C_{D_o} in the range $0.1 \leq \psi \leq 0.2$ was dependent on Mach number, nose shape, and nose length. For the secant-ogive nose configuration, increasing ψ to 0.3 increased C_{D_o} significantly at the higher Mach numbers.
3. The static stability parameter, $C_{m_{\alpha}}$, is highly sensitive to nose shape with the conical nose shape yielding the minimum instability and the tangent-ogive nose yielding the maximum instability.
4. The dynamic stability coefficients for all configurations decreased with increasing Mach number. However, the projectiles remained dynamically stable throughout the Mach number range.
5. Nonlinearities with amplitude were observed in the force and moment data and were treated, apparently adequately, using a cubic analysis.

REFERENCES

1. Murphy, C. H. and Schmidt, L. E. "The Effect of Length on the Aerodynamic Characteristics of Bodies of Revolution in Supersonic Flight." BRL Report 876 (AD23468), August 1953.
2. Dickinson, E. R. "The Effect of Boattailing on the Drag Coefficient of Cone-Cylinder Projectiles at Supersonic Velocities." BRL Memorandum Report No. 842, November 1954.

3. Greene, J. E. "Static Stability and Magnus Characteristics of the 5-Caliber and 7-Caliber Army-Navy Spinner Rocket at Low Subsonic Speeds." NAVORD Report 3884, December 1954.
4. Roschke, E. J. "The Effect of Nose Truncation on the Aerodynamic Properties of 9-Caliber Long Army-Navy Spinner Rocket Models near Sonic Velocity." BRL Technical Note No. 902, January 1955.
5. Jaeger, B. F. and Morgan, A. J. A. "A Review of Experiment and Theory Applicable to Cone-Cylinder and Ogive-Cylinder Bodies of Revolution in Supersonic Flow." NAVORD Report 5239, June 1956.
6. Luchuk, W. "The Dependence of the Magnus Force and Moment on the Nose Shape of Cylindrical Bodies of Fineness Ratio 5 at a Mach Number of 1.75." NAVORD Report 4425, April 1957.
7. Greene, J. E. "A Summary of Experimental Magnus Characteristics of a 7- and 5-Caliber Body of Revolution at Subsonic through Supersonic Speeds." NAVORD Report 6110, August 1958.
8. Dickinson, E. R. "Some Aerodynamic Effects of Blunting a Projectile Nose." BRL Memorandum Report 1596, September 1964.
9. Welsh, C. J., Winchenbach, G. L., and Madagan, A. N. "Free-Flight Investigation of the Aerodynamic Characteristics of a 10-deg Semiangle Cone at Mach Numbers from 6 to 16." AEDC-TR-69-63 (AD686407), April 1969.
10. Murphy, C. H. "The Measurement of Nonlinear Forces and Moments by Means of Free Flight Tests." BRL Report No. 974, February 1956.
11. Murphy, C. H. "Free Flight Motion of Symmetric Missiles." BRL-R-1216, July 1963.

APPENDIXES
I. ILLUSTRATIONS
II. TABLES

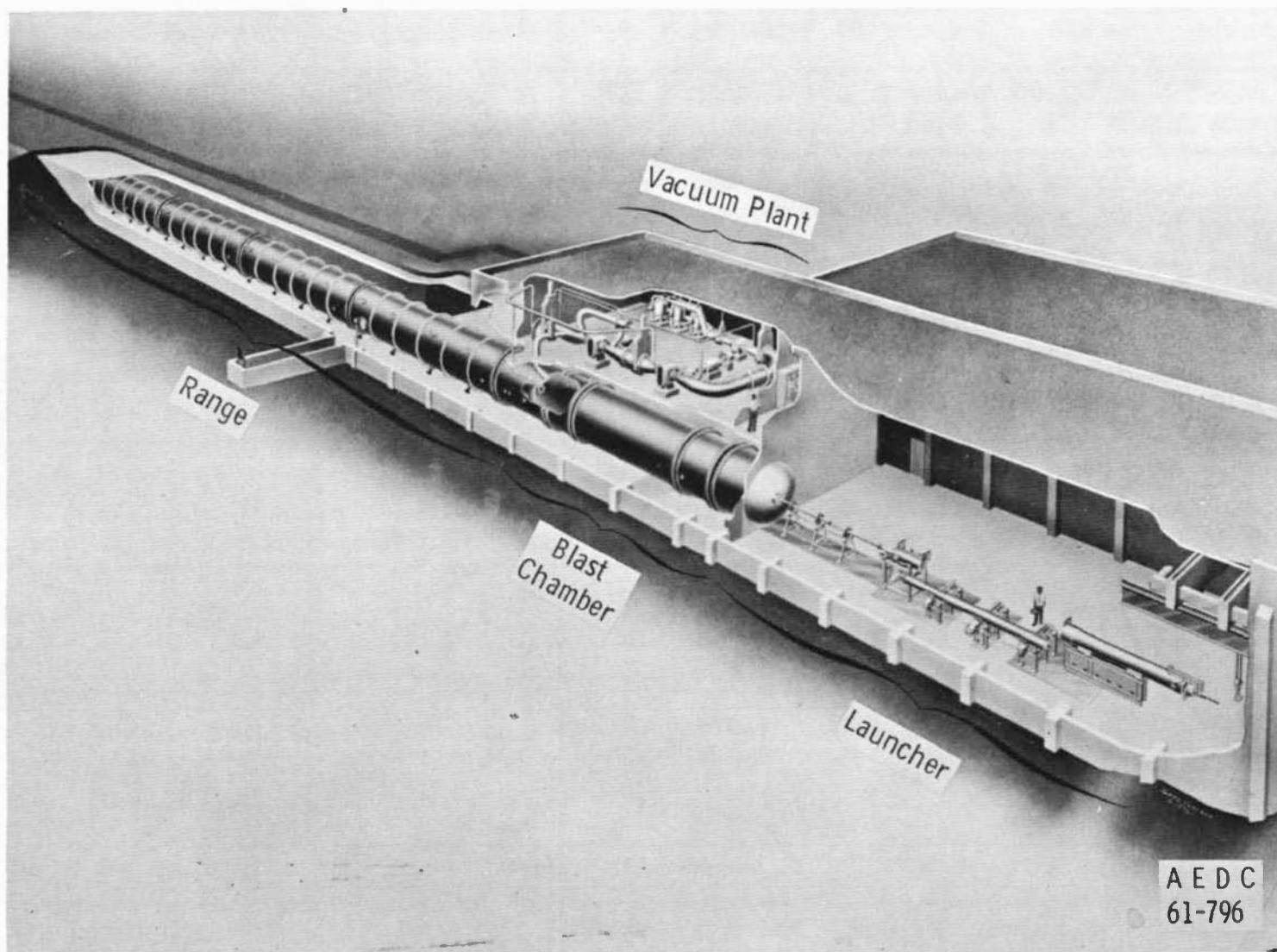


Fig. 1 Range G

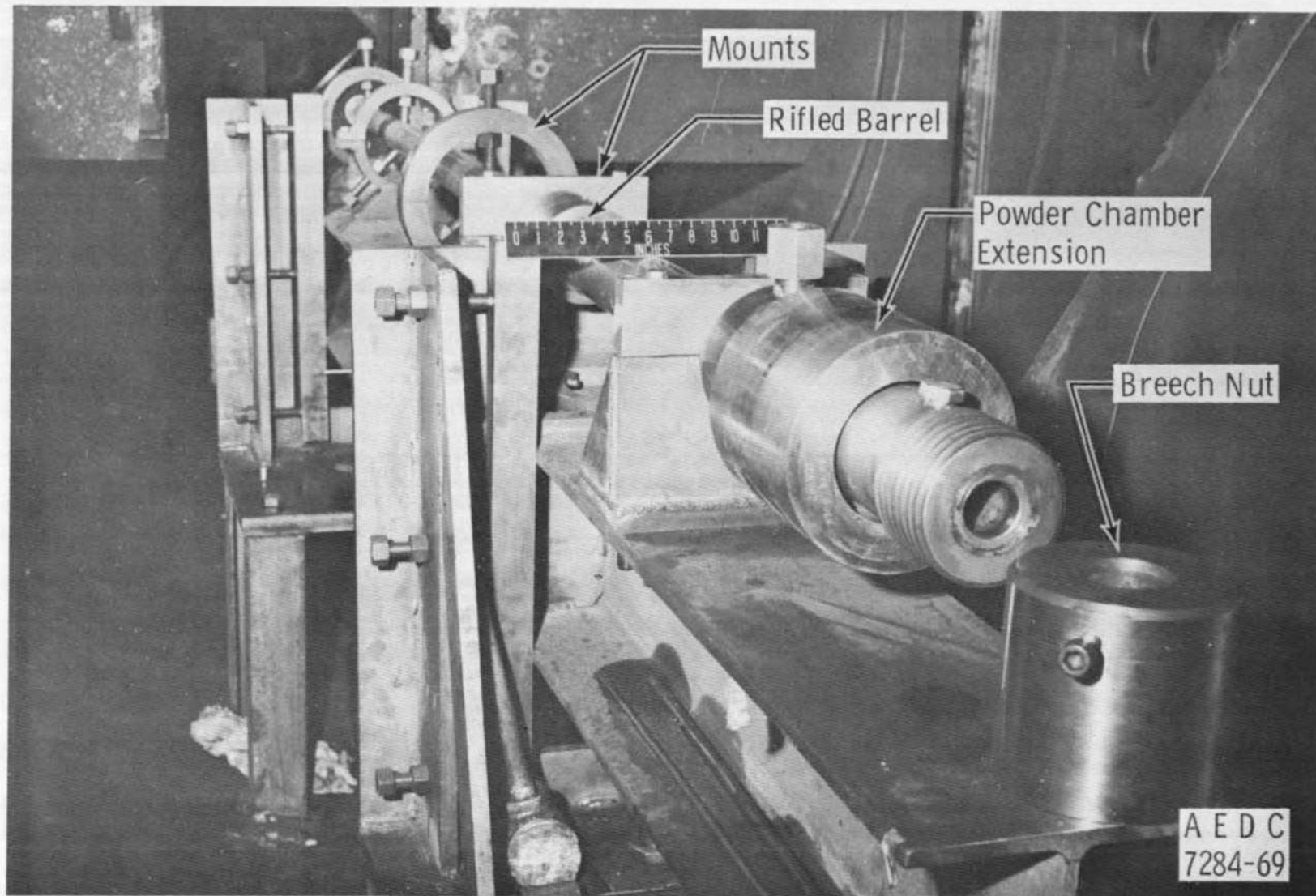
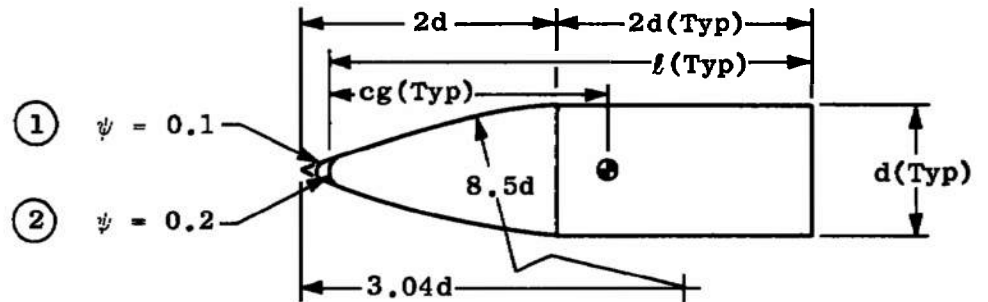
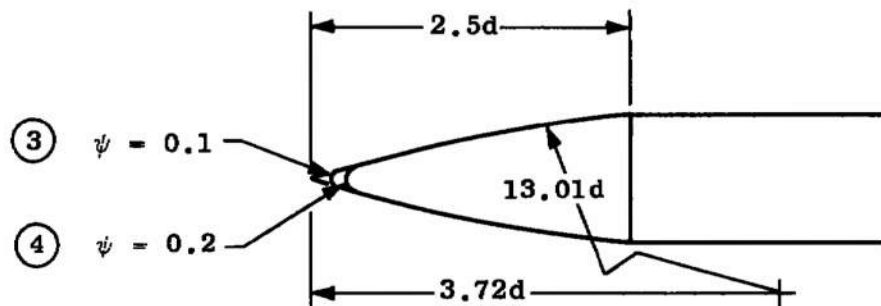


Fig. 2 Support System for the 20-mm Cannon

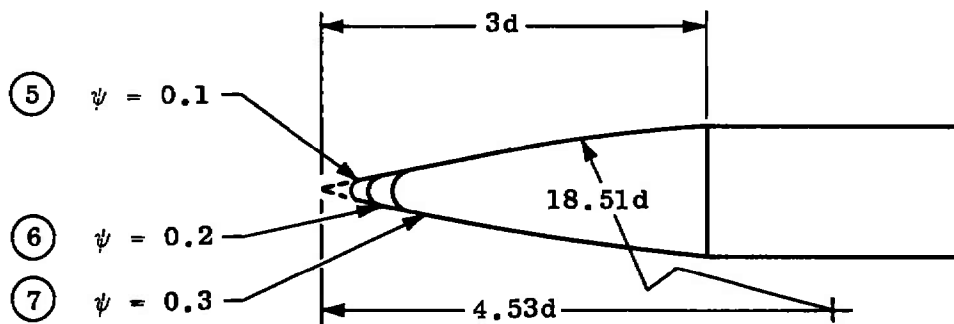
○ Configuration Number



a. 2.0-cal Secant-Ogive Nose



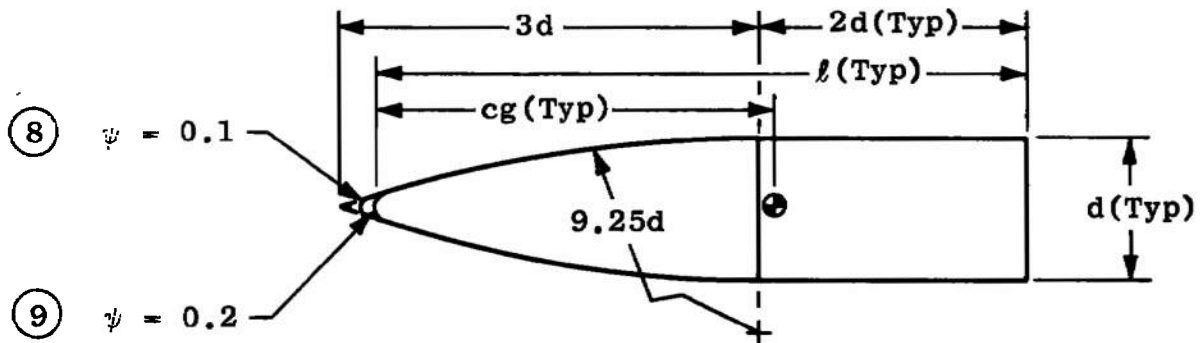
b. 2.5-cal Secant-Ogive Nose



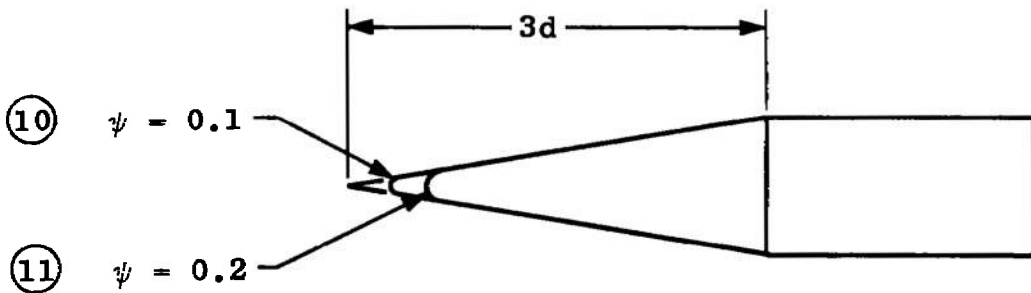
c. 3.0-cal Secant-Ogive Nose

Fig. 3 Sketches of the Projectiles

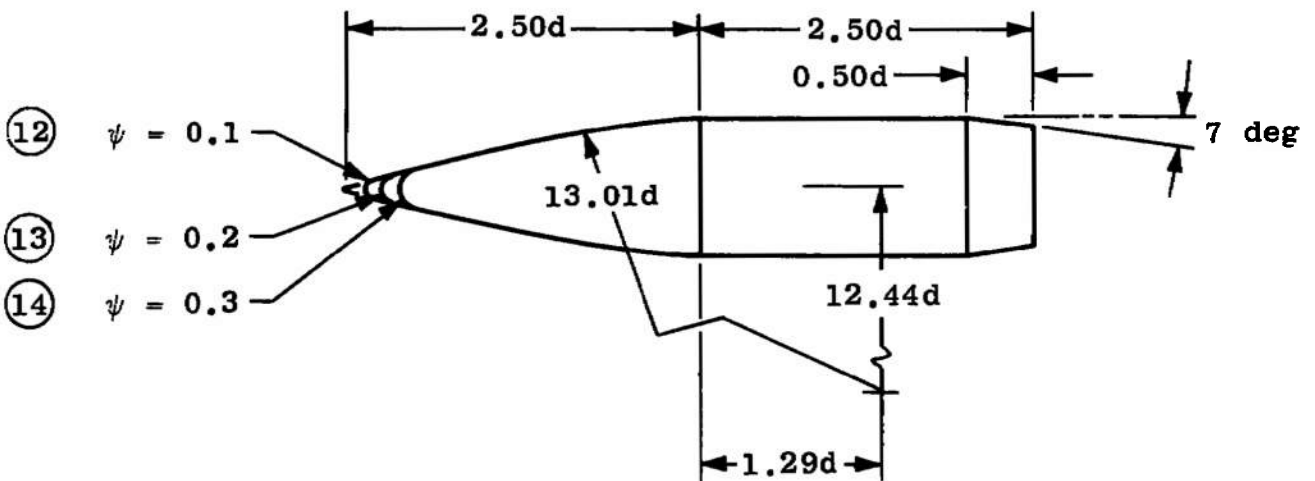
○ Configuration Number



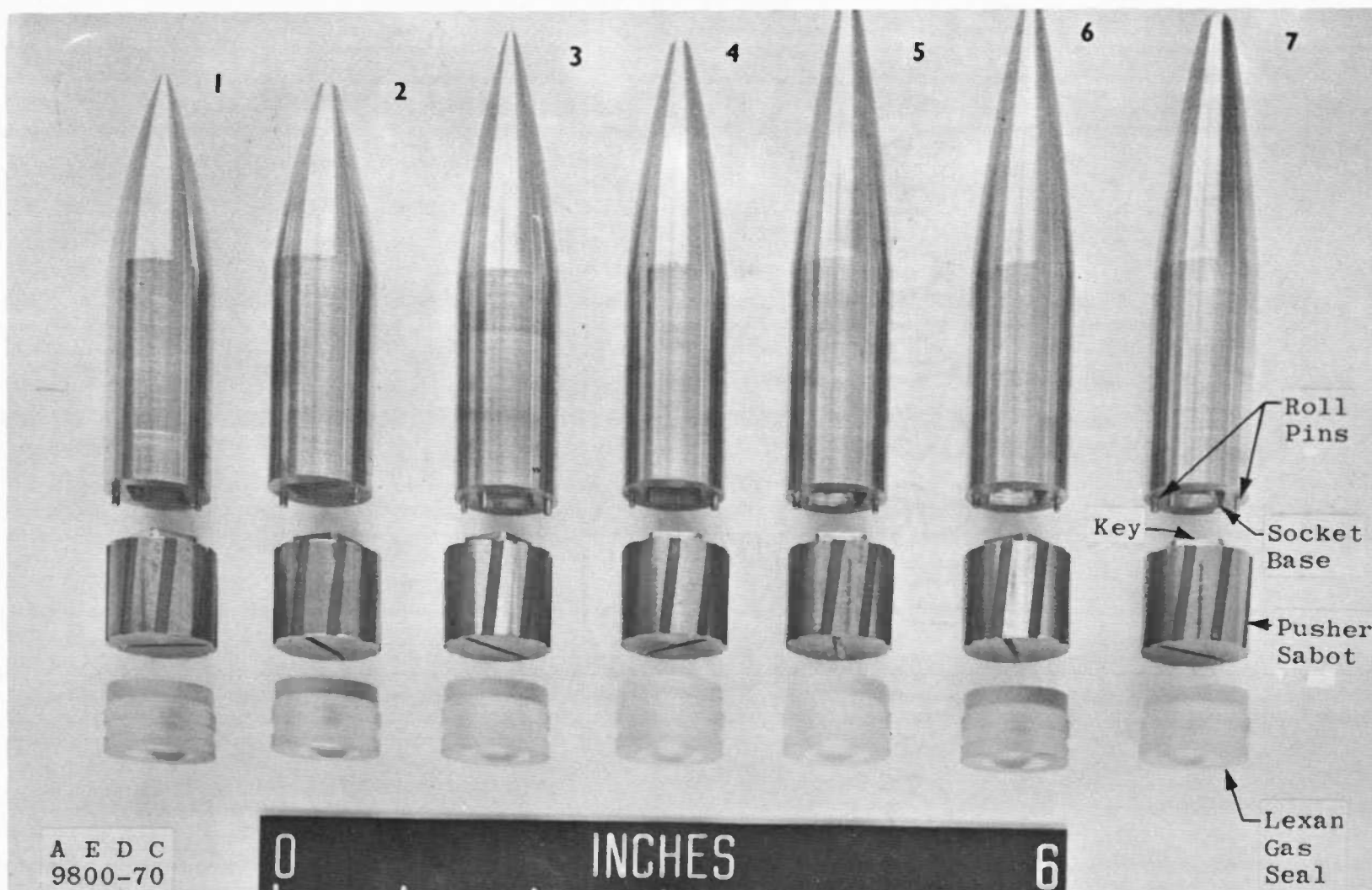
d. 3-cal Tangent-Ogive Nose



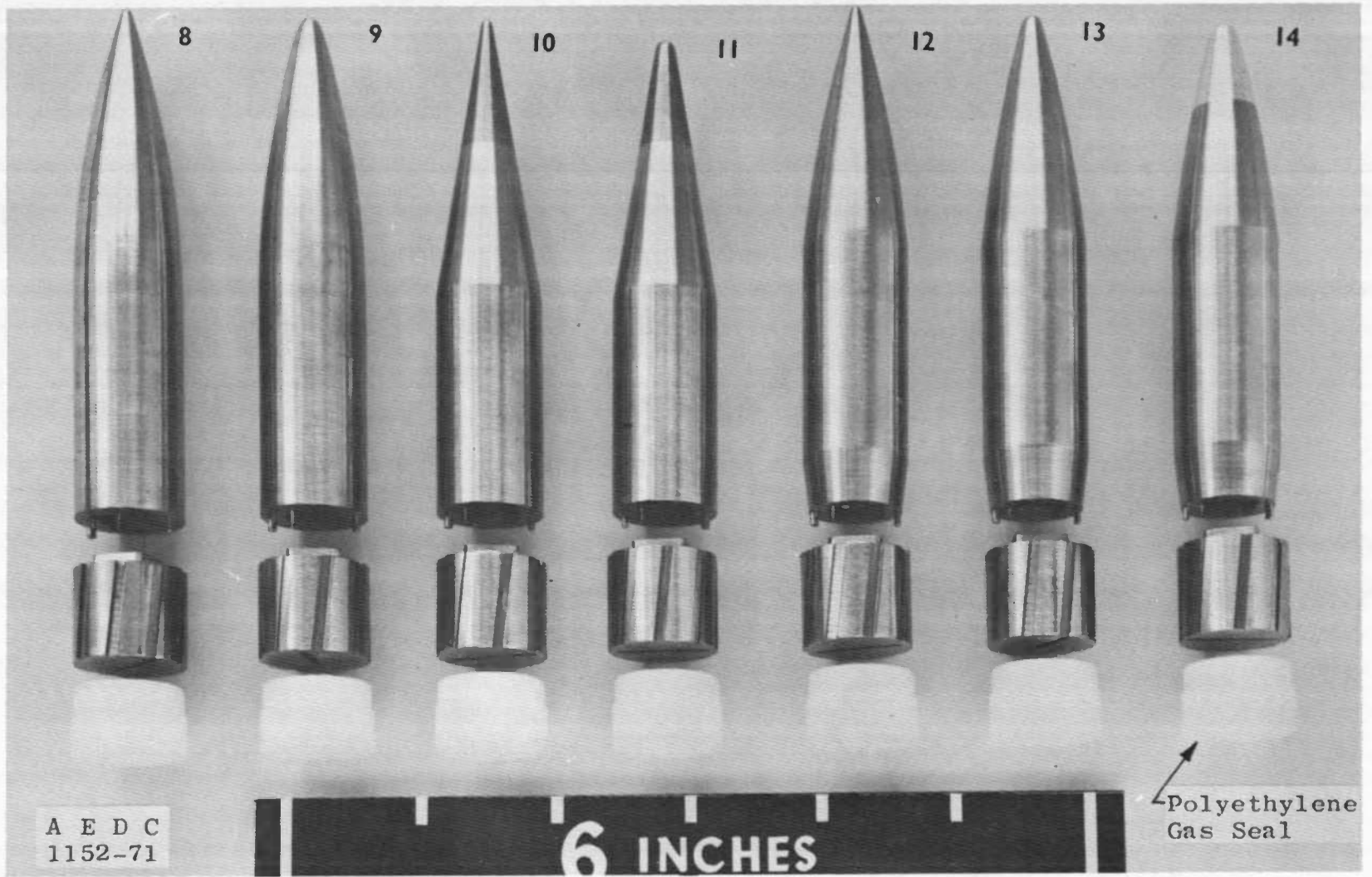
e. 3-cal Conical Nose



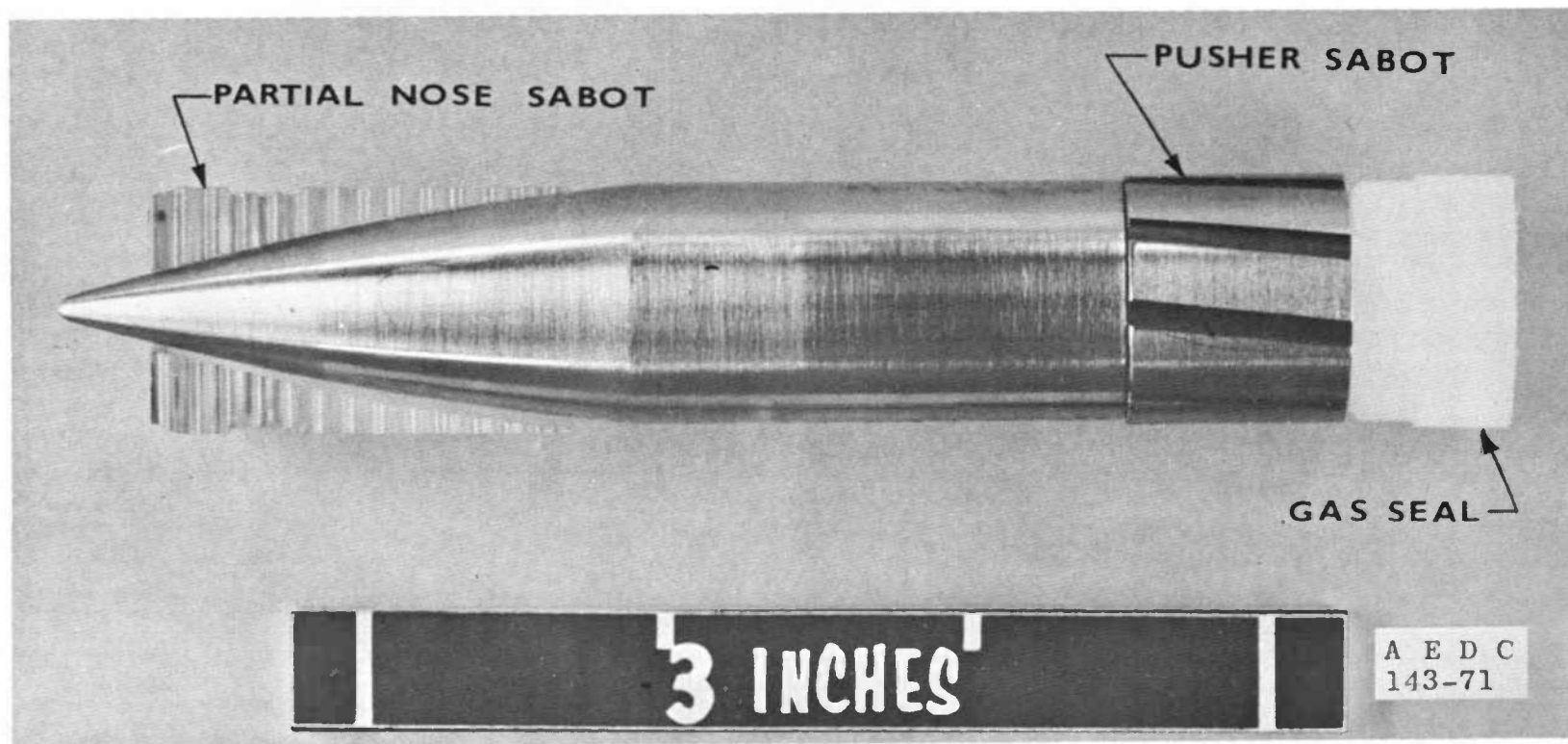
f. 2.5-cal Secant-Ogive Nose with Boattail
Fig. 3 Concluded



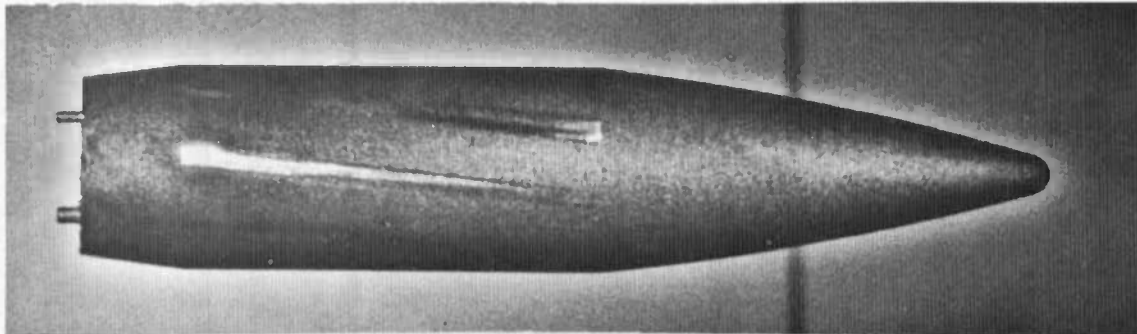
a. 4, 4.5, and 5-cal Configurations with Secant-Ogive Nose
 Fig. 4 Photograph of Projectiles, Sabots, and Gas Seals



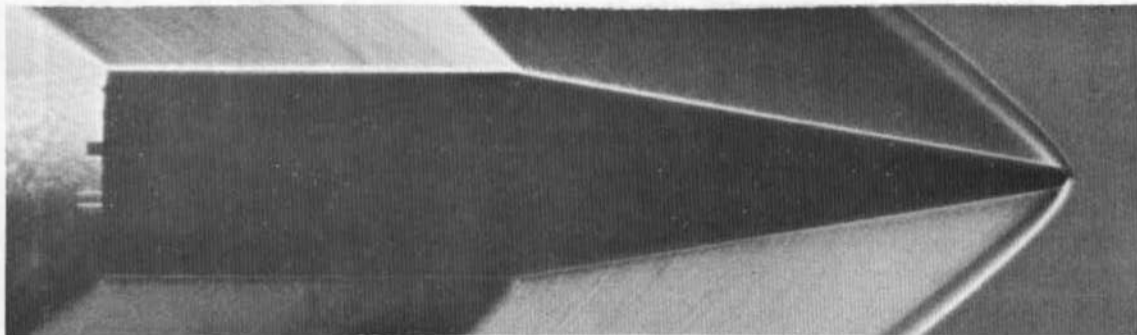
b. 5-cal Configurations with Tangent-Ogive Nose, Conical Nose, and Boattail
Fig. 4 Continued



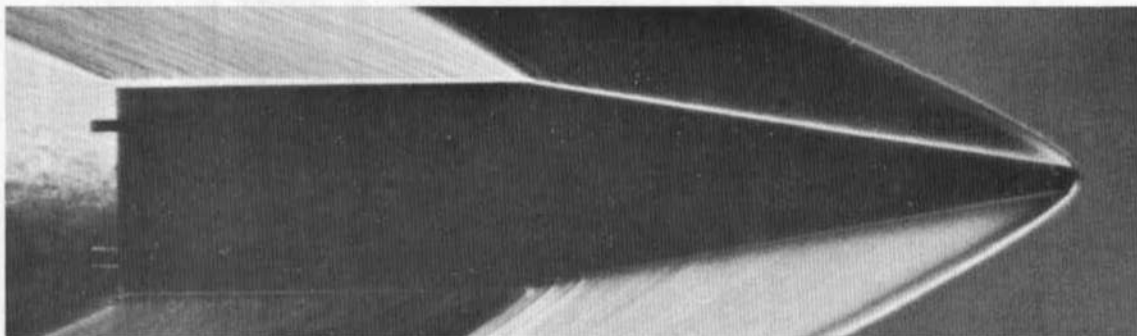
c. Partial Launch Package Assembly
Fig. 4 Concluded



a. Laser Photograph of Secant-Ogive Cylinder Configuration with Boattail

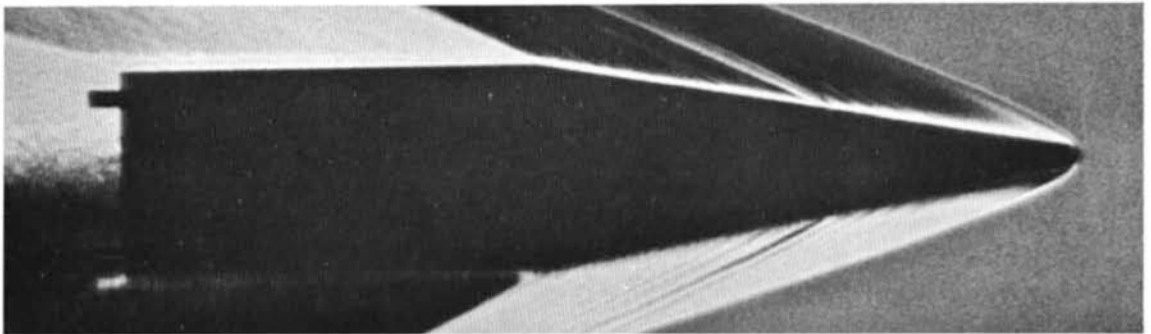


b. Schlieren Photograph of 5-cal Cone-Cylinder Configuration
at $M = 1.5$ ($Re_\ell = 3.41 \times 10^6$)

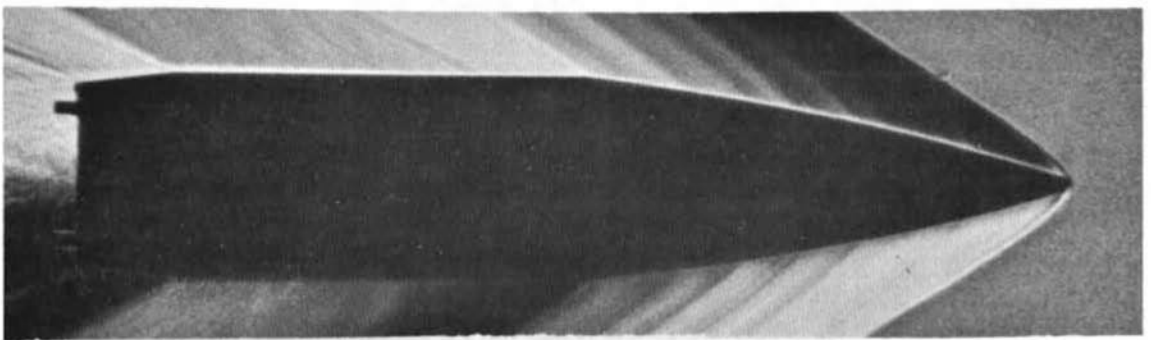


c. Schlieren Photograph of 5-cal Cone-Cylinder Configuration
at $M = 2.5$ ($Re_\ell = 5.02 \times 10^6$)

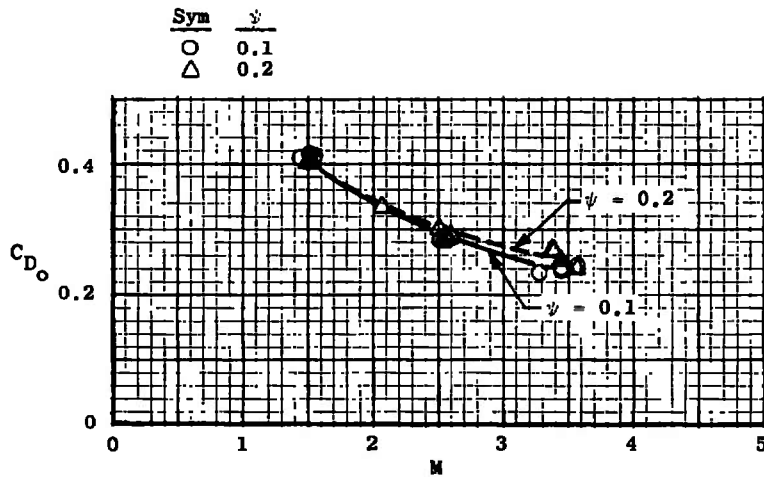
Fig. 5 Photographic Observations of Typical Configurations



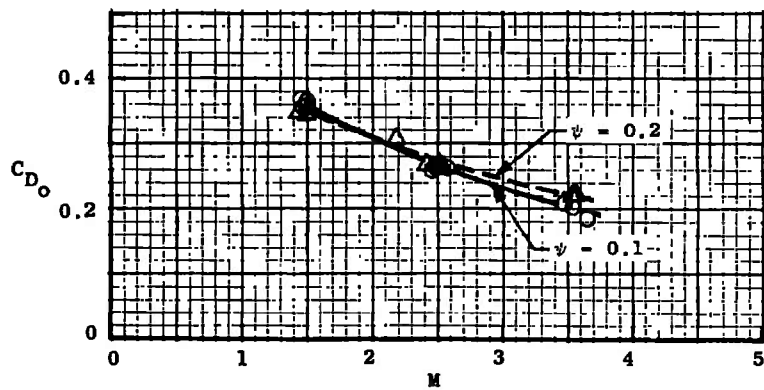
d. Schlieren Photograph of 5-cal Cone-Cylinder Configuration
at $M = 3.5$ ($Re_\ell = 6.90 \times 10^6$)



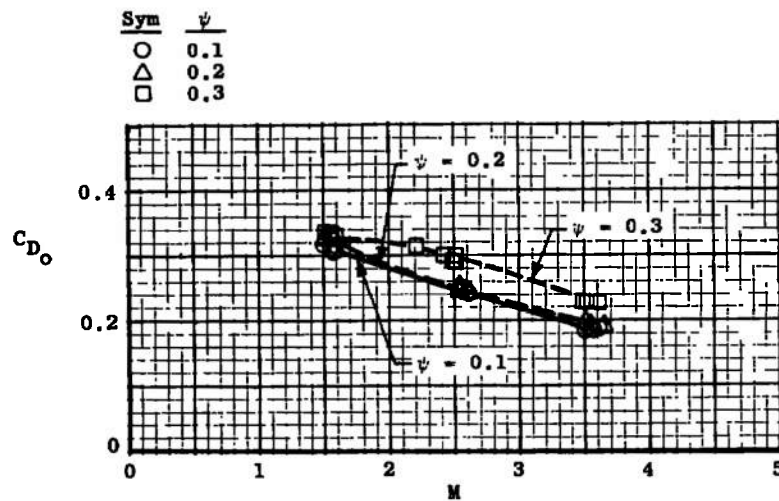
e. Schlieren Photograph of 5-cal Secant-Ogive-Cylinder Configuration
with Boattail at $M = 2$ ($Re_\ell = 4.34 \times 10^6$)
Fig. 5 Concluded



a. 2-cal Nose Length



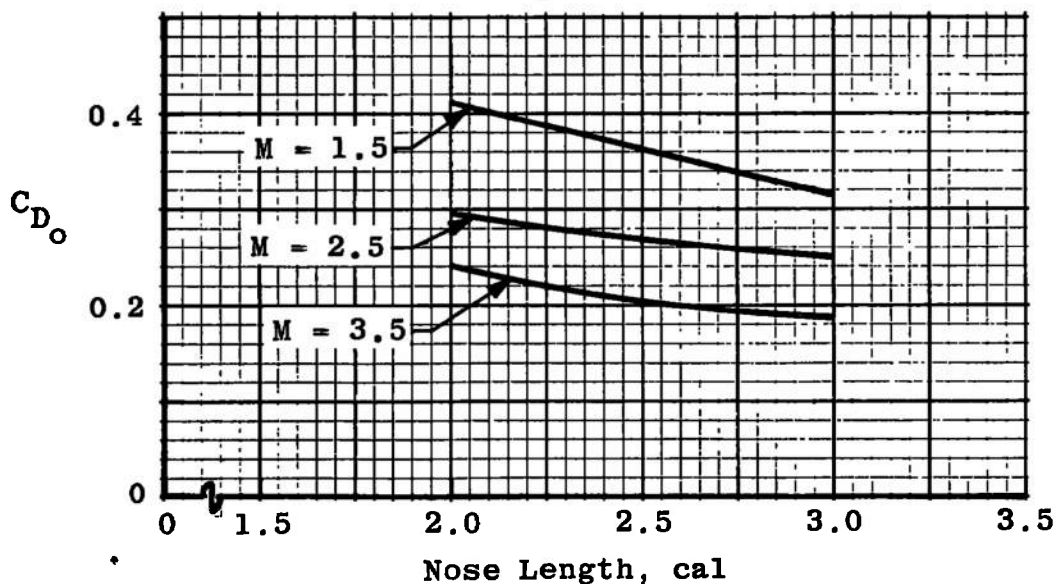
b. 2.5-cal Nose Length



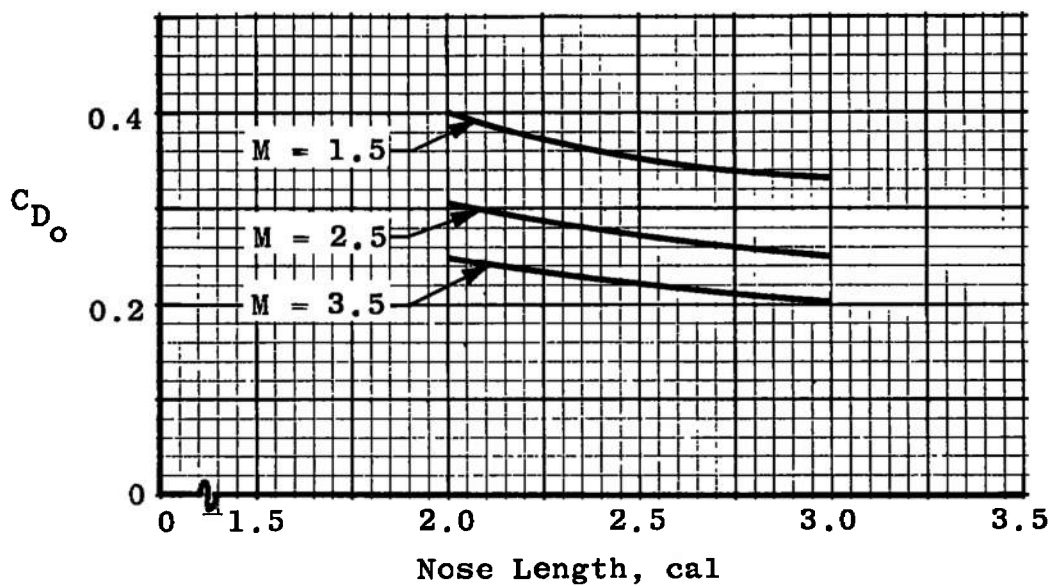
c. 3-cal Nose Length

Fig. 6 Drag Measurements for Secant-Ogive-Cylinder Configurations at Ground Level

Note: Levels Obtained by Crossplotting
Data from Fig. 6



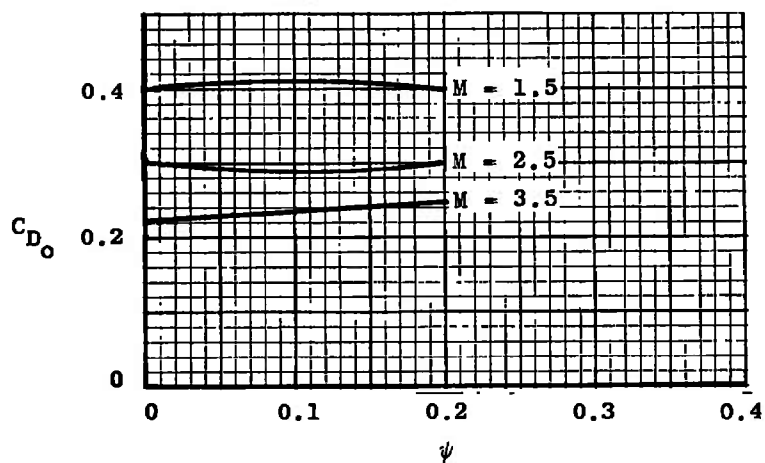
a. $\psi = 0.1$



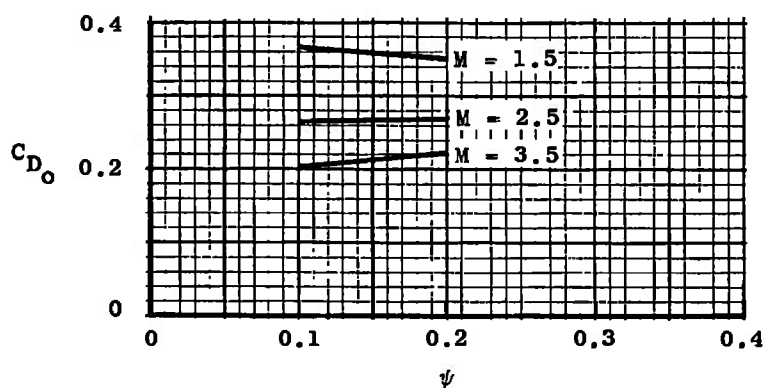
b. $\psi = 0.2$

Fig. 7 Effect of Nose Length on the Drag Coefficient of Secant-Ogive-Cylinder Configurations at Ground Level

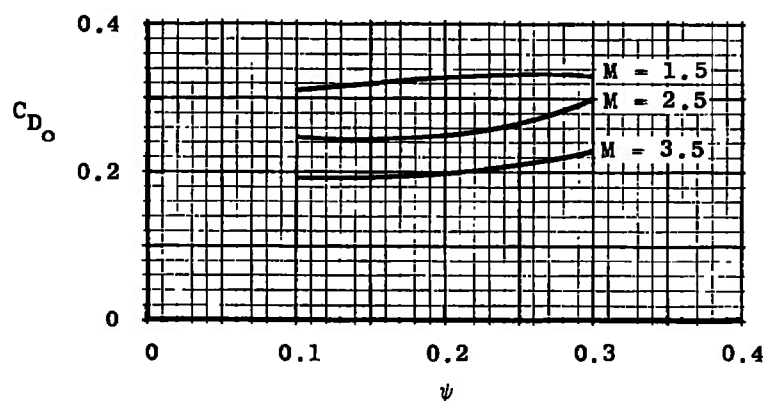
Note: Levels Obtained by Crossplotting
Data from Fig. 6



a. 2-cal Nose Length

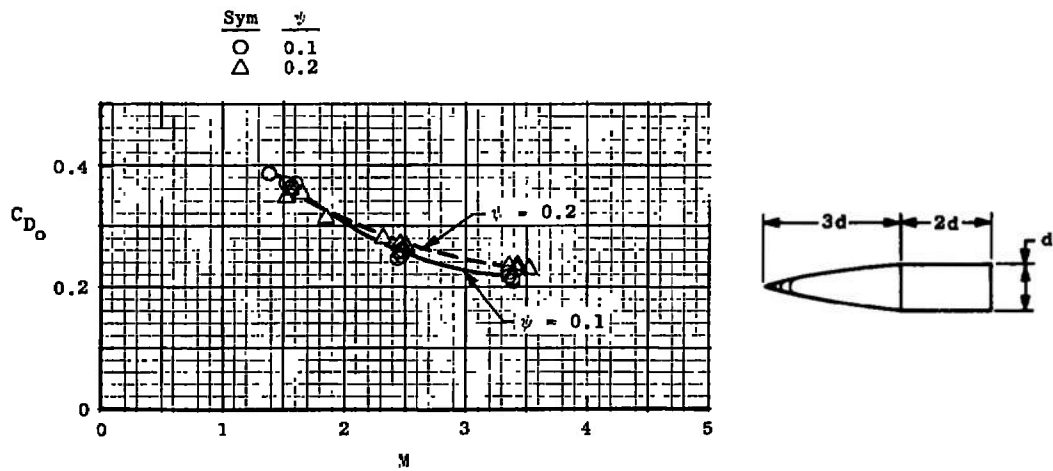


b. 2.5-cal Nose Length

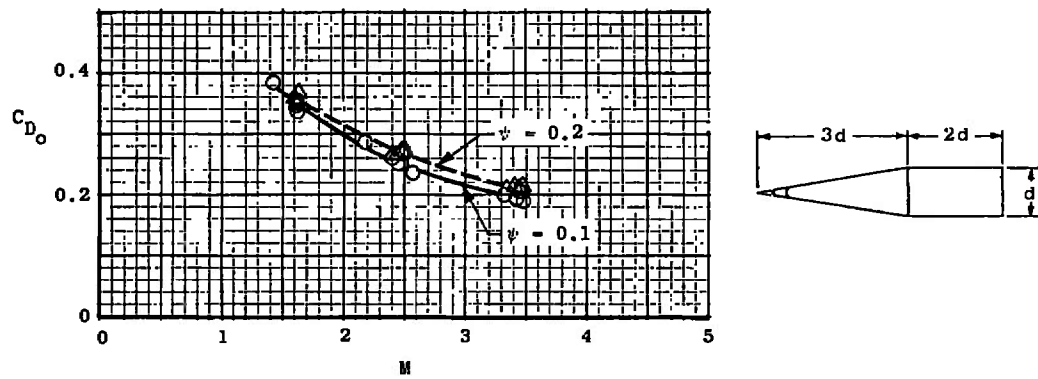


c. 3-cal Nose Length

Fig. 8 Effect of Bluntness on the Drag Coefficient of Secant-Ogive-Cylinder Configurations at Ground Level



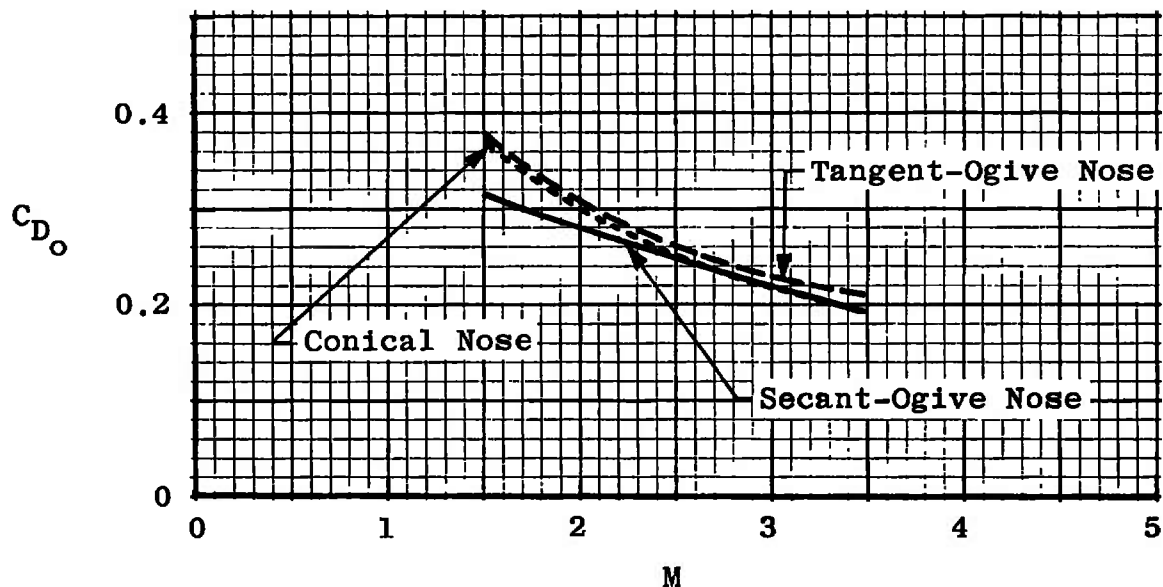
a. Tangent-Ogive Nose



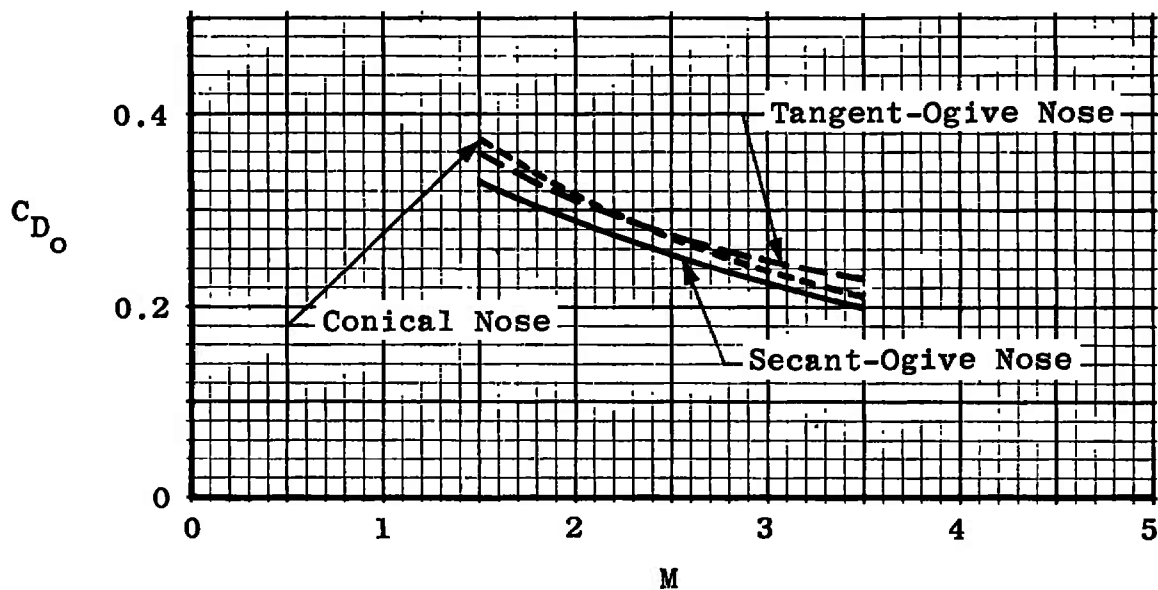
b. Conical Nose

Fig. 9 Drag Measurements for Tangent-Ogive- and Cone-Cylinder Configurations at Ground Level

Note: Levels Obtained by Crossplotting
Data from Figs. 9 and 6c



a. $\psi = 0.1$



b. $\psi = 0.2$

Fig. 10 Comparison of Drag Levels for 3-cal Nose Configurations at Ground Level

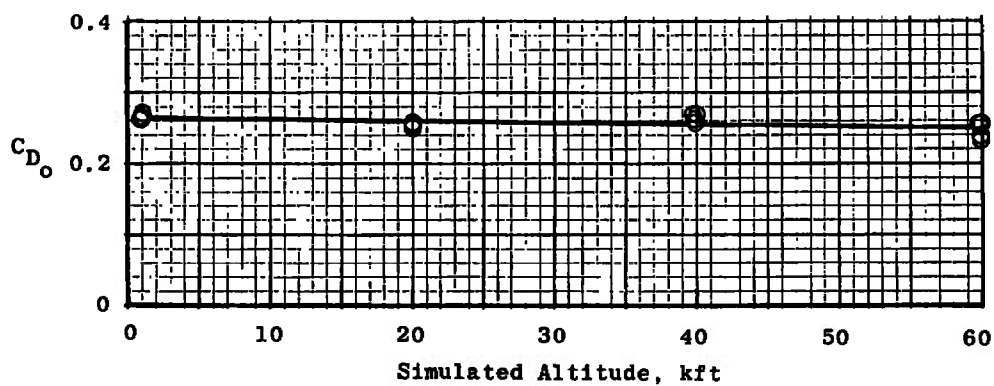
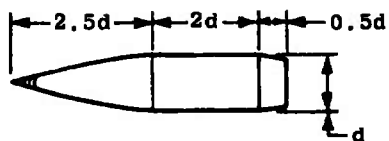
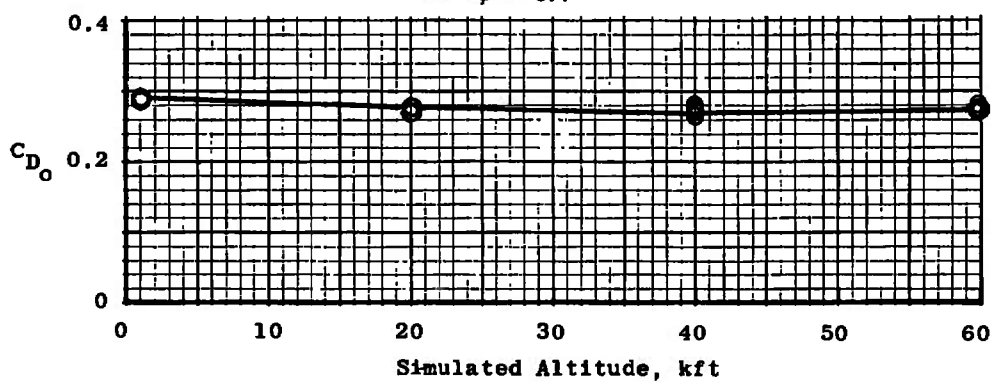
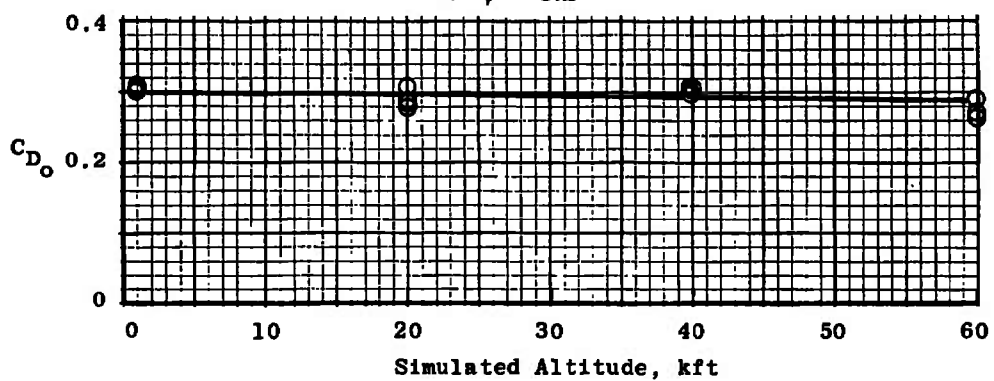
a. $\psi = 0.1$ b. $\psi = 0.2$ c. $\psi = 0.3$

Fig. 11 Drag Measurements at $M \approx 2$ for Secant-Ogive-Cylinder Configurations with Boattail

Note: Levels Obtained by Crossplotting
Data from Figs. 6b and 11

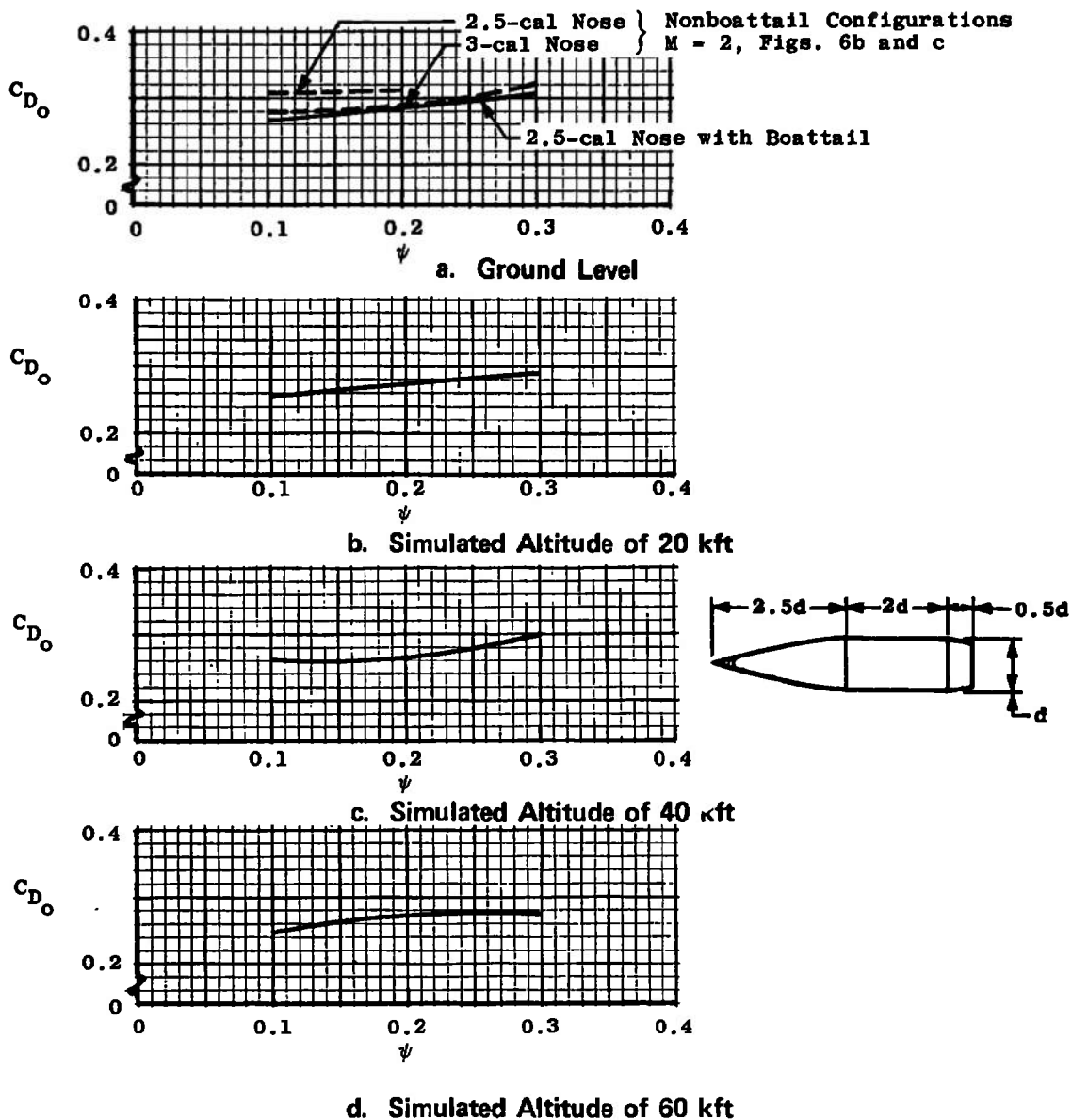
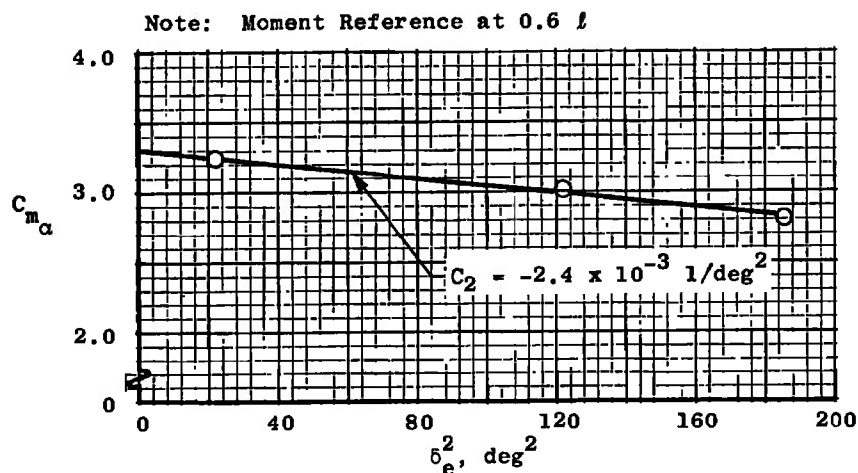
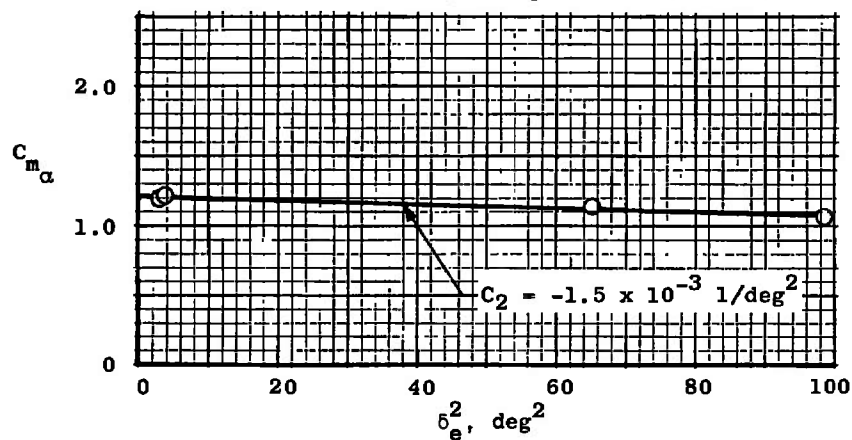


Fig. 12 Effect of Bluntness on the Drag Coefficient of Secant-Ogive-Cylinder Configurations with Boattail at $M = 2$

a. 3-cal Tangent Ogive Nose, $\psi = 0.1$, $M \approx 1.5$ b. 2.5-cal Conical Nose, $\psi = 0.1$, $M \approx 2.5$ Fig. 13 Representative Amplitude Effects on C_{m_α} for Typical Ogive- and Cone-Cylinder Configurations at Ground Level

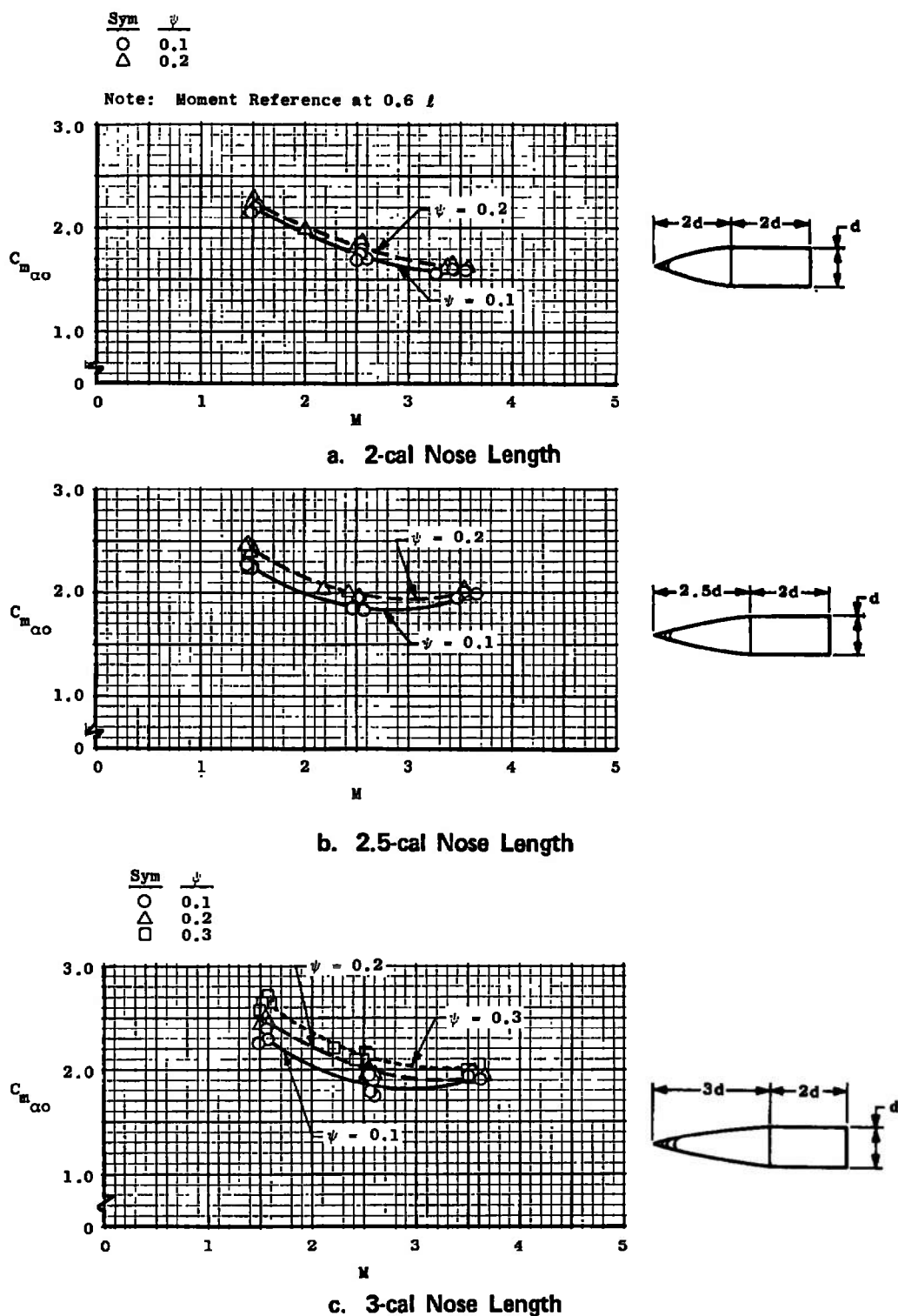
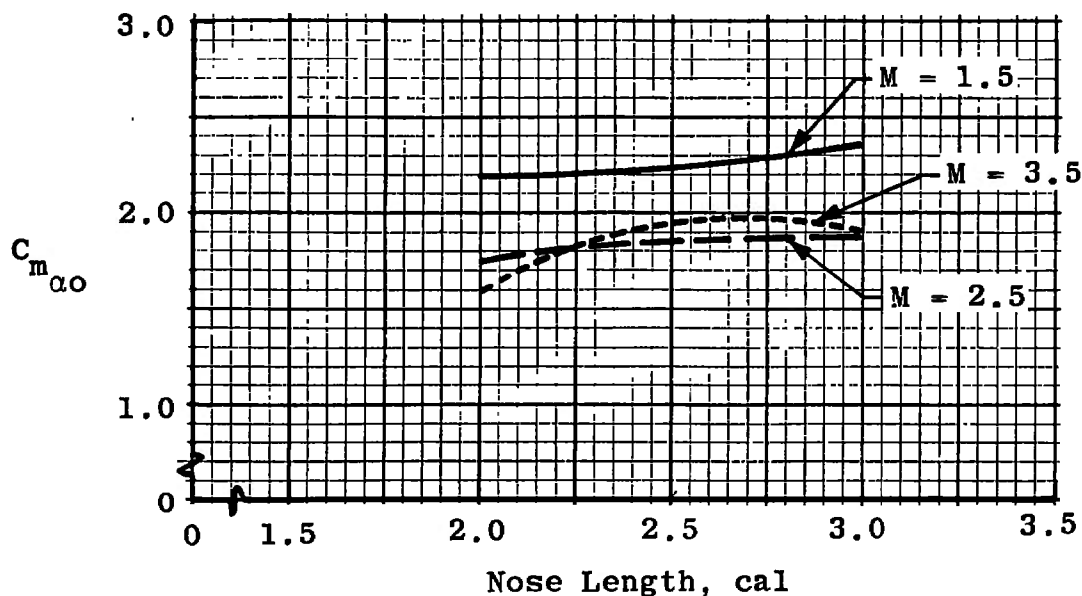
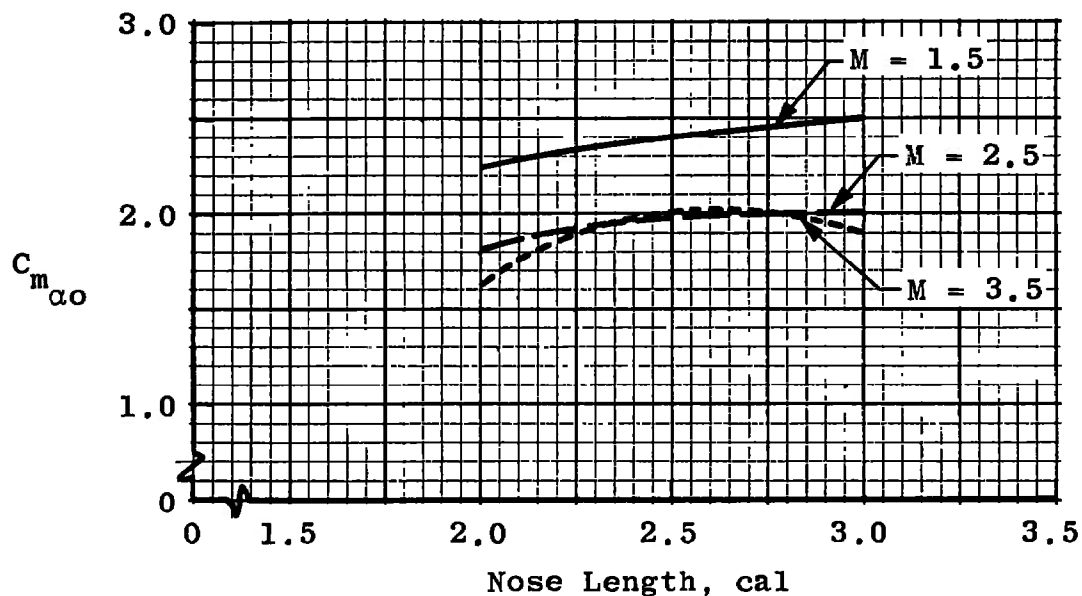


Fig. 14 Static Stability Derivatives at Zero Yaw Angle for Secant-Ogive-Cylinder Configurations at Ground Level

- Notes: 1. Levels Obtained by Crossplotting
Data from Fig. 14
2. Moment Reference at 0.6ℓ



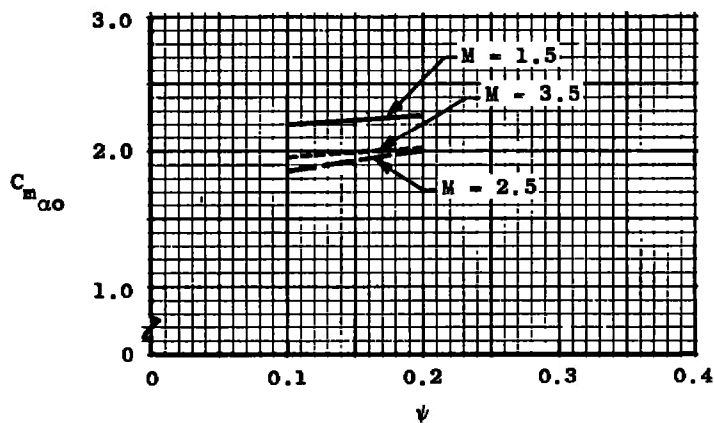
a. $\psi = 0.1$



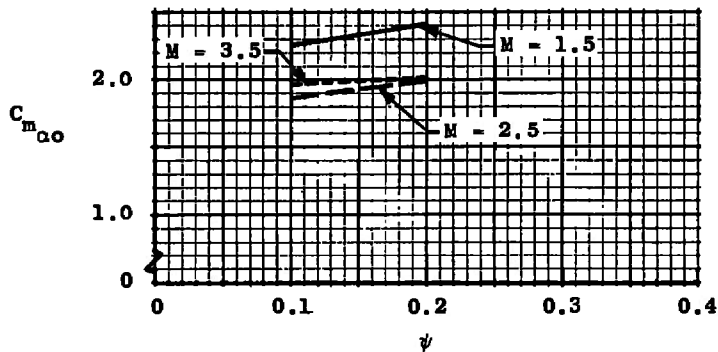
b. $\psi = 0.2$

Fig. 15 Effect of Nose Length on $C_{m\alpha_0}$ for Secant-Ogive-Cylinder Configurations at Ground Level

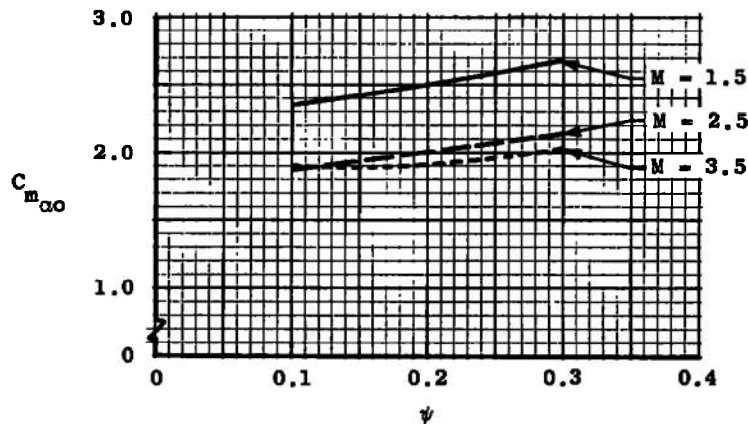
- Notes: 1. Levels Obtained by Crossplotting
Data from Fig. 14
2. Moment Reference at $0.6 l$



a. 2-cal Nose Length

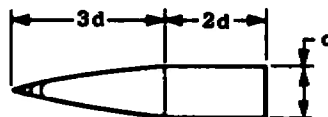
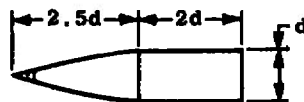
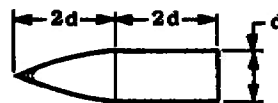


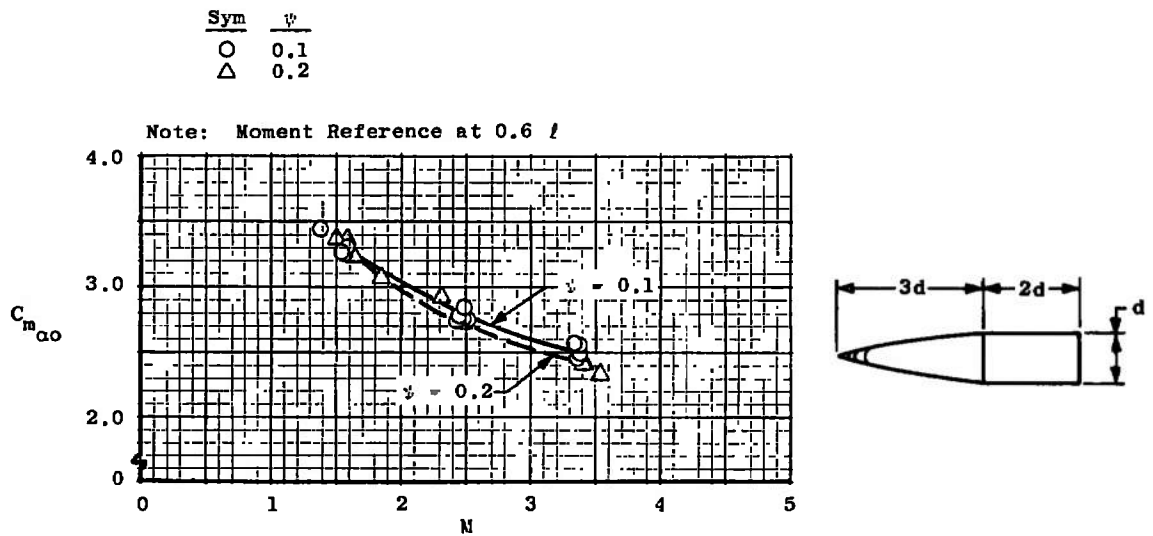
b. 2.5-cal Nose Length



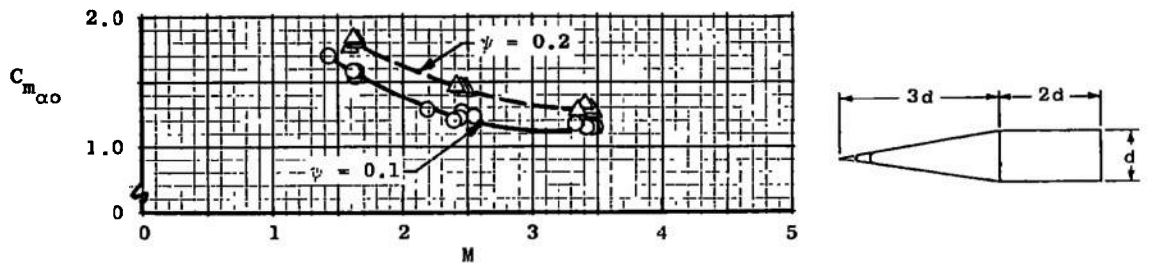
c. 3-cal Nose Length

Fig. 16 Effect of Nose Bluntness on $C_{m_{\alpha_0}}$ for Secant-Ogive-Cylinder Configurations at Ground Level





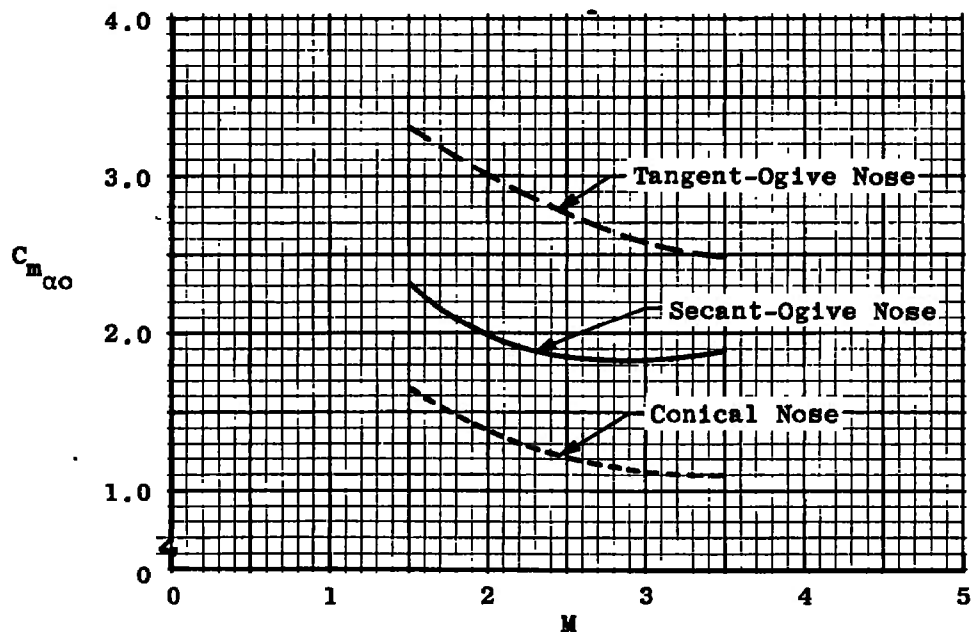
a. Tangent-Ogive Nose



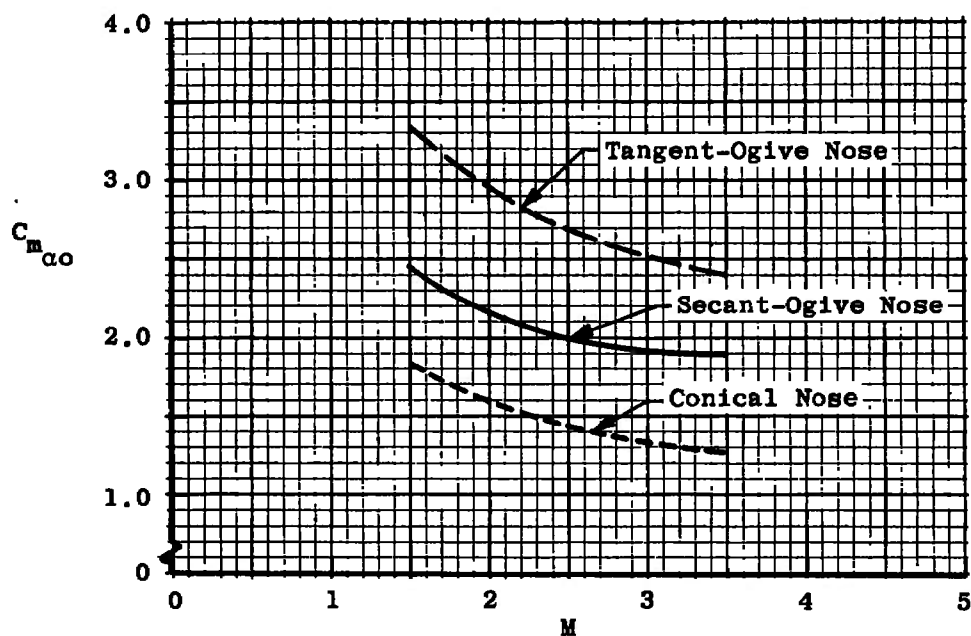
b. Conical Nose

Fig. 17 Static Stability Derivatives at Zero Yaw Angle for Tangent-Ogive- and Cone-Cylinder Configurations at Ground Level

- Notes: 1. Levels Obtained by Crossplotting
Data from Figs. 14c and 17
2. Moment Reference at 0.6 l

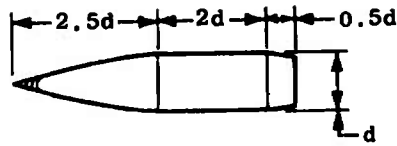


a. $\psi = 0.1$

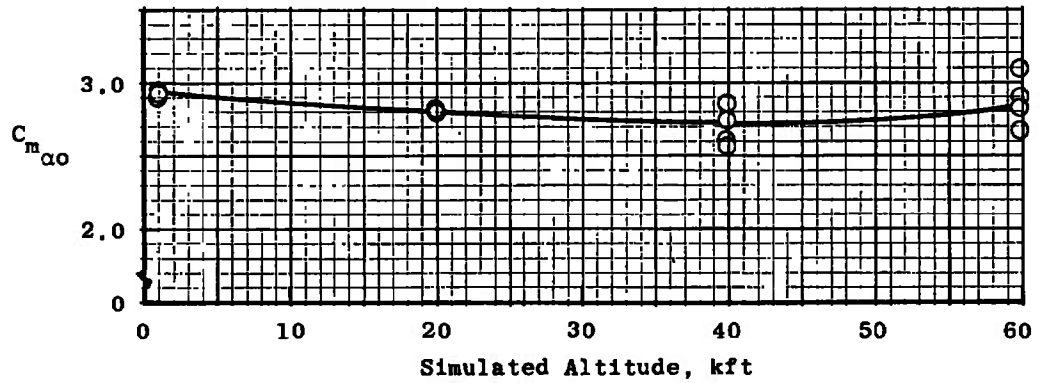


b. $\psi = 0.2$

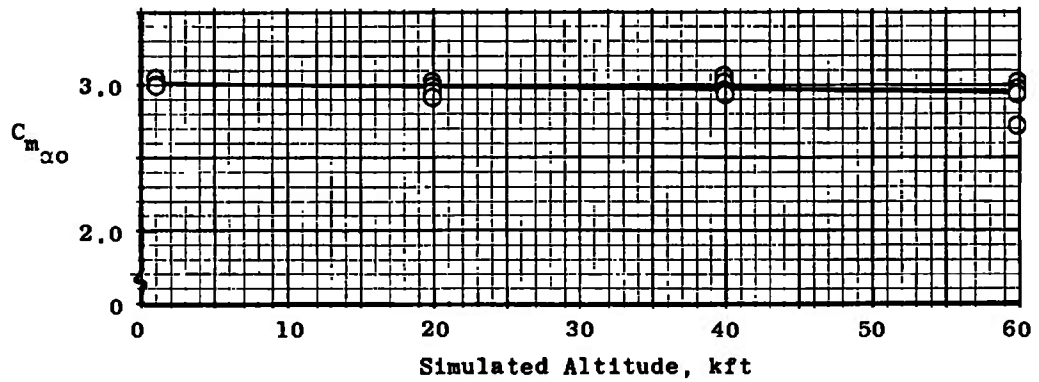
Fig. 18 Comparison of Levels of $C_{m_{\alpha 0}}$ for 3-cal Nose Configurations at Ground Level



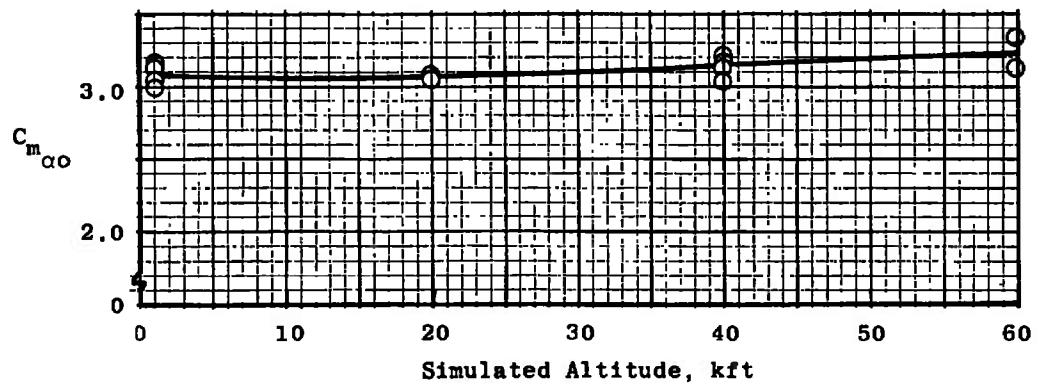
Note: Moment Reference at $0.6 l$



a. $\psi = 0.1$



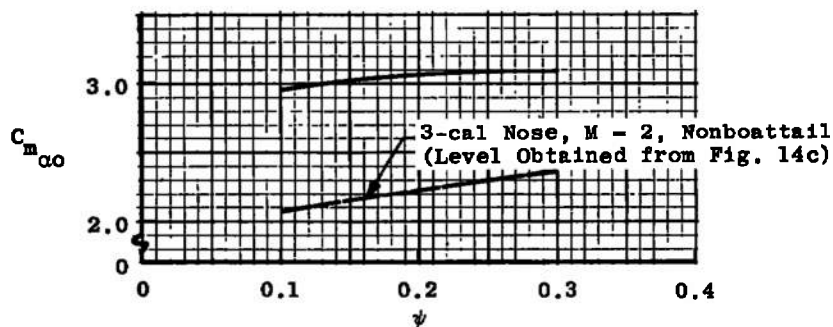
b. $\psi = 0.2$



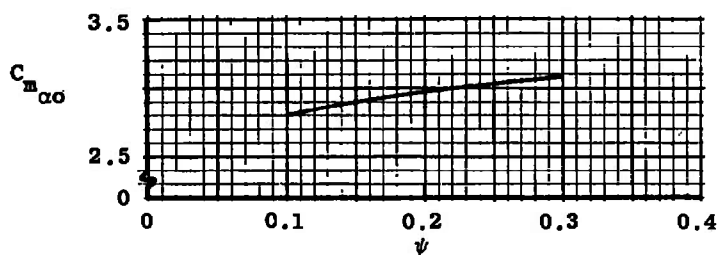
c. $\psi = 0.3$

Fig. 19 Static Stability Derivatives at $M = 2$ and Zero Yaw Angle for Secant-Ogive-Cylinder Configurations with Boattail

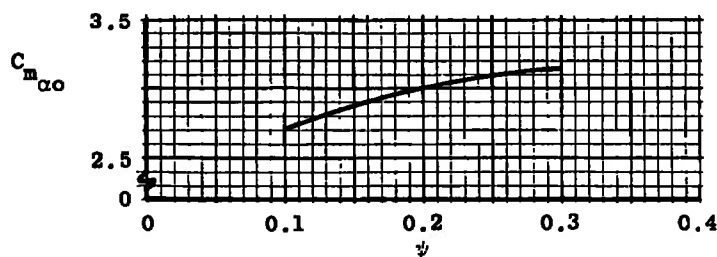
- Notes: 1. Levels Obtained by Crossplotting Data from Figs. 14b and 19
 2. Moment Reference at $0.6 l$



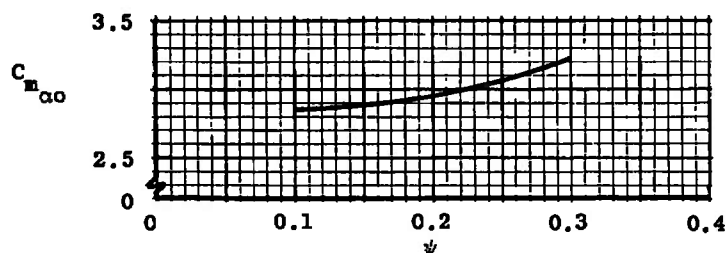
a. Ground Level



b. Simulated Altitude of 20 kft



c. Simulated Altitude of 40 kft



d. Simulated Altitude of 60 kft

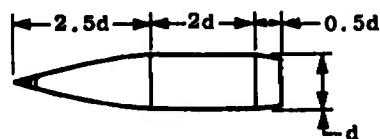
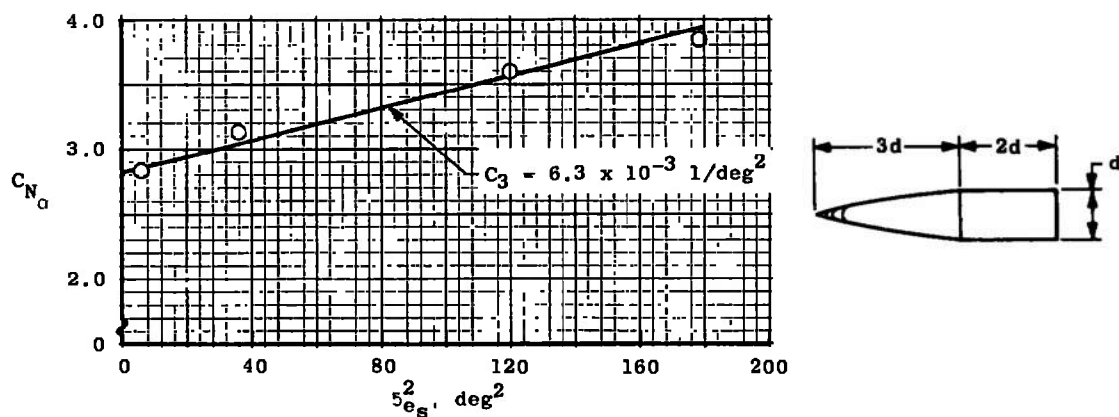
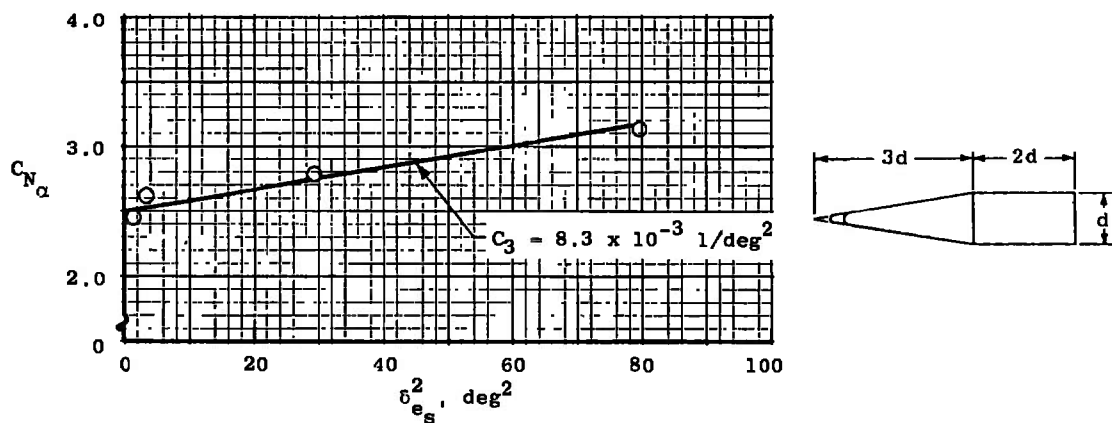


Fig. 20 Effect of Nose Bluntness on $C_{m_{\alpha 0}}$ at $M \approx 2$ for Secant-Ogive-Cylinder Configurations with Boattail



a. 3-cal Tangent Ogive Nose, $\psi = 0.2$, $M \approx 2.5$



b. 3-cal Conical Nose, $\psi = 0.1$, $M \approx 3.4$

Fig. 21 Representative Amplitude Effects on C_{N_α} for Typical Ogive- and Cone-Cylinder Configurations at Ground Level

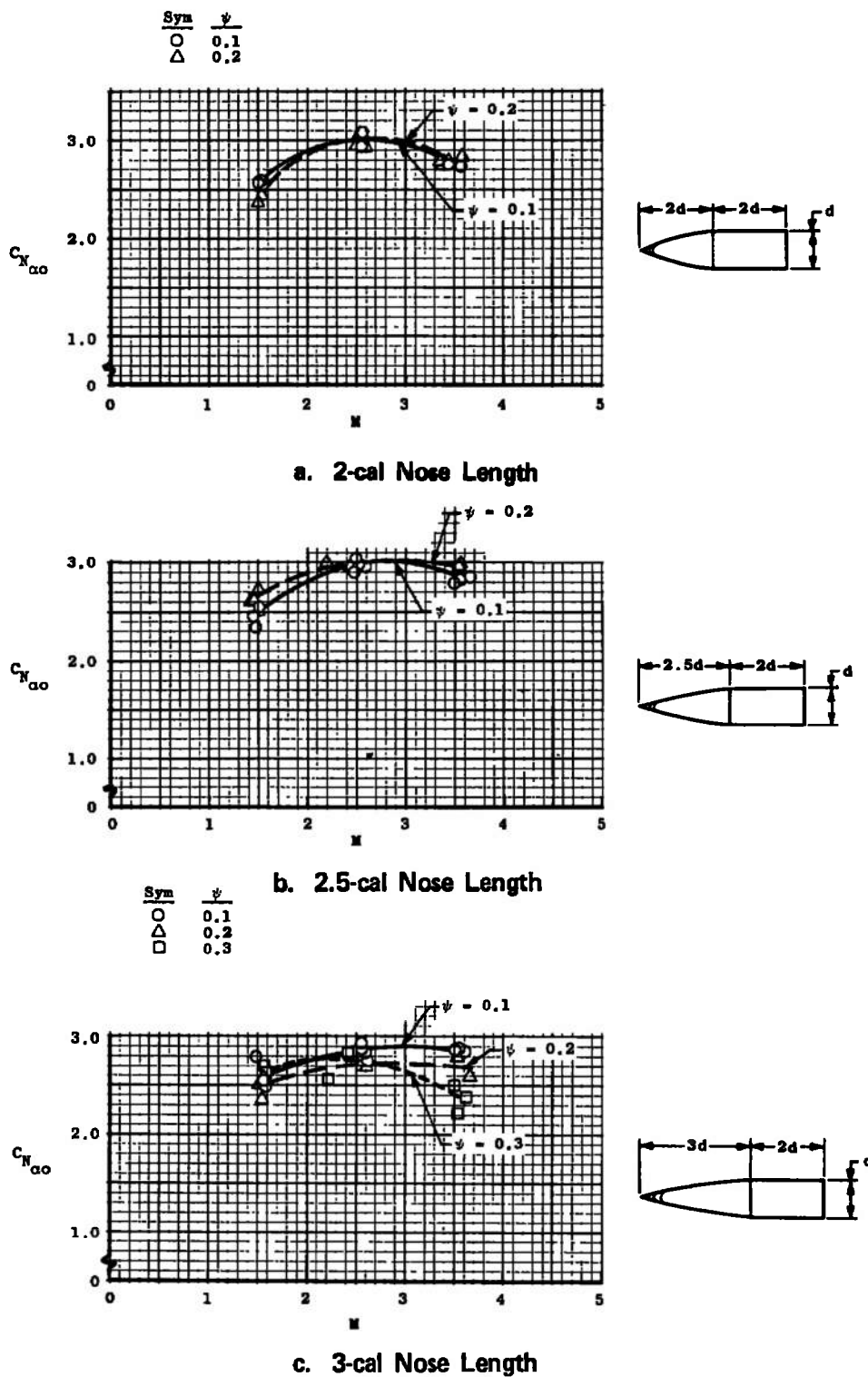
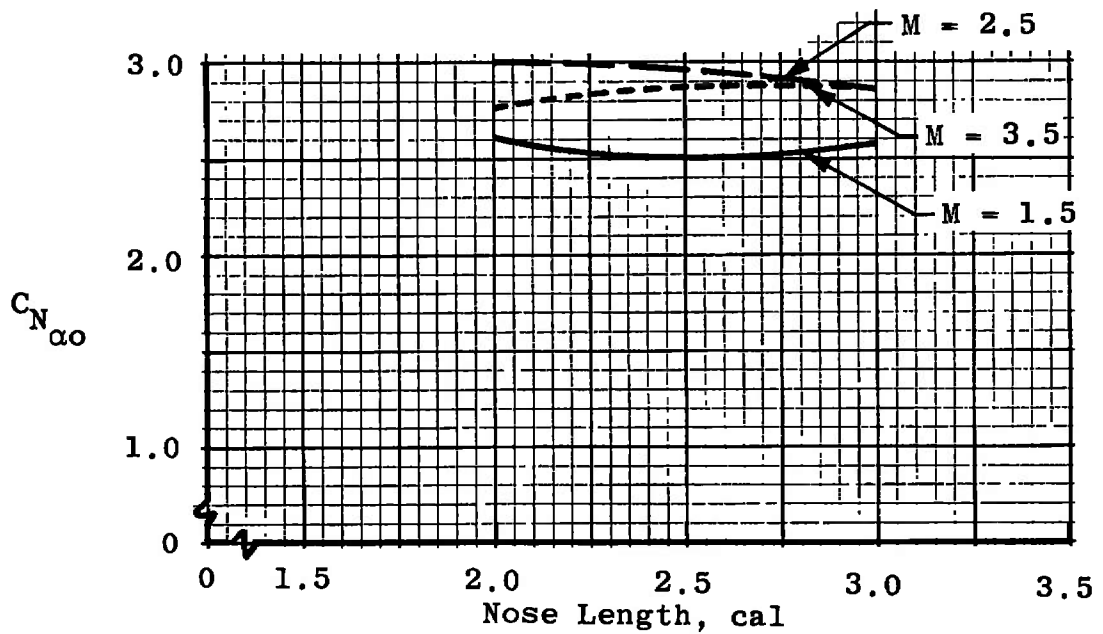
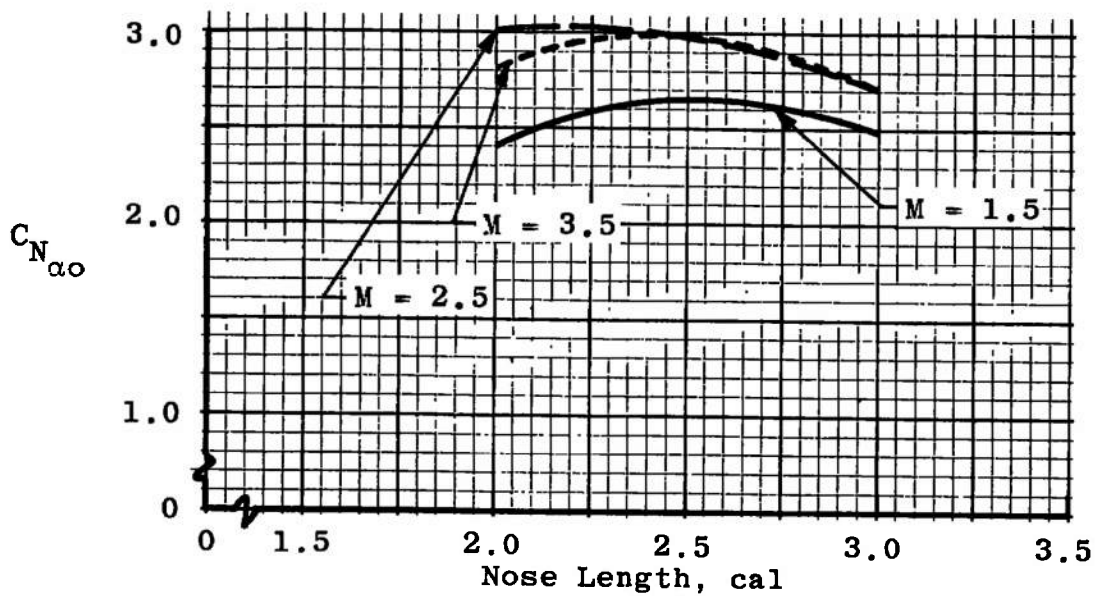


Fig. 22 Normal-Force Data at Zero Yaw Angle for Secant-Ogive-Cylinder Configurations at Ground Level

Note: Levels Obtained by Crossplotting
Data from Fig. 22



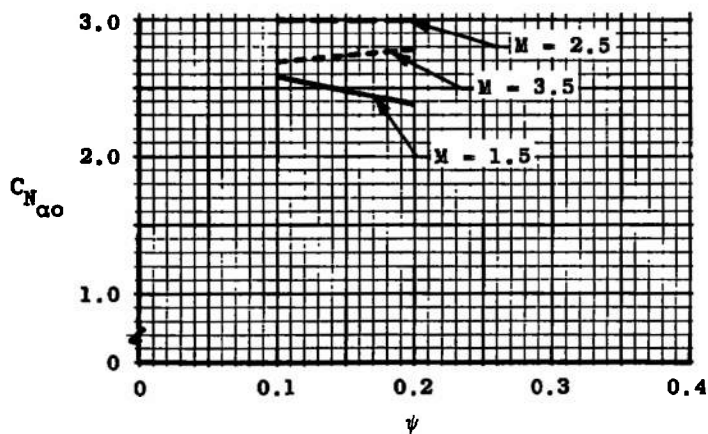
a. $\psi = 0.1$



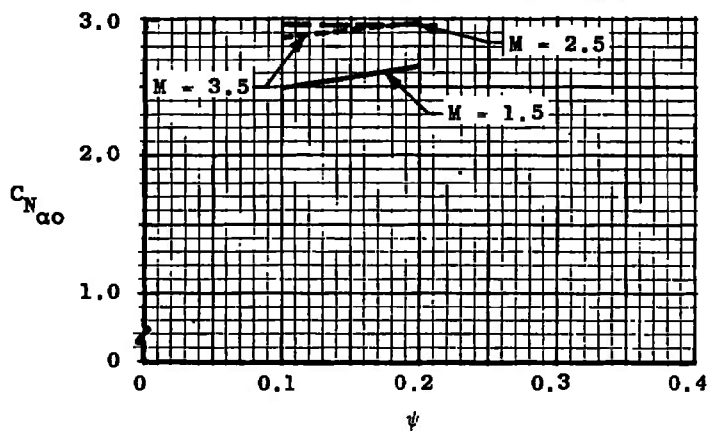
b. $\psi = 0.2$

Fig. 23 Effect of Nose Length on $C_{N_{\alpha o}}$ for Secant-Ogive-Cylinder Configurations at Ground Level

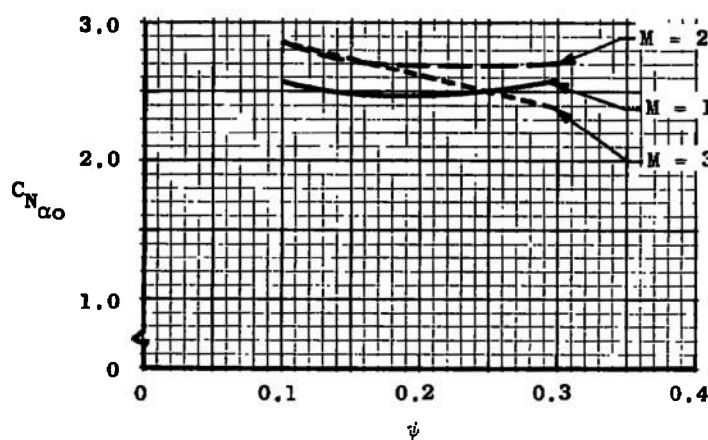
Note: Levels Obtained by Crossplotting
Data from Fig. 22



a. 2-cal Nose Length

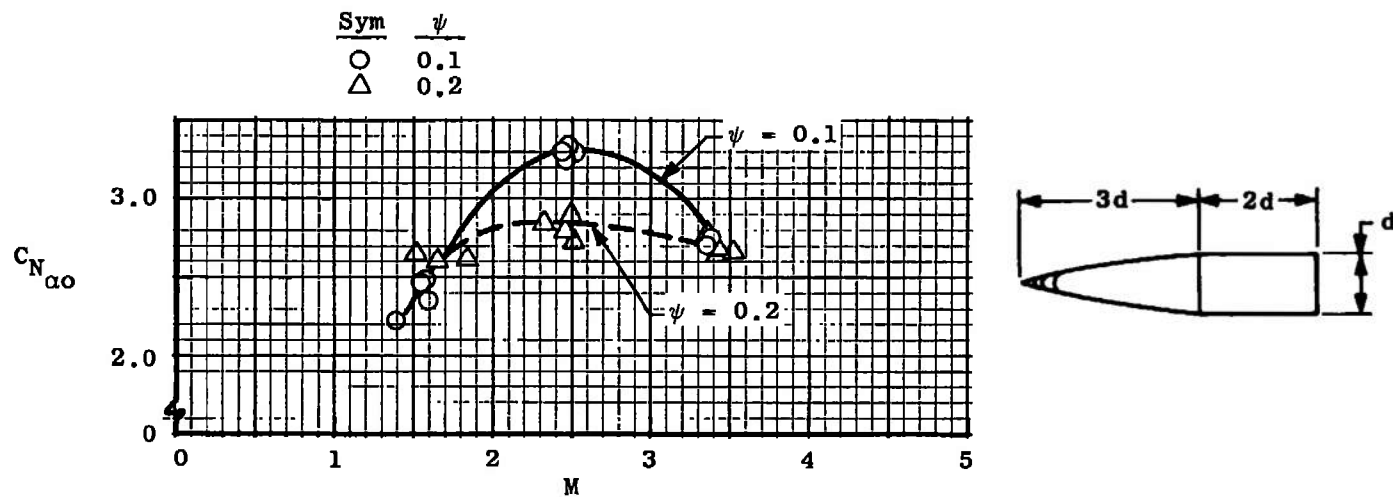


b. 2.5-cal Nose Length

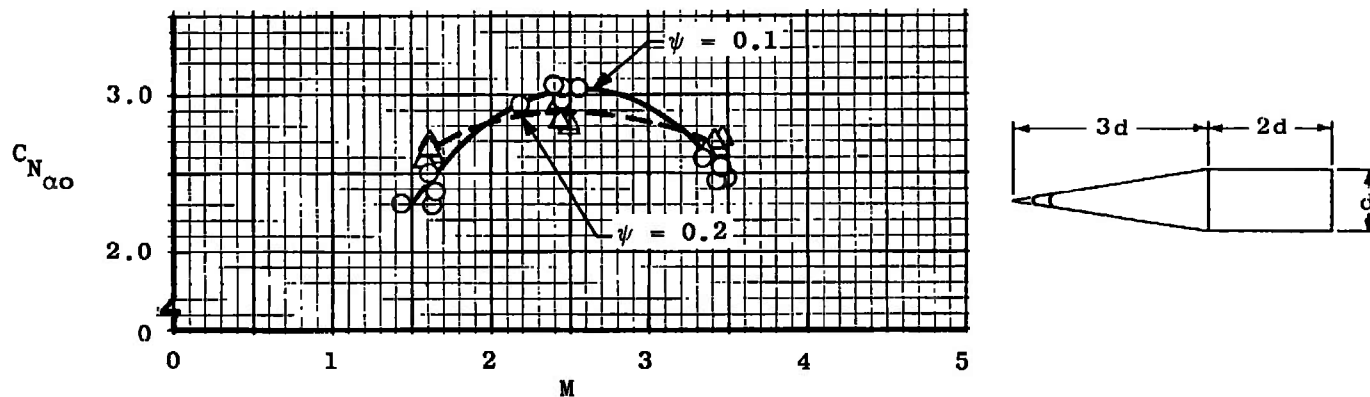


c. 3-cal Nose Length

Fig. 24 Effect of Nose Bluntness on $C_{N_{\alpha 0}}$ for Secant-Ogive-Cylinder Configurations at Ground Level



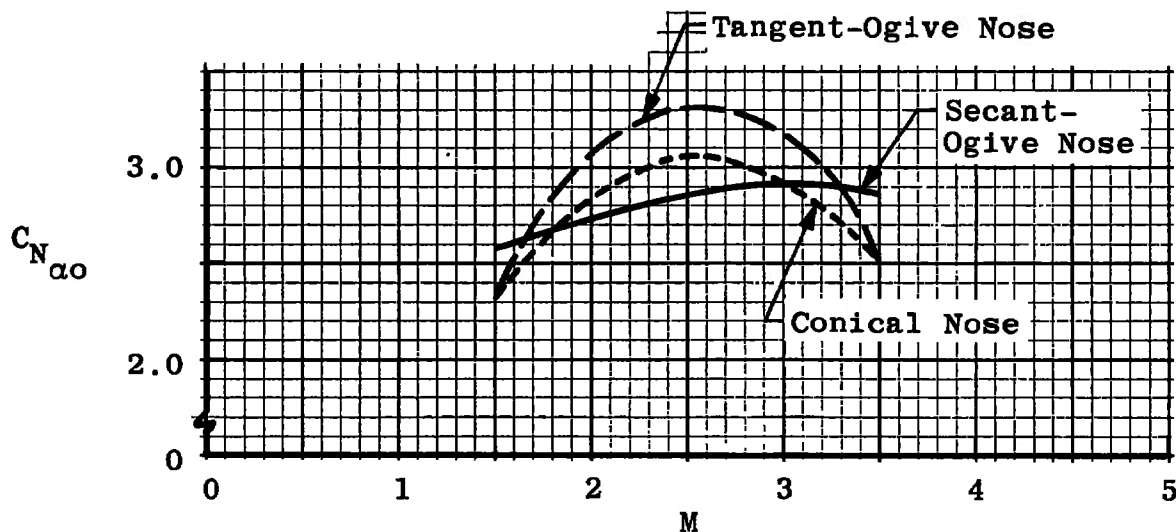
a. Tangent-Ogive Nose



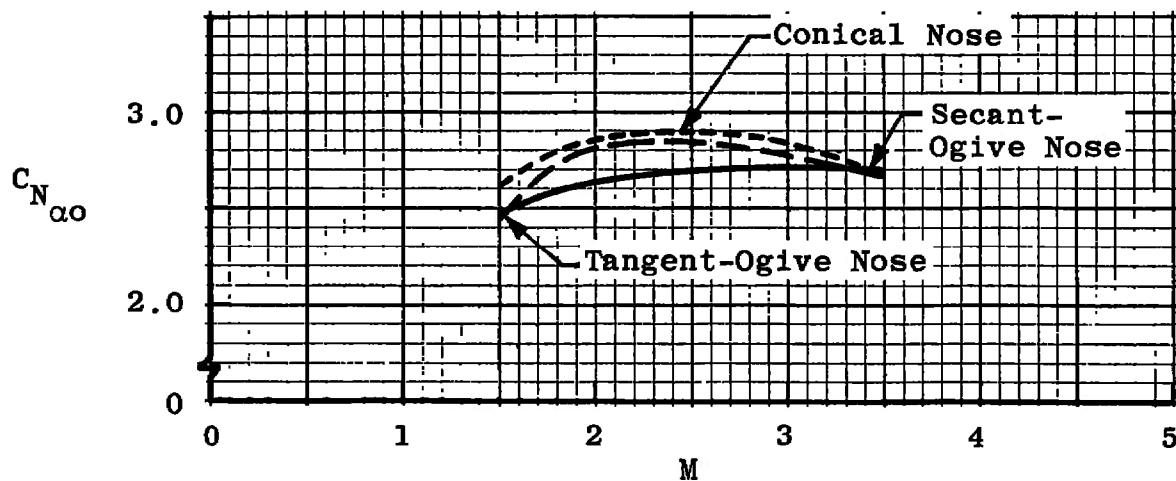
b. Conical Nose

Fig. 25 Normal-Force Data at Zero Yaw Angle for Tangent-Ogive- and Cone-Cylinder Configurations at Ground Level

Note: Levels Obtained by Crossplotting
Data from Figs. 22c and 25



a. $\psi = 0.1$



b. $\psi = 0.2$

Fig. 26 Comparison of Levels of $C_{N_{\alpha_0}}$ for 3-cal Nose Configurations
at Ground Level

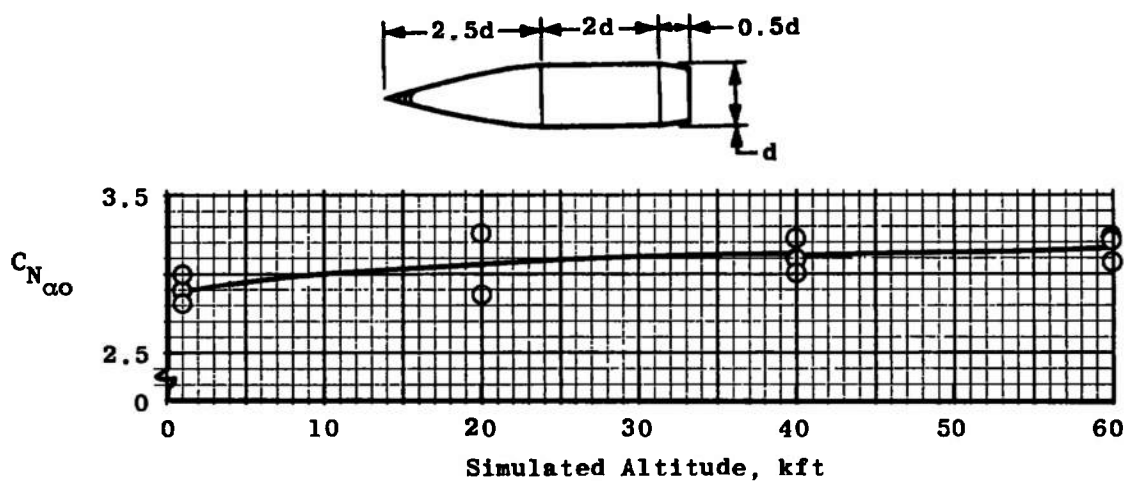
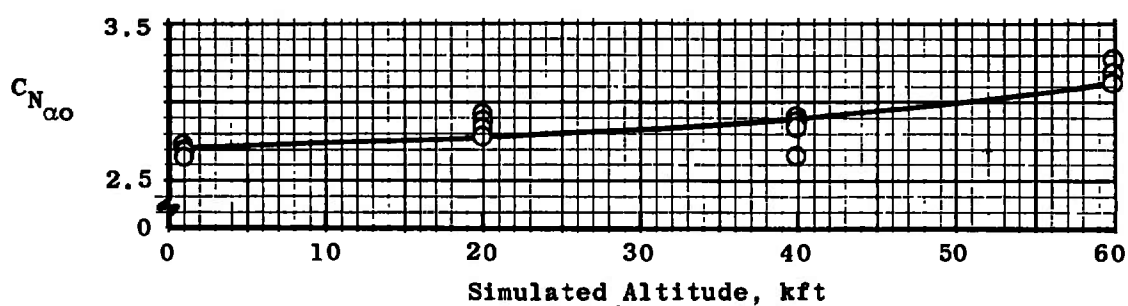
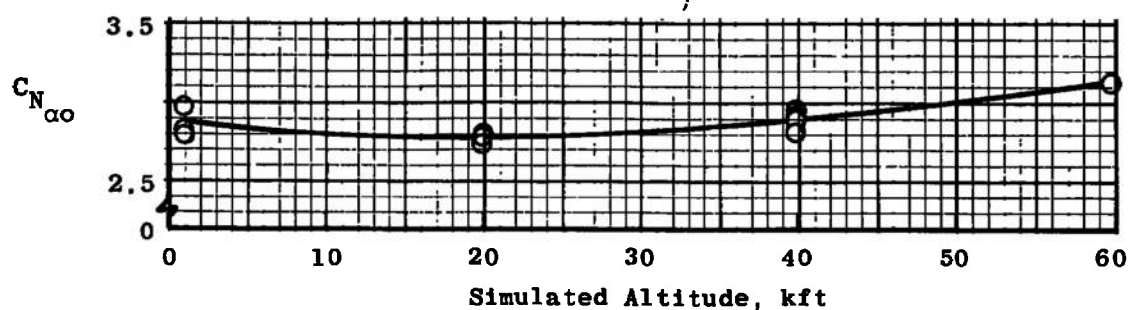
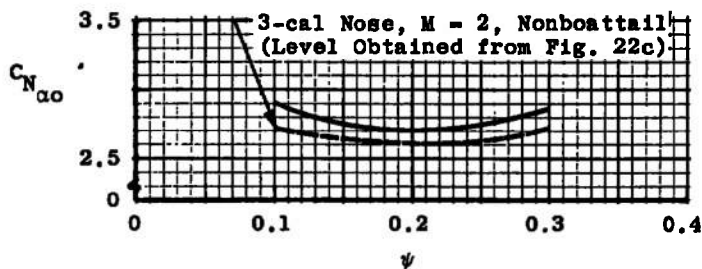
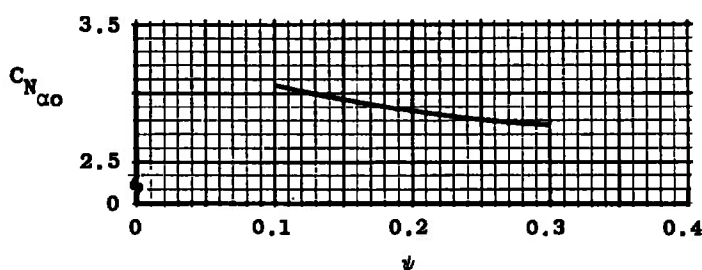
a. $\psi = 0.1$ b. $\psi = 0.2$ c. $\psi = 0.3$

Fig. 27 Normal-Force Data at $M = 2$ and Zero Yaw Angle for Secant-Ogive-Cylinder Configurations with Boattail

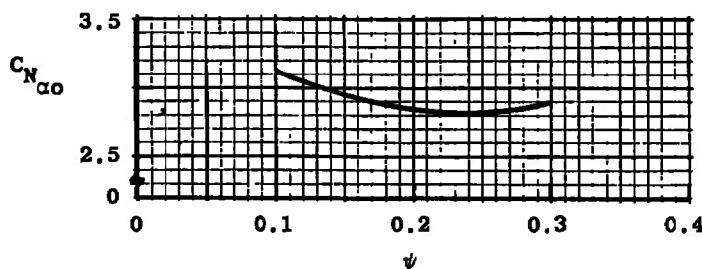
Note: Levels Obtained by Crossplotting Data from Figs. 22b and 27.



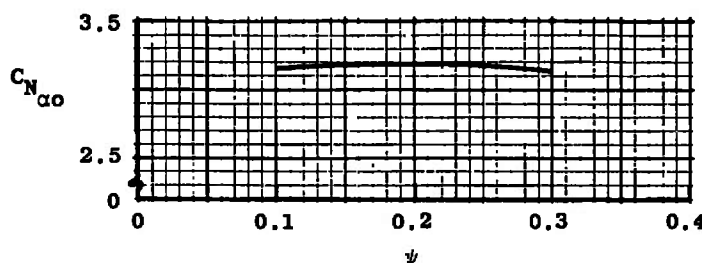
a. Ground Level



b. Simulated Altitude of 20 kft

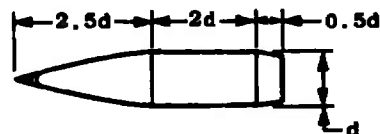


c. Simulated Altitude of 40 kft



d. Simulated Altitude of 60 kft

Fig. 28 Effect of Nose Bluntness on $C_{N_{\alpha_0}}$ at $M = 2$ for Secant-Ogive-Cylinder Configurations with Boattail



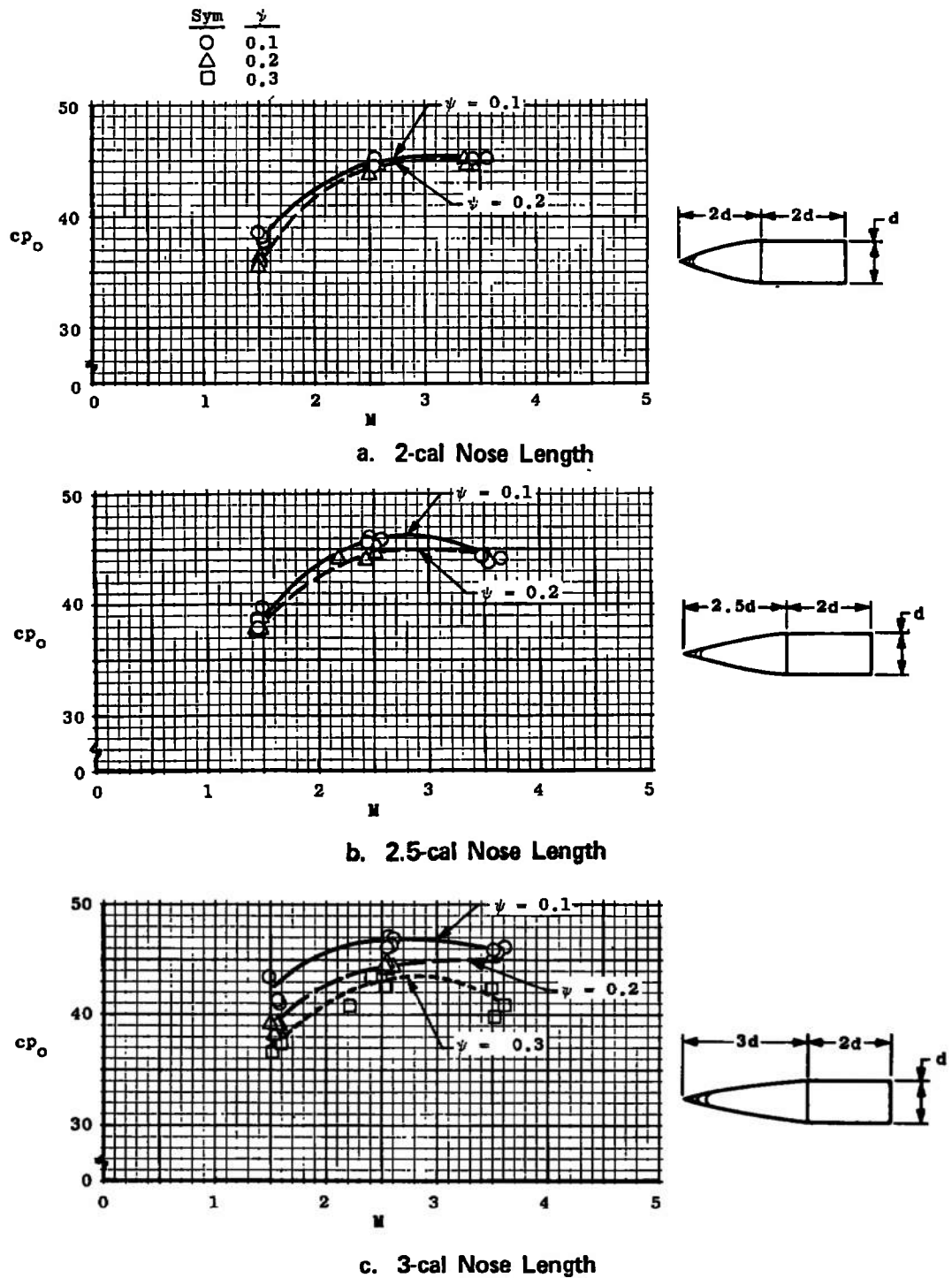


Fig. 29 Center-of-Pressure Data for Secant-Ogive-Cylinder Configurations at Ground Level (Zero Yaw Angle)

Note: Levels Obtained by Crossplotting
Data from Fig. 29

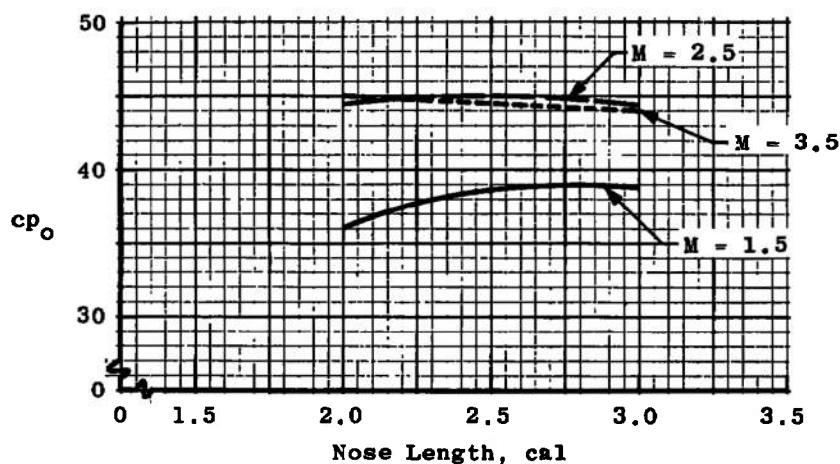
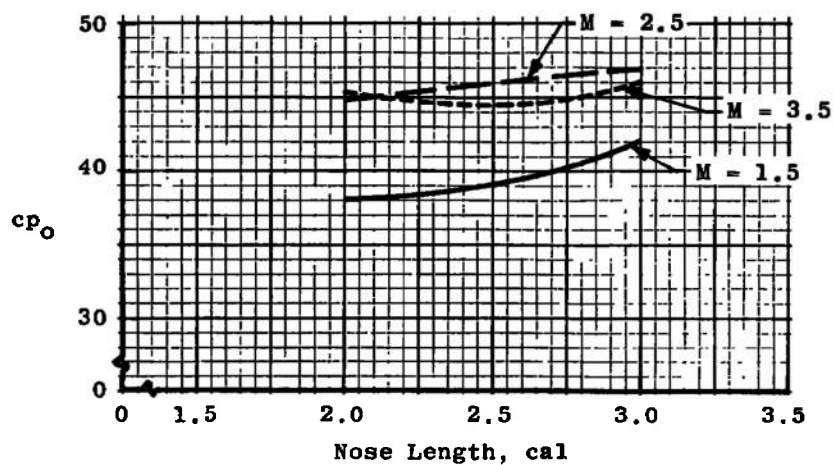


Fig. 30 Effect of Nose Length on cp_o for Secant-Ogive-Cylinder Configurations at Ground Level

Note: Levels Obtained by Crossplotting
Data from Fig. 29

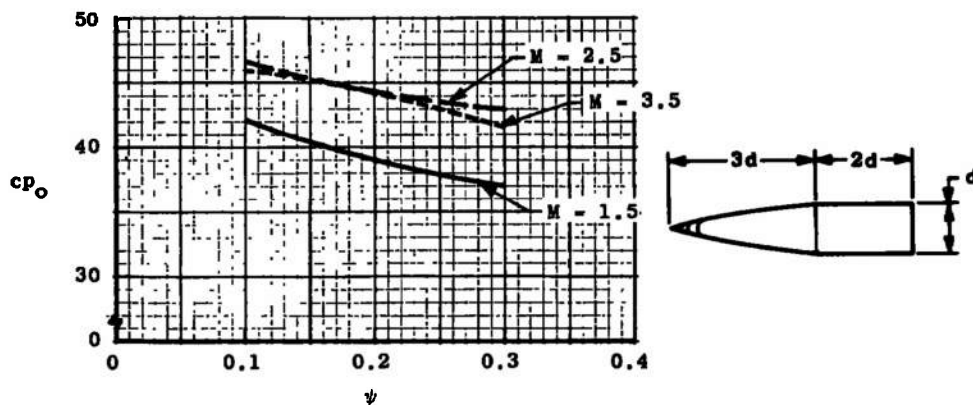
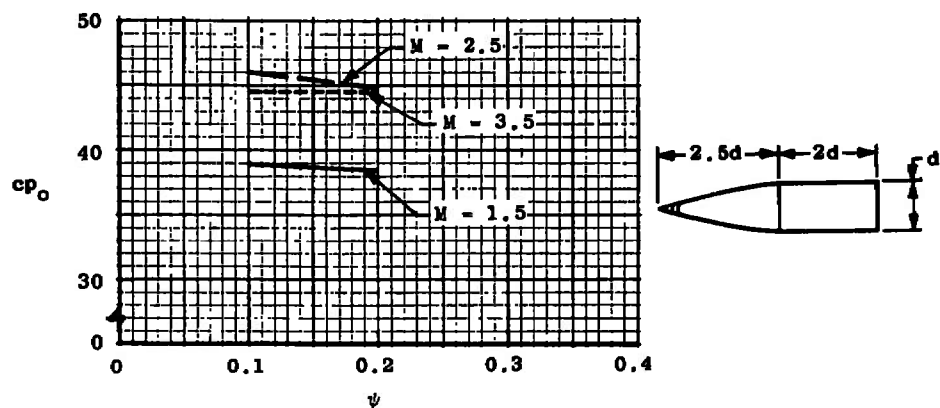
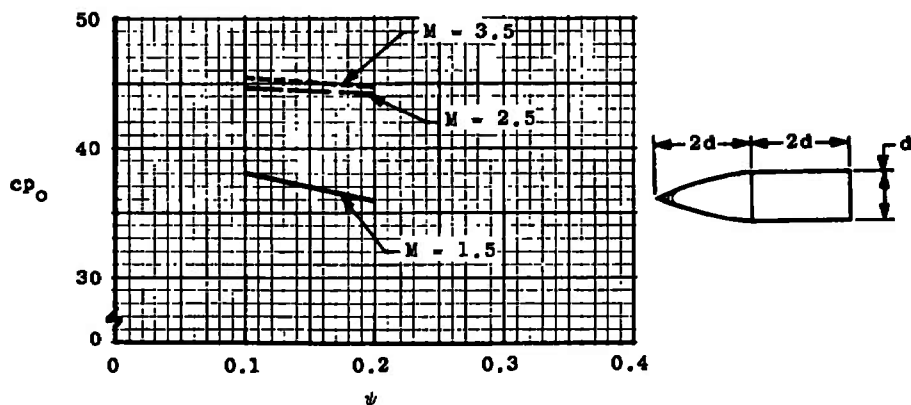
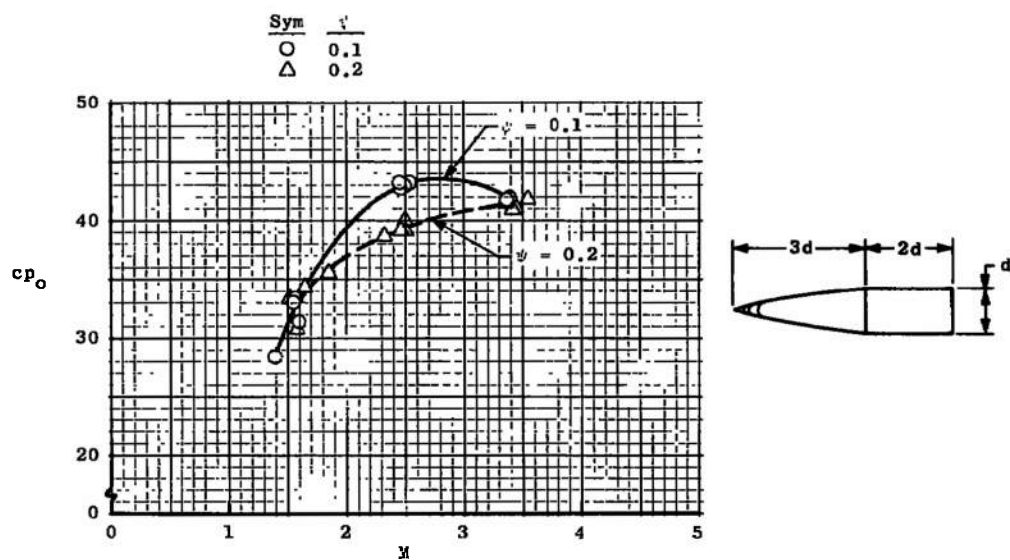
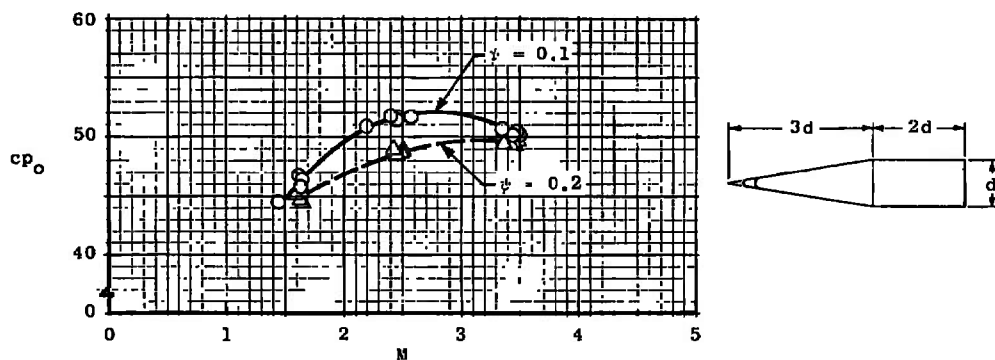


Fig. 31 Effect of Nose Bluntness on cp_o for Secant-Ogive-Cylinder Configurations at Ground Level



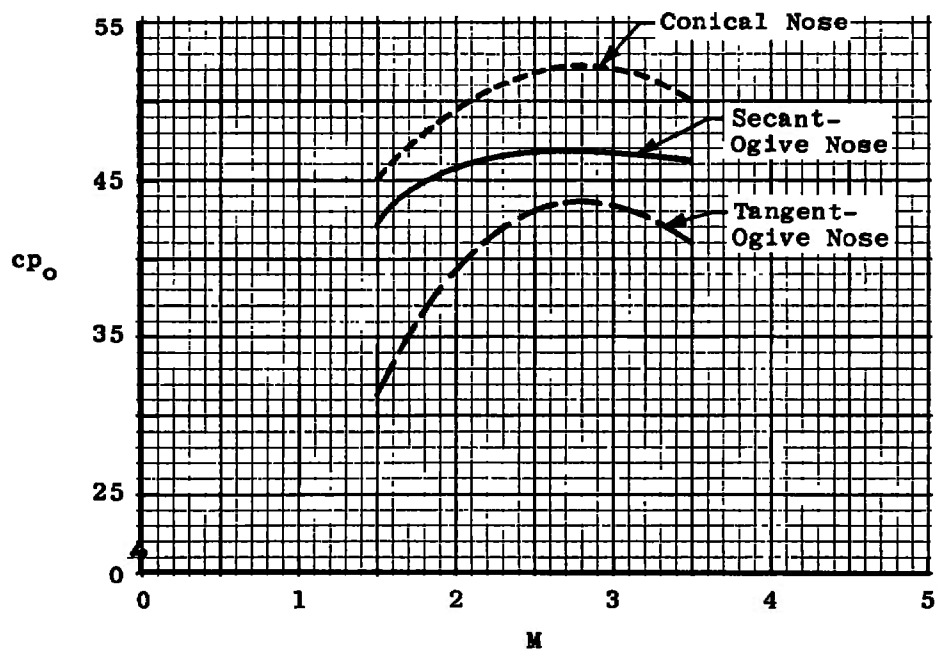
a. Tangent-Ogive Nose



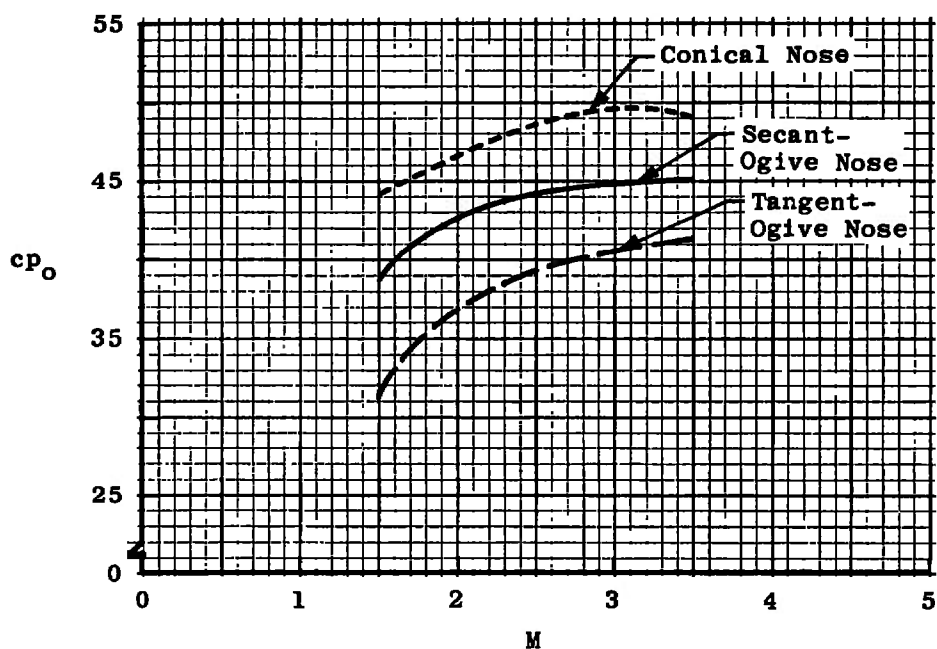
b. Conical Nose

Fig. 32 Center-of-Pressure Data for Tangent-Ogive- and Cone-Cylinder Configurations at Ground Level (Zero Yaw Angle)

Note: Levels Obtained by Crossplotting
Data from Figs. 29c and 32



a. $\psi = 0.1$



b. $\psi = 0.2$

Fig. 33 Comparison of Levels of cp_o for 3-cal Nose Configurations at Ground Level

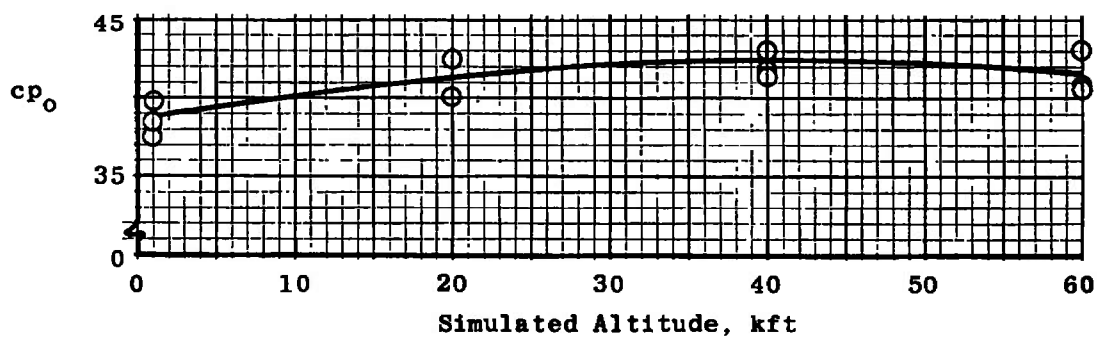
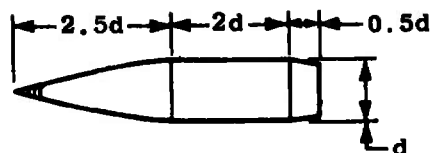
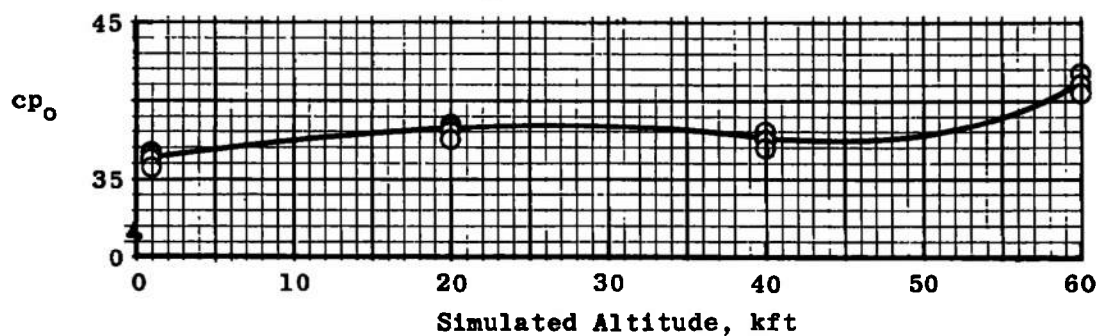
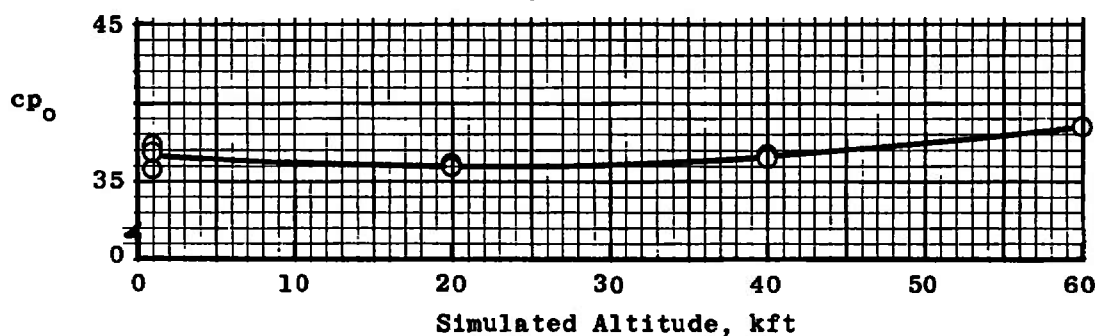
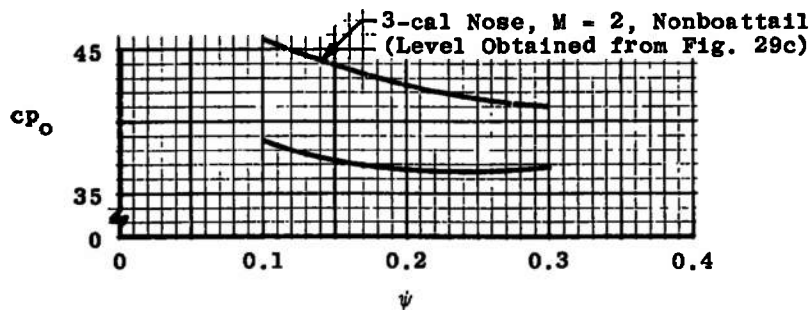
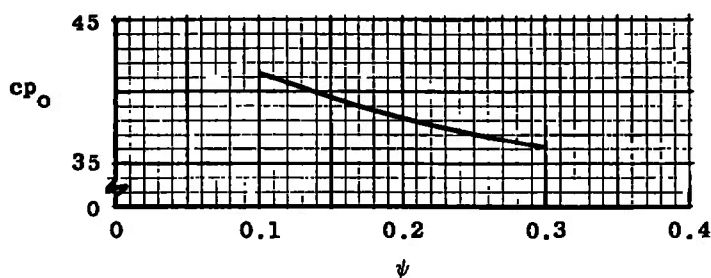
a, $\psi = 0.1$ b, $\psi = 0.2$ c, $\psi = 0.3$

Fig. 34 Center-of-Pressure Data at $M \approx 2$ for Secant-Ogive-Cylinder Configurations with Boattail (Zero Yaw Angle)

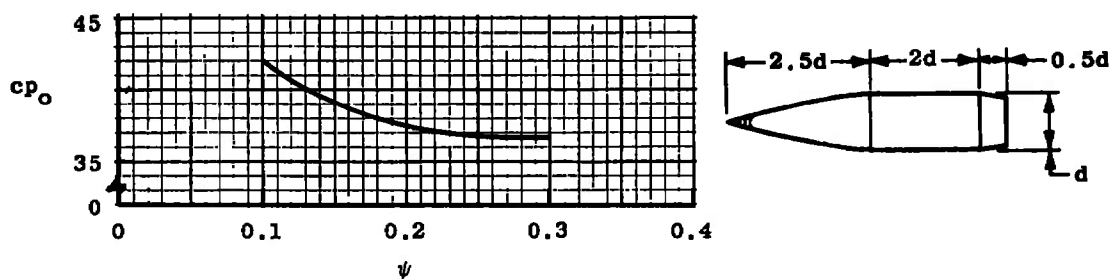
Note: Levels Obtained by Crossplotting
Data from Figs. 29b and 34



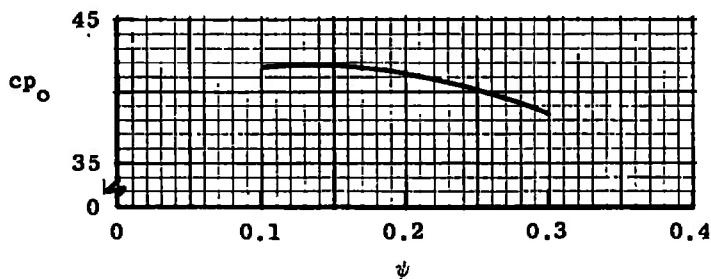
a. Ground Level



b. Simulated Altitude of 20 kft



c. Simulated Altitude of 40 kft



d. Simulated Altitude of 60 kft

Fig. 35 Effect of Nose Bluntness on cp_o at $M = 2$ for Secant-Ogive-Cylinder Configurations with Boattail

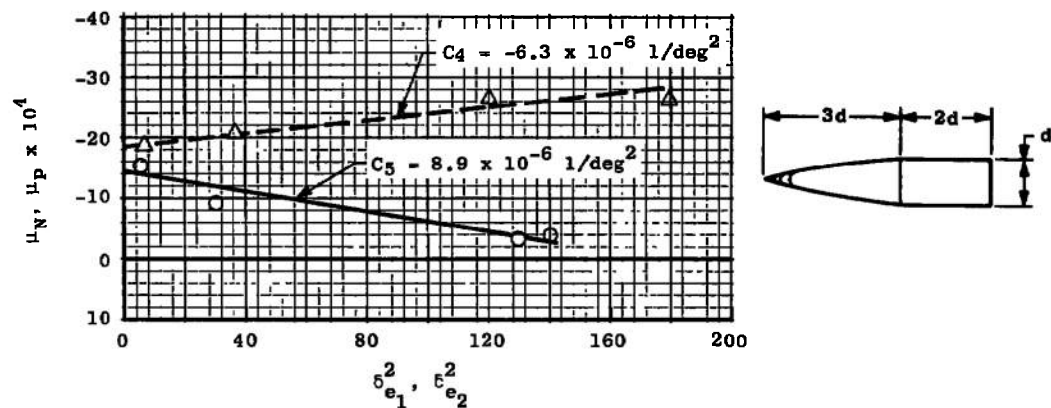
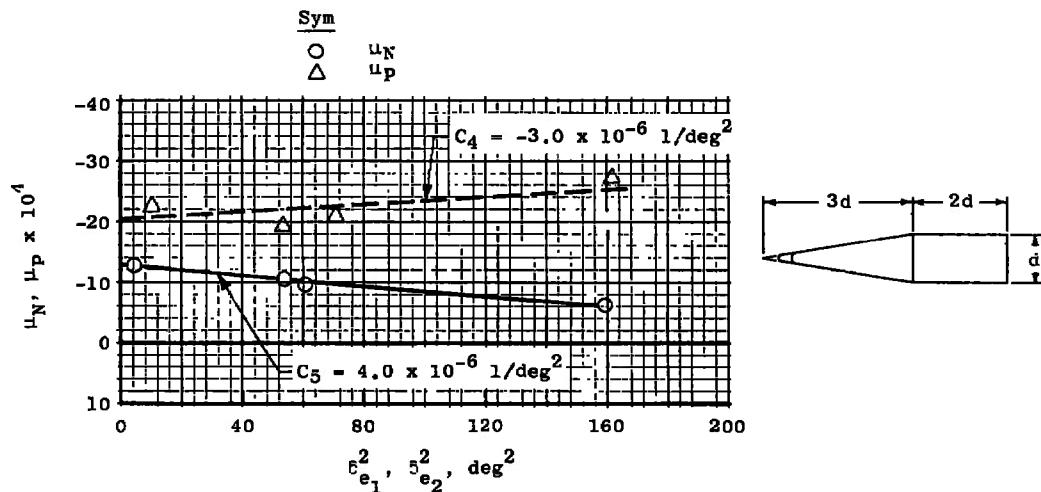


Fig. 36 Representative Amplitude Effects on Nutational and Precessional Damping Rates of Typical Ogive- and Cone-Cylinder Configurations at Ground Level

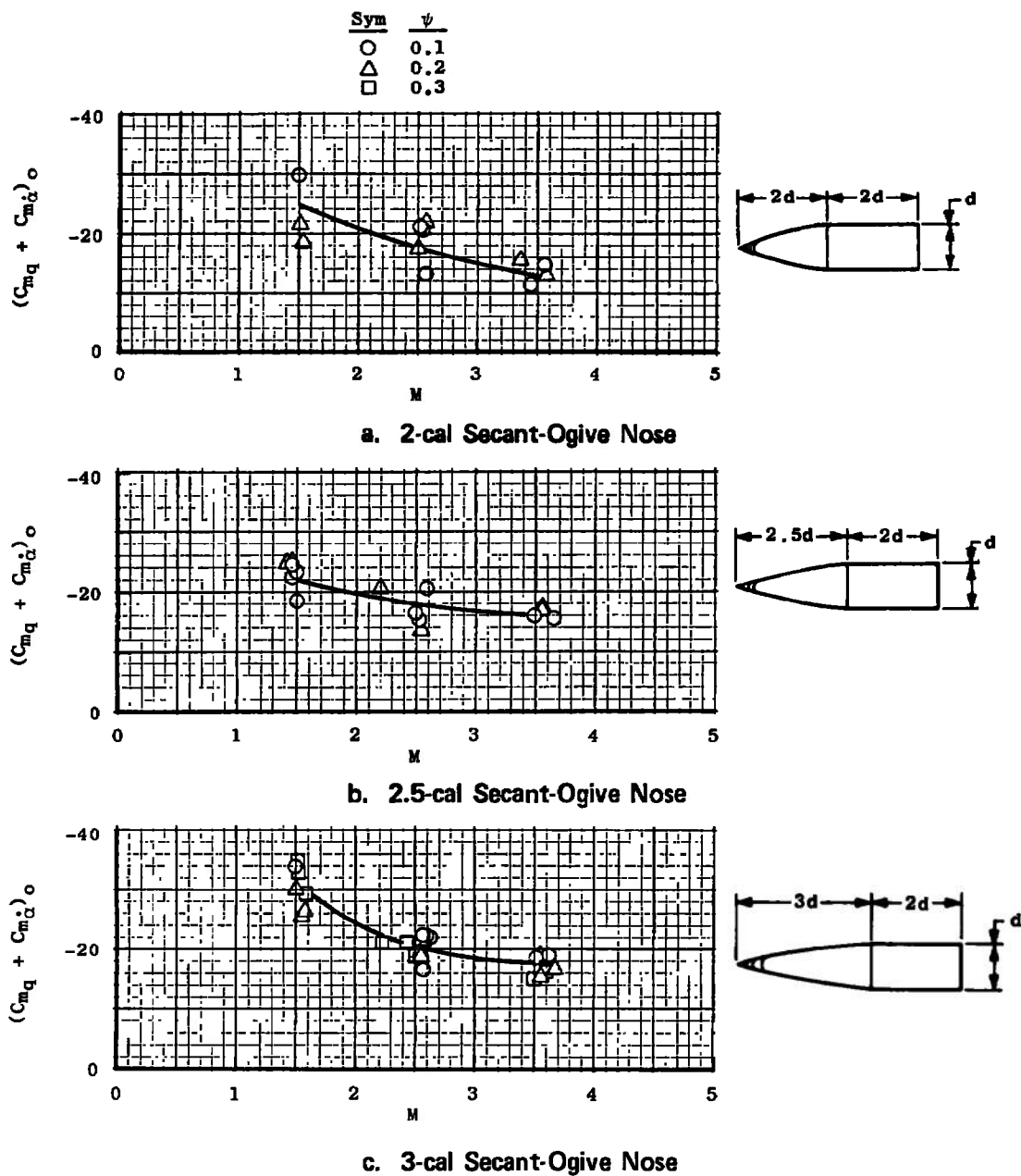
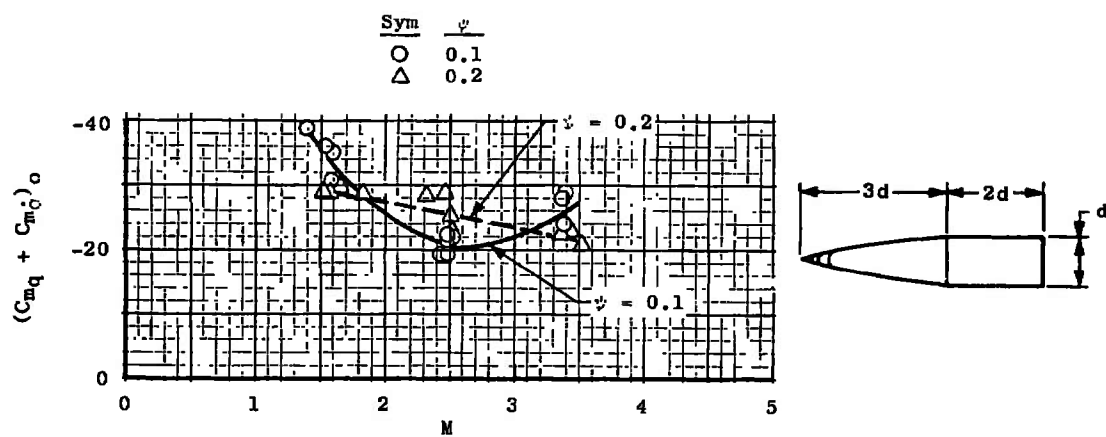
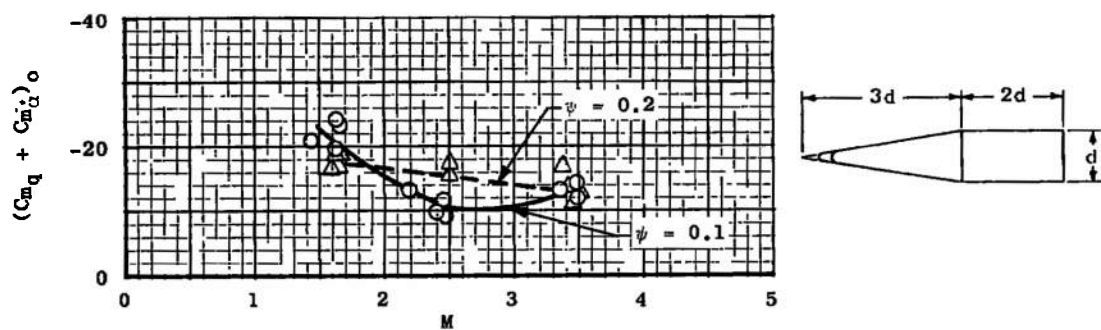


Fig. 37 Damping-in-Pitch Derivatives for Ogive- and Cone-Cylinder Configurations at Ground Level (Zero Yaw Angle)



d. 3-cal Tangent-Ogve Nose



e. 3-cal Conical Nose
Fig. 37 Concluded

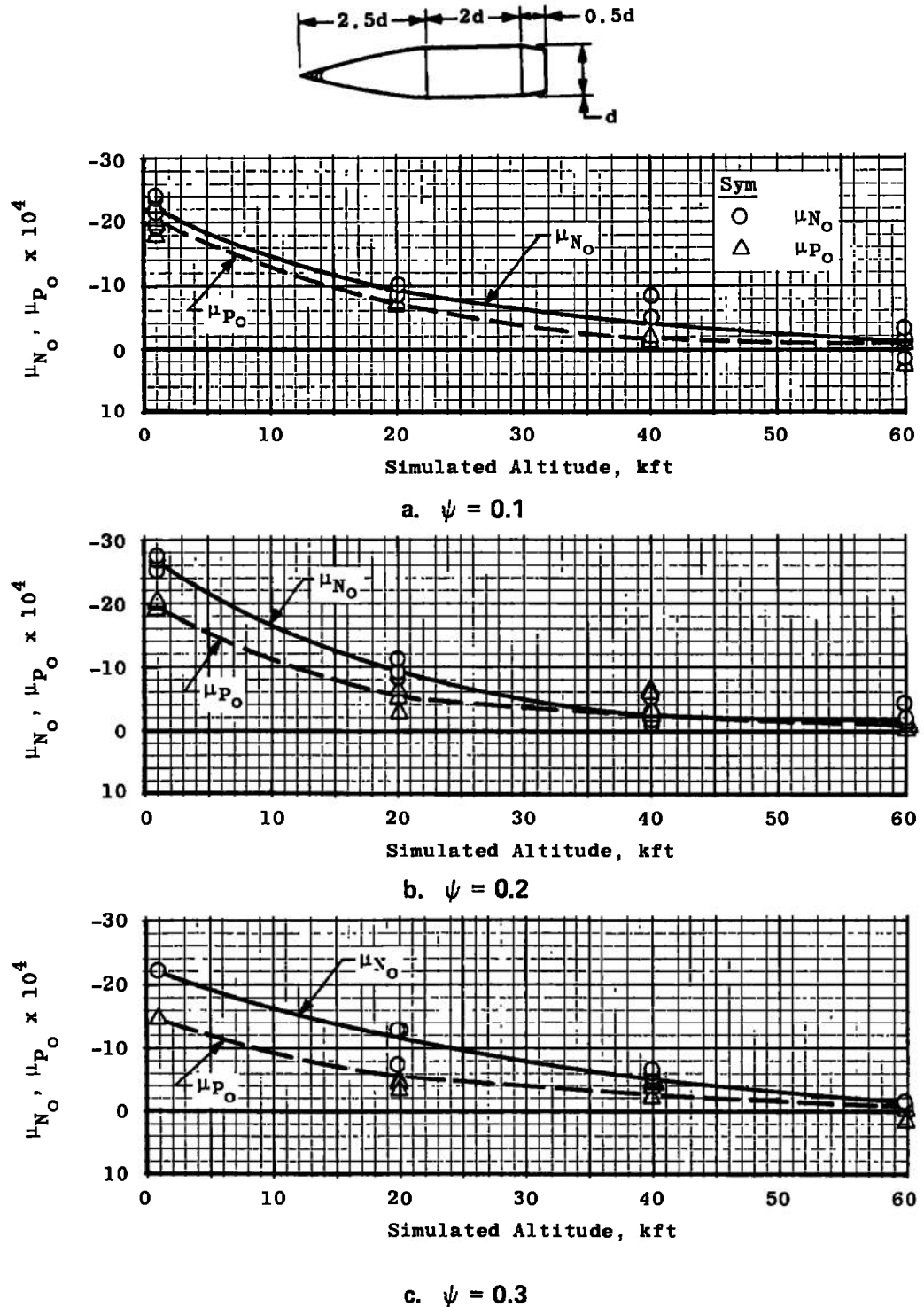


Fig. 38 Effect of Altitude on Nutational and Precessional Damping Rates for Secant-Ogive-Cylinder Configurations with Boattail (Zero Yaw Angle)

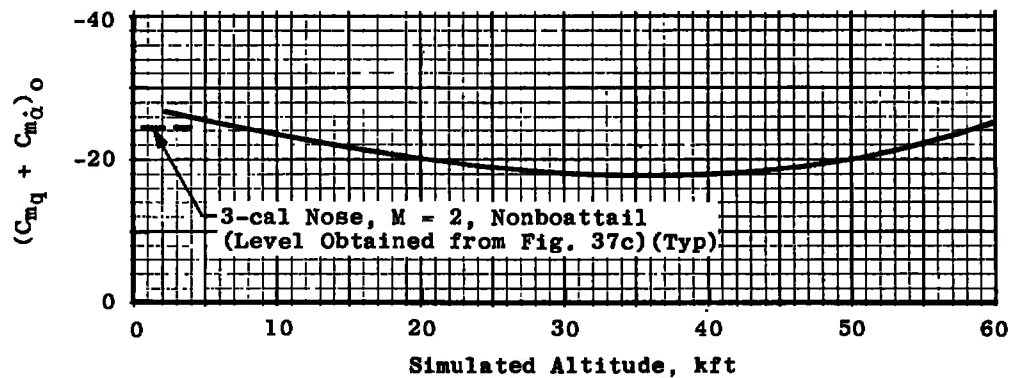
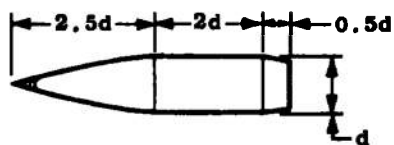
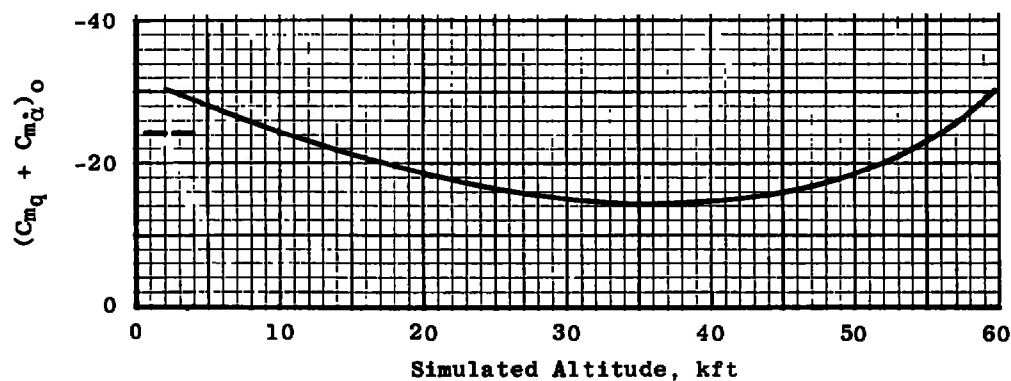
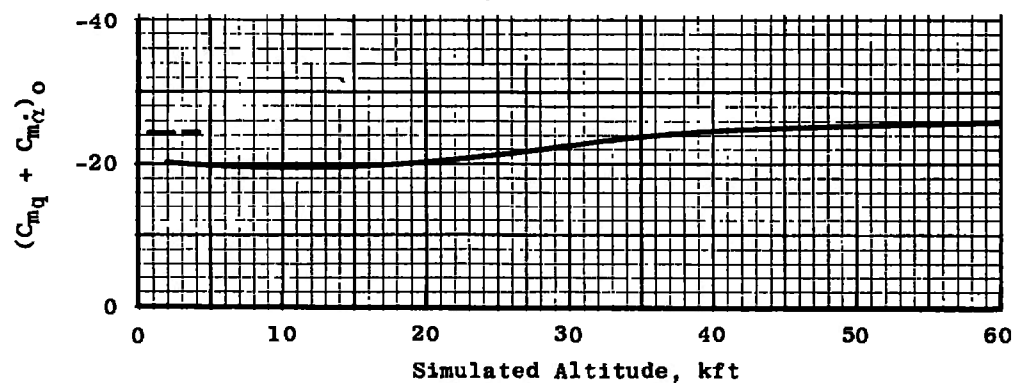
a. $\psi = 0.1$ b. $\psi = 0.2$ c. $\psi = 0.3$

Fig. 39 Damping-in-Pitch Derivatives at $M = 2$ for Secant-Ogive-Cylinder Configurations with Boattail (Zero Yaw Angle)

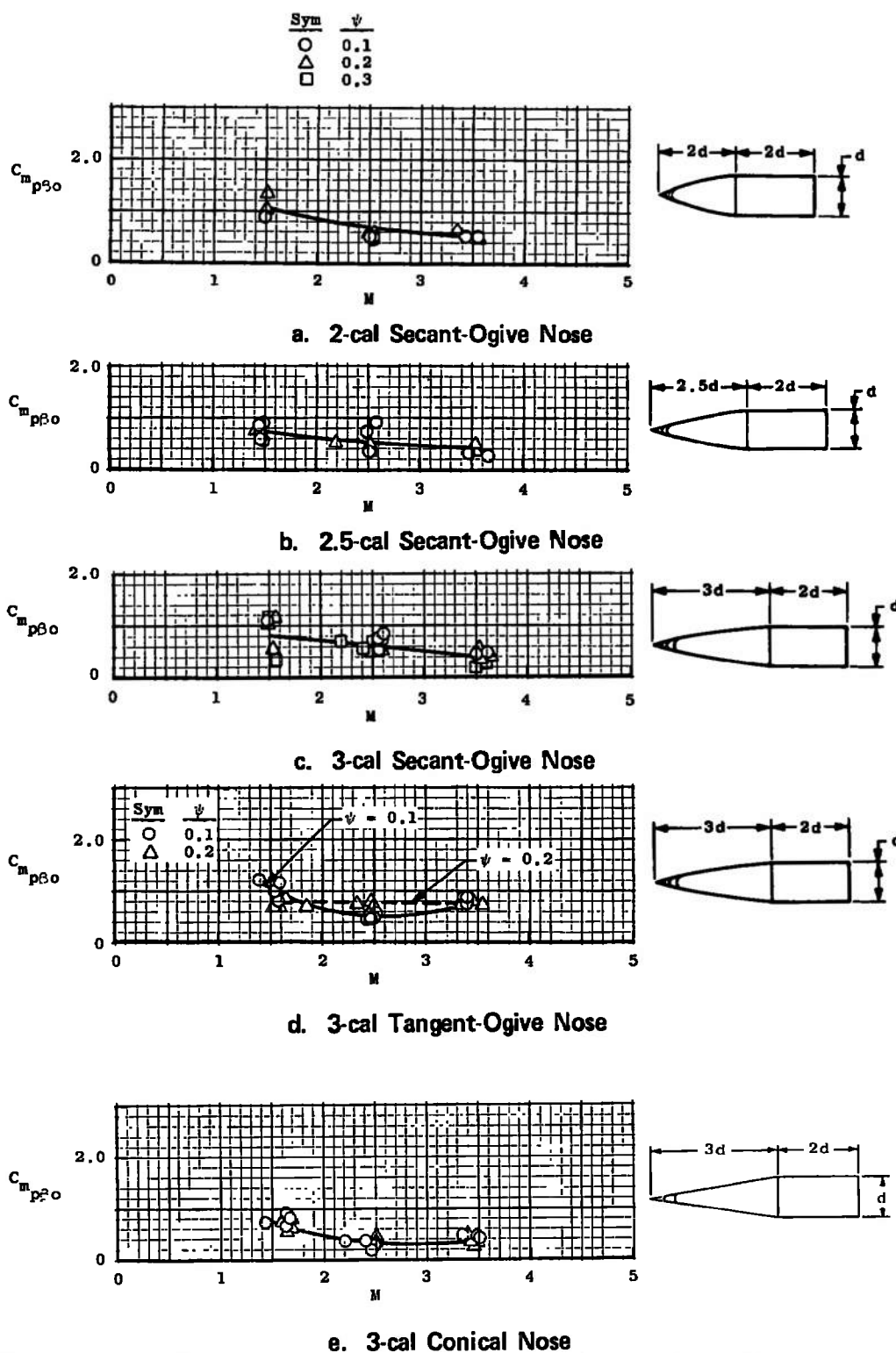
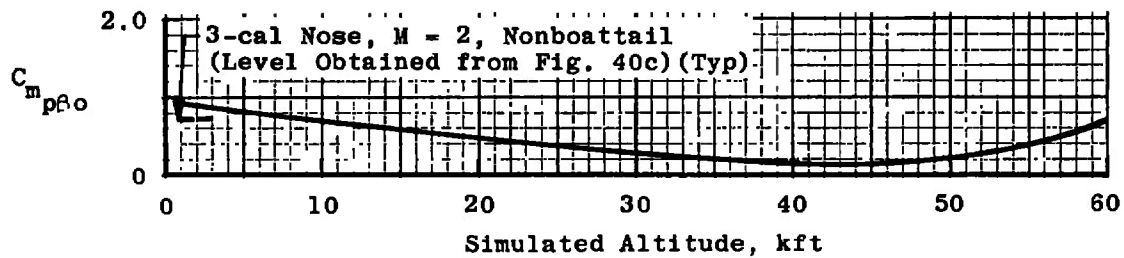
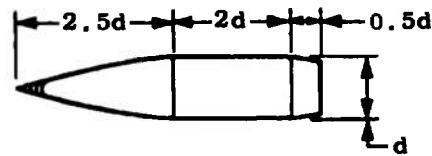
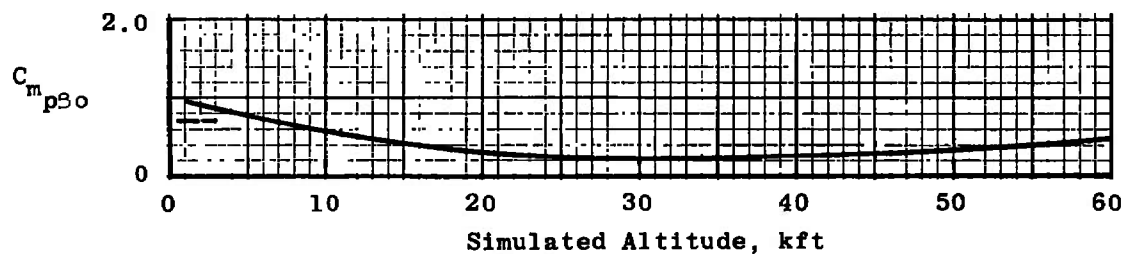


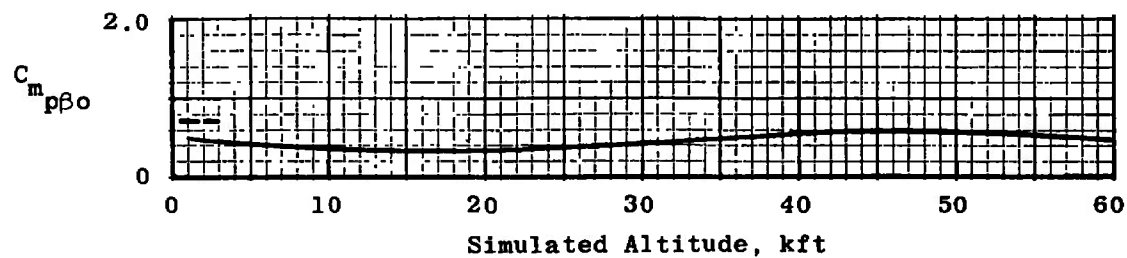
Fig. 40 Magnus-Moment Derivatives for Ogive- and Cone-Cylinder Configurations at Ground Level (Zero Yaw Angle)



a. $\psi = 0.1$

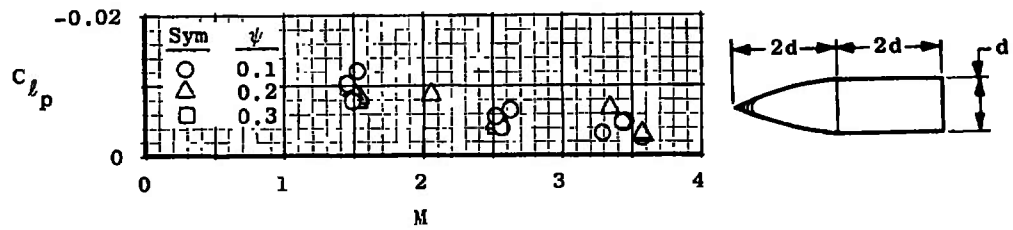


b. $\psi = 0.2$

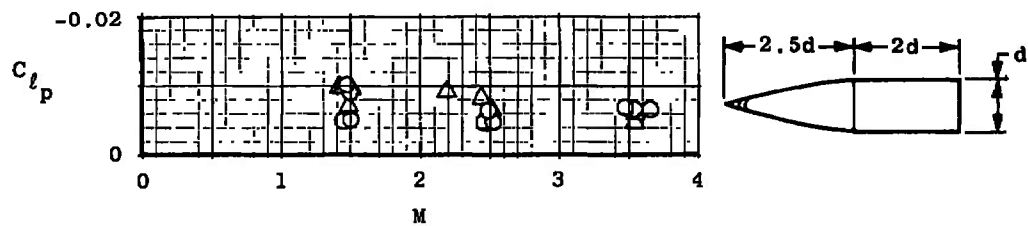


c. $\psi = 0.3$

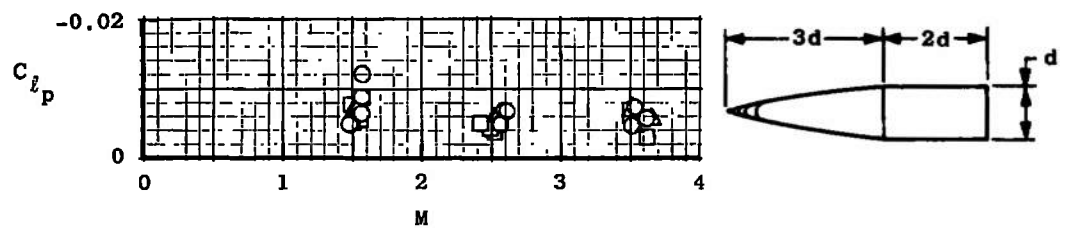
Fig. 41 Magnus-Moment Derivatives at $M = 2$ for Secant-Ogive-Cylinder Configurations with Boattail (Zero Yaw Angle)



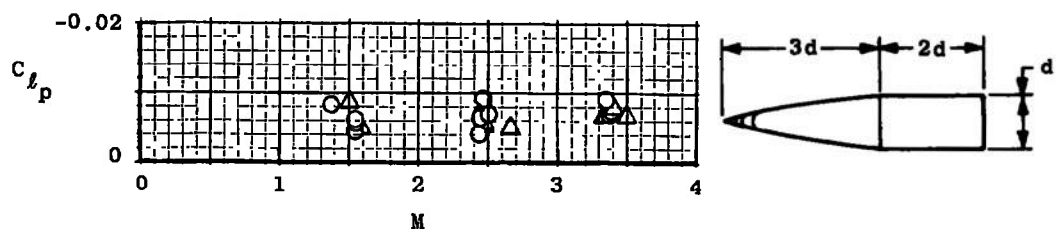
a. 2-cal Secant-Ogive Nose



b. 2.5-cal Secant-Ogive Nose

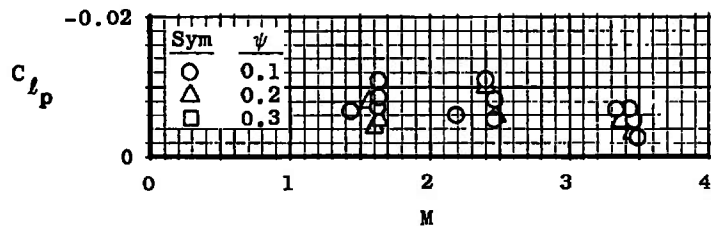


c. 3-cal Secant-Ogive Nose



d. 3-cal Tangent-Ogive Nose

Fig. 42 Roll Damping for the Ogive- and Cone-Cylinder Configurations



e. 3-cal Conical Nose

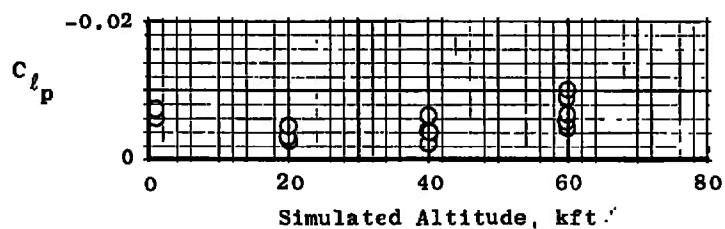
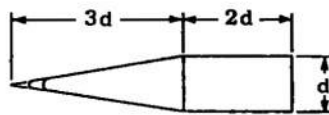
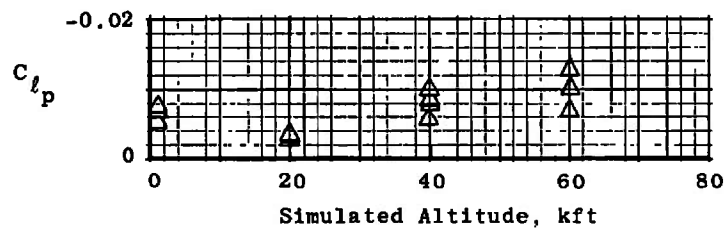
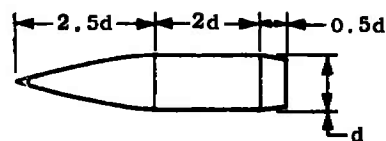
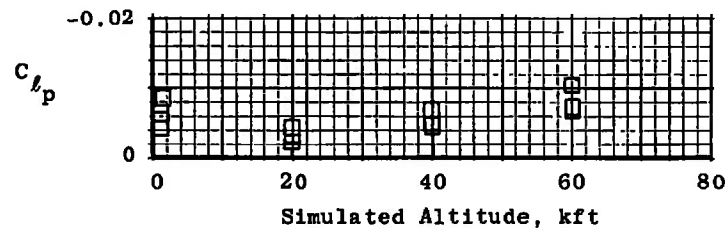
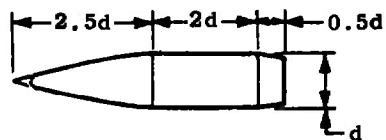
f. Boattail Configuration ($\psi = 0.1$)g. Boattail Configuration ($\psi = 0.2$)h. Boattail Configuration ($\psi = 0.3$)

Fig. 42 Concluded

TABLE I
NOMINAL PHYSICAL PROPERTIES OF THE PROJECTILES

Model* Nomenclature	Model Configuration		L, in.	m, gm	cg **	$I_y \times 10^4$, in.-lb-sec ²	$I_x \times 10^4$, in.-lb-sec ²
	Nose Length, cal	ϕ					
1V	2	0.1	3.078 ±0.004	136.3 ±0.5	91.62 ±0.05	4.08 ±0.11	0.551 ±0.003
1T		0.1	3.080 ±0.001	77.7 ±0.5	61.72 ±0.04	2.27 ±0.02	0.312 ±0.002
2V		0.2	2.593 ±0.031	135.9 ±0.3	60.69 ±0.06	3.96 ±0.06	0.548 ±0.003
2T		0.2	3.090 ±0.001	77.4 ±0.2	60.85 ±0.05	2.23 ±0.02	0.314 ±0.002
3VM	2, 5	0.1	3.442 ±0.008	154.3 ±0.7	60.34 ±0.09	6.41 ±0.09	0.388 ±0.009
3TS		0.1	3.443 ±0.003	89.6 ±0.4	59.92 ±0.04	4.34 ±0.02	0.361 ±0.003
4VM		0.2	3.337 ±0.005	153.5 ±0.7	59.26 ±0.07	6.35 ±0.07	0.591 ±0.003
4TS		0.2	3.337 ±0.001	89.5 ±0.2	58.65 ±0.08	4.31 ±0.02	0.360 ±0.002
5VM	3	0.1	3.816 ±0.002	155.5 ±1.3	61.26 ±0.26	8.30 ±0.17	0.624 ±0.005
5TS		0.1	3.788 ±0.002	93.8 ±0.2	61.42 ±0.05	5.25 ±0.02	0.376 ±0.002
6VM		0.2	3.678 ±0.003	164.8 ±1.5	60.15 ±0.20	9.08 ±0.12	0.621 ±0.004
6TS		0.2	3.659 ±0.001	93.9 ±0.2	60.14 ±0.04	5.22 ±0.02	0.374 ±0.002
7VM		0.3	3.556 ±0.003	164.4 ±0.8	59.08 ±0.48	7.86 ±0.16	0.623 ±0.003
7TS		0.3	3.528 ±0.011	93.7 ±0.5	58.75 ±0.08	5.13 ±0.06	0.379 ±0.002
9VF		0.1	3.843 ±0.005	192.4 ±2.1	58.64 ±0.48	9.84 ±0.20	0.596 ±0.009
8TV		0.1	3.894 ±0.05	104.1 ±0.3	58.55 ±0.01	5.59 ±0.04	0.403 ±0.000
9VF		0.2	3.751 ±0.003	182.3 ±3.2	57.78 ±0.23	9.70 ±0.27	0.693 ±0.004
9TV		0.2	3.752 ±0.001	104.8 ±1.6	57.42 ±0.26	5.61 ±0.11	0.401 ±0.009
10VM		0.1	3.735 ±0.032	172.2 ±0.4	60.77 ±0.60	7.72 ±0.02	0.594 ±0.003
10VF		0.1	3.735 ±0.032	171.3 ±0.5	60.29 ±0.09	7.80 ±0.03	0.596 ±0.001
10TF		0.1	3.731 ±0.002	95.5 ±0.3	59.09 ±0.06	5.04 ±0.00	0.326 ±0.001
11VM		0.2	3.557 ±0.029	171.9 ±0.5	58.26 ±0.21	7.62 ±0.01	0.597 ±0.000
11VF		0.2	3.557 ±0.029	171.7 ±0.9	59.32 ±0.05	7.73 ±0.01	0.594 ±0.000
11TF		0.2	3.567 ±0.009	95.2 ±0.7	57.59 ±0.09	4.93 ±0.05	0.328 ±0.003
12V†	2, 5	0.1	3.843 ±0.017	167.6 ±0.9	61.15 ±0.17	7.42 ±0.04	0.653 ±0.007
13V†		0.2	3.736 ±0.014	187.6 ±1.1	60.09 ±0.09	7.41 ±0.07	0.683 ±0.003
14VA†		0.3	3.641 ±0.011	163.5 ±0.8	60.31 ±0.31	6.59 ±0.04	0.861 ±0.005

*Letters following configuration number indicate afterbody and forebody material, respectively:

V - Viscount 44 S - 4130 steel
 F - Fansteel 50 A - Aluminum
 T - Titanium alloy M - Mallory 3000

**Percentage of projectile length from the nose

†Boattail configurations

Note: Projectile diameter (d) = 0.787 ± 0.002 in. for all projectiles.
 Physical measurements listed represent mean values of random samples ± maximum deviation from the mean values.

TABLE II-PART I
AERODYNAMIC PROPERTIES OF THE PROJECTILES

Shot No.	Model Nomenclature	M	Reg $\times 10^{-6}$	Simulated Altitude, kft	Range Pressure, mm Hg	C_D	δ^2 , deg ²	$C_1 \times 10^3$, 1/deg ²	C_{D0}	C_{m0}^*	δ_c^2 , deg ²	$C_2 \times 10^3$, 1/deg ²	C_{m00}	C_{N0}	δ_{cg}^2 , deg ²	$C_3 \times 10^3$, 1/deg ²	C_{N00}	C_{P0}^{**}	p , deg/ft	C_{Lp}
1	JV	1.44	2.47	Ground Level	742.0	0.410	0.6	1.50	0.408			0				6.0				-0.0101
2		1.50	2.55		738.1	0.435	13.8		0.414	2.15	8.8		2.15	2.62	9.7		2.56	38.5	184	-0.0078
3		1.54	2.62		740.6	0.480	48.8		0.407	2.20	52.2		2.20	2.89	52.3		2.58	38.2	184	-0.0122
4		1.55	2.64		740.9	0.478	41.5		0.414	2.21	50.4		2.21	2.87	51.3		2.56	37.8	185	
5		2.51	4.20		724.0	0.284	1.1	2.20	0.282	1.69	1.1		1.68			0			184	
6		2.54	4.21		728.7	0.208	1.6		0.204	1.85	0.8		1.85						182	-0.0058
7		2.55	4.45		735.8	0.308	10.6		0.308	1.76	7.8		1.76	2.93	8.4		2.93	44.6	184	-0.0053
8		2.56	4.36		736.0	0.286	2.1		0.281	1.78	1.8		1.78	3.09	1.8		3.09	45.2	184	-0.0039
9		2.61	4.36		724.2	0.304	8.0		0.286	1.70	11.2		1.70						180	-0.0066
10		3.28	5.60		733.8	0.219	2.3	1.00	0.217	1.55	0.4		1.55			6.0			178	-0.0030
11	1T	3.44	5.77		728.4	0.201	42.1		0.239	1.60	43.4		1.60	3.03	49.0		2.74	45.1	181	-0.0040
12		3.44	5.88		734.7	0.243	1.8		0.241	1.60	1.4		1.60						178	-0.0040
13		3.57	6.00		729.0	0.303	55.9		0.247	1.58	47.8		1.58	3.05	54.7		2.72	45.1	182	-0.0023
14	2V	1.48	2.46		740.4	0.407	1.7	2.20	0.403	2.12	1.2	0	2.12			8.0			181	-0.0083
15		1.50	2.48		735.8	0.406	1.6		0.402	2.24	1.1		2.24	2.40	1.1		2.39	35.4	182	-0.0085
16		1.51	2.50		738.2	0.428	11.8		0.400	2.30	8.7		2.30	2.64	10.2		2.55	36.3	182	-0.0081
17		1.52	2.52		739.1	0.430	12.9		0.402	2.24	11.8		2.24	2.55	12.0		2.44	35.9	172	-0.0084
18		2.05	3.39		734.0	0.342	2.6	1.50	0.338	1.09	0.5		1.88			0			188	-0.0087
19		2.50	4.15		736.0	0.309	5.4		0.301	1.81	2.8		1.81	2.84	3.0		2.84	43.8	184	-0.0048
20		2.53	4.20		738.2	0.285	1.8		0.282	1.80	0.8		1.80	3.08	0.8		3.08	44.7	184	-0.0042
21		2.56	4.10		732.4	0.288	2.1		0.285	1.88	0.8		1.86						193	-0.0056
22		2.59	4.22		723.3	0.320	15.7		0.296	1.72	14.8		1.72	2.82	15.5		2.82	44.5	178	
23	2T	3.38	5.50		728.5	0.294	14.6		0.272	1.60	3.0		1.60	2.82	4.4	7.5	2.78	45.1	100	-0.0087
24		3.38	5.58		733.1	0.201	8.8		0.266	1.63	1.9		1.63	2.75	2.0		2.74	44.4	181	-0.0065
25		3.44	5.68		732.0	0.270	14.3		0.257	1.64	15.8		1.64	2.91	16.5		2.79	44.6	162	
26		3.58	5.84		727.1	0.255	8.8		0.240	1.81	8.2		1.61	2.90	9.8		2.83	45.1	180	-0.0034
27	3VM	1.45	2.77		736.2	0.418	22.8	2.20	0.369	2.27	27.7		2.27	2.70	27.5	8.0	2.45	30.0	187	-0.0053
28		1.47	2.80		735.8	0.366	5.1		0.355	2.25	4.8		2.25	2.37	4.8		2.33	37.8	105	-0.0102
29		1.50	2.01		725.7	0.375	8.2		0.367	2.23	12.5		2.23						185	-0.0084
30		1.50	2.88		725.0	0.406	18.6		0.363	2.24	32.8		2.24	2.82	31.8		2.53	39.8	183	-0.0052
31		2.47	4.85		731.5	0.269	7.9	1.15	0.260	1.82	5.4	-1.80	1.83	2.82	5.8	3.8	2.80	45.8	104	-0.0052
32		2.48	4.71		733.5	0.284	17.0		0.264	1.79	28.8		1.84	3.13	28.1		3.03	46.1	183	-0.0083
33		2.52	4.77		734.1	0.280	27.8		0.266	1.86	34.6		1.92	3.09	34.7		2.97	45.2	185	-0.0046
34		2.59	4.88		731.7	0.324	51.5		0.285	1.67	82.6		1.82	3.24	81.9		2.95	45.9	186	

TABLE II-PART I (Continued)

Shot No.	Model Nomenclature	M	$R_{ef} \times 10^{-6}$	Simulated Altitude, kft	Range Pressure, mm Hg	C_D	δ^2 , deg ²	$C_1 \times 10^3$, 1/deg ²	C_{D_0}	C_{m_0}	δ_C^2 , deg ²	$C_2 \times 10^3$, 1/deg ²	$C_{m_{00}}$	C_{N_0}	$\delta_{C_0}^2$, deg ²	$C_3 \times 10^3$, 1/deg ²	$C_{N_{10}}$	cp_0^{**}	p , deg/ft	C_{Lp}
35	ATS	3.49	6.58	Ground Level	731.8	0.214	4.2	1.88	0.207	1.81	2.6	-1.80	1.84	2.80	2.7	4.0	2.79	44.3	203	-8.0071
36		3.55	6.69		730.9	0.208	3.5		0.202	2.00	1.2		2.00	2.83	1.2		2.82	43.8	205	-0.0088
37		3.66	6.06		727.0	0.270	54.5		0.183	1.82	89.0		1.88	3.23	95.4		2.85	44.1	205	-0.0067
38	4VM	1.43	2.80		725.4	0.553	90.1	2.08	0.147	2.18	197.2	-1.25	2.43	3.14	186.2	3.0	2.58	37.8	185	-0.0094
39		1.46	2.66		725.6	0.388	11.8		0.163	2.13	11.4		2.44	2.60	11.0		2.56	37.5	188	-0.0080
40		1.49	2.70		725.5	0.348	1.3		0.348	2.30	0.0		2.38	2.50	0.8		2.50	27.6	187	-0.0076
41		1.49	2.68		725.8	0.358	2.5		0.353	2.43	1.9		2.43	2.72	2.2		2.71	38.8	188	-0.0074
42		2.19	4.02		731.7	0.316	6.5	1.48	0.307	2.01	4.5	-2.50	2.02	3.01	4.7		3.00	44.1	188	-0.0092
43		2.43	4.46		732.4	0.270	1.3		0.268	1.98	8.9		2.00	2.94	0.9		2.94	44.0	189	-0.0081
44		2.52	4.60		730.8	0.117	34.5		0.260	1.83	46.1		1.95	3.10	46.6		2.96	44.5	188	-0.0060
45		2.53	4.62		730.0	0.276	6.8		0.266	1.83	8.0		1.85						186	-0.0062
46	4TS	3.53	6.40		726.9	0.361	112.0	1.25	0.222	1.72	202.0	-1.30	1.90	3.33	194.5	2.0	2.96	44.2	207	
47		3.54	6.48		732.2	0.258	24.3		0.226	1.95	25.1		1.98	2.97	26.1		2.92	44.0	206	-0.0048
48		3.55	6.50		735.3	0.231	6.3		0.223	2.01	8.0		2.04	3.01	8.0		2.90	43.0	205	-0.0060
49	5VM	1.49	3.12		733.6	0.468	80.3	1.90	0.315	2.18	16.7	-1.25	2.24	2.94	42.2	3.7	2.78	43.4	187	-0.0052
50		1.57	3.20		734.8	0.492	80.9		0.304	2.05	187.0		2.28	3.16	171.7		2.52	41.3	184	-0.0063
51		1.58	3.20		731.6	0.316	8.0		0.302	2.38	8.1		2.39						182	-0.0091
52		1.59	3.31		730.5	0.331	6.2		0.313	2.27	10.4		2.28	2.52	9.5		2.48	41.0	184	-0.0123
53	5TS	2.56	5.33		731.9	0.350	88.1	1.20	0.244	1.82	131.8	1.00	1.95	3.64	122.3	6.0	2.01	46.1	203	
54	5VM	2.57	5.42		735.2	0.286	34.1		0.245	1.73	54.9		1.70	3.17	53.8		2.85	47.1	181	-0.0053
55		2.60	5.49		736.5	0.276	28.8		0.240	1.04	45.3		1.88	3.09	44.2		2.82	46.2	186	-0.0064
56		2.62	5.53		736.4	0.345	87.4		0.240	1.61	129.2		1.74	3.51	129.4		2.73	46.0	185	-0.0065
57	5TS	3.51	7.24		727.3	0.216	21.0	1.50	0.184	1.94	18.1	0	1.94	2.99	18.3	7.0	2.86	45.9	202	-0.0042
58		3.58	7.35		727.9	0.187	1.8		0.184	1.98	1.9		1.90	2.08	1.3		2.80	45.7	201	-0.0076
59		3.62	7.52		727.4	0.201	10.0		0.108	1.90	5.9		1.90	2.90	9.3		2.83	46.1	195	-0.0059
60	6VM	1.50	3.04		736.5	0.447	54.8	2.20	0.328	2.38	59.0	-0.50	2.42	2.97	48.3	9.8	2.50	39.3	189	
61		1.54	3.10		731.8	0.389	23.7		0.337	2.40	15.5		2.41	2.52	15.9		2.36	38.2	184	-0.0069
62		1.57	3.18		733.9	0.342	6.1		0.329	2.49	12.3		2.50	2.68	12.0		2.56	39.1	182	-0.0066
63		1.58	3.19		731.2	0.345	8.8		0.326	2.45	12.9		2.46	2.64	12.6		2.52	39.1	182	-0.0067
64		2.53	5.10		730.6	0.248	3.2	1.60	0.243	1.95	3.8	-2.00	1.88	2.74	3.8	7.0	2.71	44.5	180	-0.0056
65		2.54	5.16		737.0	0.331	48.1		0.252	1.83	74.4		1.88	3.28	73.1		2.77	44.7	184	
66		2.54	5.17		737.4	0.292	24.5		0.253	1.95	32.0		2.01	2.94	31.4		2.72	44.2	185	-0.0054
67		2.60	5.28		737.3	0.378	86.0		0.247	1.71	118.3		1.95	3.53	122.2		2.67	44.4	185	
68	8TS	3.53	7.04		728.5	0.239	27.6	1.50	0.198	1.91	42.0	0	1.92	3.00	30.9		2.78	45.2	204	-0.0044

TABLE II-PART I (Continued)

Shot No	Model Nomenclature	M	$Re_f \times 10^{-6}$	Simulated Altitude, kft	Range Pressure, mm Hg	C_D	$\frac{\delta^2}{deg^2}$	$C_1 \times 10^4, 1/deg^2$	C_{D_0}	$C_{m_0}^*$	$\frac{\delta e_s^2}{deg^2}$	$C_2 \times 10^3, 1/deg^2$	$C_{m_{ro}}$	C_{N_0}	$\frac{\delta C_{N_0}^2}{deg^2}$	$C_3 \times 10^3, 1/deg^2$	$C_{N_{oo}}$	$C_{P_0}^{**}$	p, deg/ft	C_{L_P}	
69	6TS	3.54	7.06	Ground Level	727.2	0.198	1.3	1.50	0.197	1.95	1.0	0	1.85			7.0		202	-0.0071		
70	6TS	3.66	7.38		734.9	0.223	21.1	1.50	0.191	1.93	32.3	0	1.93	2.81	31.6		7.0	2.59	45.2	202	-0.0059
71	7VM	1.50	2.99		741.2	0.429	32.4	3.09	0.328	2.57	20.1	-0.50	2.58				0		195	-0.0052	
72		1.52	2.96		731.2	0.407	22.6		0.337	2.82	17.9		2.63	2.50	17.5			2.50	36.7	196	-0.0076
73		1.58	3.13		742.4	0.351	5.5		0.334	2.70	5.3		2.70	2.70	5.8			2.70	37.9	180	-0.0055
74		1.59	3.14		742.4	0.347	5.4		0.430	2.65	7.4		2.65	2.81	7.5			2.91	37.5	192	-0.0086
75		2.22	4.34		733.9	0.318	5.3	1.20	0.412	2.20	5.5	-1.80	2.20	2.65	18.7	5.5		2.54	40.9	193	
76		2.42	4.74		731.0	0.325	21.0		0.300	2.04	24.0		2.08	2.45	25.2			2.81	43.6	197	-0.0055
77		2.50	4.99		735.8	0.328	20.7		0.294	2.02	37.6		2.09	3.04	37.2			2.84	43.7	188	-0.0044
78		2.51	4.90		731.9	0.287	10.9		0.294	2.10	17.4		2.13							194	-0.0054
79		2.53	4.94		731.6	0.400	94.1		0.209	1.88	126.0		2.12	3.38	128.1			2.68	42.6	195	-0.0037
80	7TS	3.50	6.74		727.1	0.232	3.3		0.228	1.99	2.7	-2.00	1.99	2.51	2.7	7.0		2.49	42.2	201	-0.0094
81		3.52	6.75		727.5	0.231	1.5		0.229	2.04	0.8		1.99	2.21	0.7			2.20	38.8	201	-0.0070
82		3.62	6.95		727.2	0.328	85.5		0.220	1.99	70.5		2.03	2.98	88.2			2.36	40.8	203	-0.0033
83	8VFF	1.39	2.06		740.8	0.448	45.8	1.43	0.384	3.26	74.7	2.40	3.44	2.64	65.8	6.4		2.22	29.3	188	-0.0095
84		1.54	3.23		732.0	0.395	21.2		0.365	3.23	22.4		3.28	2.82	22.4			2.48	32.8	186	-0.0063
85		1.57	3.33		740.6	0.551	131.0		0.364	2.81	186.6		3.26	3.86	182.4			2.48	33.2	197	-0.0048
86		1.59	3.37		740.8	0.480	78.0		0.368	3.01	122.6		3.30	3.36	157.1			2.35	31.2	199	-0.0057
87		2.44	5.18		738.3	0.318	30.1	1.88	0.246	2.63	56.8	-2.00	2.74	3.30	54.3	0		3.30	43.0	192	-0.0039
88		2.46	5.24		739.4	0.291	11.1		0.260	2.75	12.7		2.78	3.25	12.7			3.25	42.5	185	-0.0064
89		2.48	5.19		729.8	0.258	2.1		0.254	2.76	2.4		2.76							181	-0.0080
90		2.49	5.18		729.5	0.273	5.9		0.262	2.81	8.0		2.83	3.34	7.7			3.34	42.9	194	-0.0079
91		2.52	5.36		737.7	0.313	24.4		0.267	2.68	27.6		2.74	3.30	28.7			3.30	43.0	194	-0.0070
92	8TV	3.35	7.20		738.1	0.230	5.2	1.60	0.222	2.58	10.5	4.40	2.58			9.4				188	-0.0096
93		3.37	7.18		741.9	0.240	13.0		0.219	2.37	18.3		2.45	2.90	10.7			2.70	41.7	183	
94		3.39	7.40		741.9	0.268	32.9		0.218	2.17	88.4		2.48	3.14	41.3			2.75	41.8	177	-0.0073
95		3.39	7.19		740.0	0.216	2.4		0.212	2.55	2.2		2.58							182	-0.0079
96	8VFF	1.51	3.11		730.9	0.345	1.3	1.74	0.343	3.37	1.3	-0.60	3.37	2.66	2.9	6.0		2.64	33.2	180	-0.0005
97		1.50	3.31		744.0	0.460	58.0		0.459	3.32	79.0		3.37	2.89	80.3			2.41	30.7	199	-0.0047
98		1.65	3.41		740.5	0.457	60.9		0.352	3.15	100.0		3.21	3.18	96.5			2.00	34.1	186	-0.0054
99		1.84	3.82		741.4	0.563	149.2	1.88	0.312	2.51	233.3	-2.50	3.09	3.96	225.4			2.81	35.2	184	
100		2.32	4.80		738.1	0.425	97.1	1.49	0.280	2.61	118.3	-2.5	2.81	3.60	120.3	8.3		2.94	39.5	199	
101		2.46	5.07		731.6	0.285	6.3		0.276	2.77	6.9		2.78	2.83	6.7			2.79	38.0	191	-0.0079
102		2.49	5.09		730.0	0.310	24.0		0.274	2.67	17.8		2.76	3.13	36.3			2.80	40.0	190	-0.0058

TABLE II—PART I (Continued)

Shot No.	Model Nomenclature	M	$Re_g \times 10^{-8}$	Simulated Altitude, kft	Range Pressure, mm Hg	C_D	δ^2 , deg ²	$C_1 \times 10^3$, 1/deg ²	C_{D_0}	$C_{m\alpha}^*$	δe^2 , deg ²	$C_2 \times 10^3$, 1/deg ²	$C_{m\alpha_0}$	$C_{N\alpha}$	δe^2 , deg ²	$C_3 \times 10^3$, 1/deg ²	$C_{N\alpha_0}$	$C_{P_0}^{**}$	P , deg/ft	C_{I_P}
103	HVF	2.50	5.20	Ground Level	739.7	0.430	109.0	1.49	0.260	2.26	185.4	-2.5	2.72	3.85	178.9	6.3	2.72	79.0	184	-0.0056
104	9TV	3.36	6.97		740.9	0.245	9.3	1.10	0.238	2.44	7.5	-2.25	2.46	2.92	19.6	7.0	2.79	11.4	196	-0.0066
105	10VM	3.41	7.08		741.3	0.229	8.2	1.56	0.226	2.40	3.1	-1.70	2.41	2.65	2.1	4.9	2.64	40.8	195	-0.0075
106		3.42	7.06		739.4	0.325	83.0		0.234	2.11	135.6		2.42	3.47	114.1		2.67	41.0	191	-0.0074
107		3.53	7.31		740.0	0.242	12.1		0.229	2.28	23.2		2.33	2.78	16.9		2.60	41.6	192	-0.0069
108		1.43	2.96		745.0	0.456	45.8		0.305	1.58	72.1		1.70	2.65	70.6		2.30	44.4	186	-0.0065
109	10VF	1.61	3.32		741.3	0.415	36.5	1.64	0.458	1.47	64.4	-1.50	1.58	2.78	53.6	1.2	2.50	46.7	184	-0.0076
110		1.62	3.35		742.1	0.508	105.9		0.343	1.29	183.6		1.57	3.00	163.1		2.29	45.6	197	-0.0109
111		1.64	3.41		744.0	0.347	6.4		0.337	1.53	0.8		1.55	2.43	9.5		2.39	48.3	185	-0.0086
112		2.19	4.49		734.1	0.358	44.8		0.284	1.18	74.4		1.29	3.03	74.2		2.04	50.9	186	-0.0059
113	10'V'	2.40	4.93		735.0	0.283	2.0	1.28	0.260	1.20	3.2	-0.5	1.20	3.07	4.0	0.3	3.06	51.7	103	-0.0106
114		2.45	5.02		735.2	0.237	3.2		0.252	1.21	3.9		1.22	2.96	3.9		2.96	51.3	194	-0.0080
115		2.46	5.05		733.8	0.326	44.9		0.252	1.14	65.9		1.24	3.11	66.0		3.03	51.4	195	-0.0054
116		2.57	5.31		736.9	0.338	62.5		0.236	1.07	97.4		1.22	3.15	98.7		3.03	51.5	185	-0.0068
117	11VM	3.34	6.90		741.9	0.204	3.2	1.73	0.700	1.18	3.9	-1.65	1.18	2.62	3.5	2.7	2.59	50.4	195	-0.0070
118		3.43	7.04		739.2	0.190	1.3		0.196	1.16	1.7		1.16	2.45	1.6		2.44	50.0	184	-0.0052
119		3.46	7.12		740.3	0.225	18.3		0.202	1.15	31.0		1.16	2.78	29.4		2.54	50.4	102	-0.0022
120		3.49	7.21		742.9	0.252	49.0		0.188	1.12	92.7		1.16	3.14	79.9		2.48	50.1	195	-0.0076
121	11VF	1.59	3.13		742.1	0.438	47.0	1.48	0.357	1.76	67.7	-1.40	1.78	2.77	65.5	1.1	2.59	45.0	189	-0.0043
122		1.92	3.16		740.1	0.603	142.6		0.356	1.36	294.8		1.85	3.43	287.6		2.85	44.6	184	0.0032
123		1.62	3.20		740.6	0.446	57.9		0.446	1.98	72.6		1.80	2.88	73.1		2.68	45.1	185	-0.0099
124		1.63	3.22		743.6	0.467	56.8		0.369	1.66	103.0		1.83	2.89	103.9		2.60	44.4	195	-0.0084
125	11TF	2.42	4.73		734.1	0.268	1.3	1.18	0.268	1.49	1.7	-1.1	1.48	2.93	1.7	5.7	2.03	49.9	187	-0.0057
126		2.44	4.76		737.2	0.268	2.0		0.285	1.48	2.5		1.48	2.82	2.5		2.02	48.4	187	-0.0057
127		2.49	4.92		738.2	0.294	15.6		0.271	1.43	21.9		1.49	2.93	21.5		2.91	40.5	188	-0.0057
128		2.49	4.92		737.6	0.315	29.6		0.271	1.38	51.9		1.45	2.98	51.4		2.82	48.6	185	-0.0054
129	12V	3.36	8.63		741.6	0.210	6.4	3.04	0.210	1.27	5.9	-2.1	1.28	2.85	5.6	7.5	2.62	49.2	184	-0.0064
130		3.41	6.73		742.5	0.221	7.0		0.213	1.30	10.4		1.31	2.75	9.0		2.69	49.2	195	-0.0037
131		3.45	6.81		743.2	0.279	59.4		0.209	1.19	94.1		1.29	3.15	91.2		2.63	49.2	181	-0.0051
132		3.47	6.80		747.9	0.235	15.2		0.217	1.25	27.2		1.28	2.86	26.3		2.71	49.6	182	-0.0082
133	136	2.01	4.16		724.5	0.319	16.8		0.268	2.80	21.9		2.94	2.96	21.6		2.90	39.5	182	-0.0075
134		1.97	4.13		733.7	0.333	19.9		0.273	2.91	18.4		2.95	2.84	17.7		2.71	37.7	184	-0.0075
135		2.05	4.34		734.9	0.291	0.3		0.260	2.91	0.7		2.91						199	-0.0075
136		1.98	4.14		731.2	0.346	28.3		0.260	2.78	80.5		2.95	3.25	33.5		3.00	48.9	184	

TABLE II-PART I (Concluded)

Shot No.	Model Nomenclature	M	$Re_L \times 10^{-6}$	Simulated Altitude, kft	Range Pressure, mm Hg	C_D	δ^2 , deg ²	$C_1 \times 10^3$, 1/deg ²	C_{D_0}	$C_{m_{\alpha}}$	δe^2 , deg ²	$C_2 \times 10^3$, 1/deg ²	$C_{m_{\alpha\alpha}}$	$C_{N_{\alpha}}$	δe_{α}^2 , deg ²	$C_3 \times 10^3$, 1/deg ²	$C_{N_{\alpha\alpha}}$	C_{p_0} **	P, deg/ft	C_{L_p}
137	13V	1.97	3.97	Ground Level	724.3	0.332	16.7	2.16	0.286	3.02	13.8	-0.0	3.03	3.08	51.7	7.5	2.69	36.3	185	
130	↓	2.00	4.06	↓	732.7	0.361	34.2	↓	0.287	2.86	48.3	↓	3.00	3.04	45.0	↓	2.70	36.6	108	-0.0054
139	↓	1.99	4.03	↓	723.9	0.309	9.1	↓	0.289	3.05	12.8	↓	3.06	2.75	12.2	↓	2.66	35.8	183	-0.0077
140	↓	1.97	3.99	↓	730.1	0.299	4.7	↓	0.289	3.02	3.6	↓	3.02	2.77	3.7	↓	2.74	36.8	184	-0.0072
141	14VA	2.00	3.92	↓	724.2	0.300	1.3	3.56	0.295	3.08	1.7	0	3.06			↓			183	-0.0041
142	↓	1.98	3.93	↓	732.1	0.301	0.8	↓	0.299	3.00	0.3	↓	3.00	2.81	0.3	↓	2.81	38.9	201	-0.0083
143	↓	1.90	3.87	↓	722.8	0.314	3.3	↓	0.302	3.13	2.4	↓	3.13	2.01	3.1	↓	2.79	35.8	182	-0.0081
144	↓	1.98	3.89	↓	723.7	0.335	7.6	↓	0.308	3.15	4.9	↓	3.15	3.02	5.0	↓	2.98	37.2	183	-0.0073
145	12V	2.03	1.96	20	436.7	0.294	9.1	4.40	0.254	2.80	11.0	↓	2.80	2.92	11.2	4.4	2.87	40.0	182	-0.0026
146	↓	2.07	2.03	↓	742.0	0.281	5.1	↓	0.258	2.80	6.4	↓	2.80	3.28	6.5	↓	3.25	42.4	181	-0.0044
147	↓	2.06	2.02	↓	342.2	0.258	1.4	↓	0.252	2.80	1.2	↓	2.80			↓			183	-0.0031
148	13V	2.04	1.93	↓	338.9	0.295	6.4	2.94	0.276	2.99	6.0	↓	2.99	2.95	6.4	↓	2.92	38.4	184	-0.0027
149	↓	2.80	2.00	↓	344.6	0.279	3.6	↓	0.268	2.97	5.3	↓	2.97	2.81	5.3	↓	2.79	37.6	182	-0.0028
150	↓	2.04	1.96	↓	343.9	0.302	11.0	↓	0.268	2.91	13.3	↓	2.91	2.91	13.8	↓	2.85	38.5	181	-0.0033
151	↓	2.02	1.93	↓	345.2	0.300	8.2	↓	0.276	3.02	8.8	↓	3.02	2.94	9.0	↓	2.90	38.1	184	
152	14VA	2.05	1.92	↓	344.0	0.303	3.7	2.34	0.284	3.04	3.8	↓	3.04	2.79	4.0	↓	2.77	36.0	183	-0.0032
153	↓	2.97	1.94	↓	344.0	0.289	0.2	↓	0.288			↓				↓				
154	↓	2.04	1.90	↓	343.9	0.353	24.8	↓	0.295	3.07	29.1	↓	3.07	2.90	30.4	↓	2.77	36.0	181	-0.0023
155	↓	2.03	1.89	↓	341.1	0.328	9.4	↓	0.308	3.04	14.9	↓	3.04	2.02	14.8	↓	2.75	36.1	180	-0.0042
156	12V	2.02	0.83	40	144.9	0.258	0.5	2.66	0.257	2.57	0.6	↓	2.57	3.10	0.6	0	3.10	43.0	100	-0.0043
157	↓	2.04	0.04	↓	143.5	0.292	11.4	↓	0.262	2.74	15.4	↓	2.74	3.01	15.4	↓	3.01	41.4	182	-0.0040
158	↓	2.00	0.70	↓	146.8	0.280	5.2	↓	0.266	2.61	9.8	↓	2.61			↓			181	-0.0061
159	↓	2.04	0.83	↓	142.8	0.292	9.5	↓	0.267	2.85	9.6	↓	2.85	3.23	9.8	↓	3.23	41.9	179	-0.0023
160	13V	2.04	0.83	↓	146.1	0.286	3.7	2.36	0.277	3.00	4.4	-3.5	3.02	2.93	4.4	5.5	2.91	30.1	181	-0.0056
161	↓	2.04	0.81	↓	141.9	0.322	18.1	↓	0.279	3.01	17.5	↓	3.07	2.94	18.0	↓	2.88	37.5	180	-0.0076
162	↓	2.03	0.82	↓	144.9	0.287	1.9	↓	0.262	2.91	2.6	↓	2.92	2.60	2.6	↓	2.67	37.0	180	-0.0052
163	↓	2.04	0.79	↓	139.2	0.372	42.1	↓	0.273	2.74	62.9	↓	2.96	3.07	63.3	↓	2.85	38.1	180	-0.0098
164	14VA	2.03	0.78	↓	142.0	0.381	20.3	2.80	0.303	3.04	70.3	-1.0	3.16	3.12	30.5	6.4	2.92	36.6	180	-0.0043
165	↓	2.85	0.78	↓	139.4	0.320	7.6	↓	0.288	3.16	10.7	↓	3.20	3.03	10.8	↓	2.96	36.6	182	-0.0046
166	↓	2.05	0.77	↓	139.6	0.310	2.8	↓	0.302	3.01	4.8	↓	3.03	2.84	4.8	↓	2.81	36.7	179	-0.0065
167	↓	2.03	0.78	↓	141.8	0.361	22.7	↓	0.296	2.97	40.6	↓	3.13	3.16	40.7	↓	2.90	38.7	181	-0.0048
168	12V	1.99	0.31	60	54.4	0.309	17.3	3.00	0.257	2.66	7.2	0	2.66	3.29	37.1	2.0	3.22	43.1	181	-0.0092
169	↓	1.98	0.30	↓	53.0	0.282	0.0	↓	0.250	3.09	10.6	↓	3.09	3.26	10.6	↓	3.24	40.5	180	-0.0051
170	↓	1.99	0.29	↓	51.5	0.280	13.8	↓	0.239	2.90	18.6	↓	2.90	3.12	18.6	↓	3.00	40.7	180	-0.0083
171	↓	2.00	0.30	↓	53.0	0.248	4.3	↓	0.235	2.82	5.2	↓	2.82			↓			182	-0.0103
172	13V	2.00	0.30	↓	54.4	0.335	23.5	2.46	0.277	3.02	30.1	↓	3.02			↓			180	-0.0129
173	↓	1.99	0.29	↓	52.1	0.376	42.6	↓	0.271	2.71	58.3	↓	2.71	3.27	58.8	↓	3.15	41.9	179	
174	↓	1.99	0.30	↓	54.7	0.326	21.2	↓	0.274	2.98	27.3	↓	2.98	3.26	27.4	↓	3.20	40.4	178	-0.0072
175	↓	1.99	0.30	↓	53.0	0.380	40.8	↓	0.280	2.94	73.4	↓	2.94	3.44	73.2	↓	3.29	41.2	181	-0.0100
176	14VA	1.99	0.28	↓	52.4	0.408	64.5	2.08	0.266	3.12	81.7	↓	3.12	3.29	81.5	↓	3.13	38.4	180	-0.0069
177	↓	2.02	0.31	↓	56.2	0.268	1.8	↓	0.284			↓				↓				-0.0070
178	↓	2.02	0.30	↓	54.9	0.355	32.4	↓	0.289	3.32	44.8	↓	3.32			↓			180	-0.0102

*Moment reference at 0.60L measured from the nose

**Percentage of projectile length measured from the nose

TABLE II--PART II

Shot No.	Model Nomenclature	M	$Re_f \times 10^{-8}$	Range Pressure, mm Hg	$\mu_N \times 10^4$, 1/ft	δe_2^2 , deg ²	$C_0 \times 10^6$, 1/deg ² ft	$\mu_{N_0} \times 10^4$, 1/ft	$\mu_F \times 10^4$, 1/ft	δe_1^2 , deg ²	$C_4 \times 10^6$, 1/deg ² ft	$\mu_{P_0} \times 10^4$, 1/ft	$\phi N'$, deg/ft	$\phi P'$, deg/ft	K_N , deg	K_P , deg	K_T , deg	$(C_{m_q} + C_{m_d})_0$	C_{mp80}
1	1V	1.44	2.47	742.0			0				0		22.46	2.98	0.43	0.06	0.02		
2		1.50	2.53	738.1	-58.7	17.3		-58.7	-20.5	9.7		-20.5	22.44	2.49	4.20	5.00	0.32	-28.8	0.87
3		1.54	2.62	740.8									22.28	2.37	4.86	5.30	0.19		
4		1.55	2.64	740.9									22.38	2.57	4.80	5.96	0.17		
5		2.31	4.20	724.0	-41.6	1.1		-41.6	-17.2	1.1		-17.2	22.68	1.94	1.20	0.83	0.12	-21.0	0.48
6		2.54	4.21	728.7	-40.1	1.2		-40.1	-17.8	0.9		-17.8	23.95	2.02	2.33	1.57	0.02	-20.4	0.48
7		2.57	4.35	735.8	-24.1	13.4		-24.1	-17.9	8.4		-17.0	22.88	2.00	2.09	4.08	0.19	-13.4	0.43
8		2.56	4.36	736.0									22.89	2.10	1.52	1.74	0.08		
8		2.61	4.36	724.2									22.62	1.99	2.18	1.81	0.10		
10	1T	3.28	5.60	733.8									21.05	3.66	3.42	3.07	0.04		
11		3.44	5.77	729.4	-32.1	76.8		-32.1	-33.1	49.0		-33.1	21.31	3.58	4.22	8.53	0.06	-11.6	0.49
12		3.44	5.88	734.7									20.80	3.74	2.31	2.14	0.01		
13	2V	4.57	6.00	729.0	-48.4	90.0		-46.4	-31.0	54.7		-31.0	21.72	3.52	5.74	11.13	0.08	-14.4	0.50
14		1.48	2.46	740.4									22.59	2.40	2.73	0.62	0.03		
15		1.50	2.48	745.8									22.62	2.52	1.30	1.54	0.14		
16		1.51	2.50	738.2	-34.7	13.5		-34.7	-25.8	10.2		-25.9	22.59	2.58	3.23	4.19	0.13	-21.7	1.01
17		1.52	2.52	738.1	-20.6	14.5		-20.6	-31.8	14.5		-31.0	22.67	2.49	3.03	3.61	0.08	-18.5	1.32
18		2.05	3.39	734.0									24.11	2.15	0.03	2.99	0.08		
19		2.50	4.15	736.0	-34.2	4.8		-34.2	-19.0	3.0		-19.0	23.17	2.00	2.46	3.25	0.08	-17.7	0.53
20		2.53	4.20	736.2									23.08	1.88	1.85	1.86	0.01		
21		2.56	4.10	732.4	-43.7	0.8		-43.7	-19.7	0.8		-19.7	24.82	1.82	3.14	1.28	0.06	-21.8	0.56
22		2.50	4.22	723.3									23.04	1.89	1.96	3.98	0.21		
23	2T	3.36	5.50	728.5	-47.2	7.0		-47.2	-35.7	4.4		-35.7	21.67	3.35	5.73	8.36	0.03	-15.7	0.81
24		3.38	5.56	733.1									21.74	3.41	5.44	7.64	0.15		
25		3.44	5.69	732.8									18.32	4.09	4.18	4.25	0.49		
26		3.58	5.84	727.1	-38.3	12.9		-38.3	-32.8	8.8		-32.8	21.69	3.36	3.34	4.58	0.17	-12.8	0.48
27	JVM	1.45	2.77	738.2	-22.8	26.9		-22.8	-20.8	27.5		-20.8	14.74	2.38	5.94	5.41	0.04	-24.6	0.83
28		1.47	2.80	735.8	-25.0	5.4		-25.0	-15.6	4.8		-15.6	14.61	2.39	3.06	2.50	0.16	-22.0	0.59
29		1.50	2.81	725.7	-17.8	11.9		-17.8	-16.4	12.4		-16.4	14.62	2.36	3.13	2.83	0.02	-18.5	0.55
30		1.50	2.69	725.8	-19.0	26.7		-19.0	-22.6	31.8		-22.6	14.42	2.40	5.02	4.13	0.06	-23.2	0.87
31		2.47	4.65	731.5									15.09	1.85	3.35	4.18	0.02		
32		2.49	4.71	733.5	-10.4	23.9		-10.4	-23.3	28.1		-23.3	14.82	1.88	3.74	3.42	0.10	-16.4	0.73
33		2.52	4.77	734.1	-15.4	35.4		-15.4	-15.5	34.7		-15.5	15.18	1.78	5.18	5.51	0.07	-15.4	0.35
34		2.59	4.88	731.7	-15.0	76.4		-15.0	-25.1	81.9		-25.1	15.31	1.71	6.66	6.00	0.10	-20.7	0.88

TABLE II—PART II (Continued)

Shot No.	Model Nomenclature	M	$Re_l \times 10^{-6}$	Range Pressure, mm Hg	$\mu_N \times 10^4$, 1/ft	δe_2^2 , deg ²	$C_3 \times 10^6$, 1/deg ² ft	$\mu_{N_0} \times 10^4$, 1/ft	$\mu_P \times 10^4$, 1/ft	δe_1^2 , deg ²	$C_4 \times 10^6$, 1/deg ² ft	$\mu_{P_0} \times 10^4$, 1/ft	ϕ_N , deg/ft	ϕ_P , deg/ft	K_N , deg	K_P , deg	K_T , deg	$(C_{mq} + C_{md})_0$	$C_{mp\beta_0}$
35	3TS	3.49	6.50	731.8	-28.3	2.0	11.0	-20.6	-21.9	2.7	-10.6	-21.6	13.70	3.13	3.01	2.52	0.10	-16.0	0.27
36	↓	3.55	6.69	730.9									13.78	3.23	3.21	2.37	0.14		
37	4VM	3.88	6.86	727.0	-19.6	80.9		-28.5	-31.5	93.4		-21.4	14.26	2.80	8.12	7.54	0.13	-15.7	0.24
38	↓	1.43	2.60	725.4	-10.8	121.8		-24.2	-29.4	186.3	-5.1	-19.9	14.79	2.12	10.33	6.05	0.04	-25.2	0.78
39	↓	1.46	2.86	725.6	-23.0	13.0		-24.5	-20.2	11.8	-5.1	-19.6	14.83	2.39	3.60	4.20	0.85	-25.3	0.77
40	↓	1.49	2.70	725.5									14.72	2.36	2.42	0.54	0.06		
41	↓	1.49	2.69	725.8									14.81	2.39	1.70	2.32	0.06		
42	↓	2.19	4.02	731.7	-22.9	6.4	0	-22.9	-17.6	4.7	0	-17.6	15.33	1.92	2.84	3.43	0.12	-20.9	0.52
43	↓	2.43	1.46	732.4									15.28	1.86	1.06	1.79	0.12		
44	↓	2.52	4.80	730.8	-14.8	45.5		-14.8	-18.0	46.0		-18.0	15.45	1.70	5.29	5.55	0.04	-15.9	0.48
45	↓	2.53	4.62	730.8	-14.5	10.9		-14.5	-15.4	0.9		-15.4	15.19	1.87	1.97	2.60	0.85	-13.7	0.37
46	4TS	3.53	6.40	726.9									14.98	2.27	11.02	8.21	0.20		
47	↓	3.54	6.48	732.2	-21.6	30.2		-21.6	-31.1	26.0		-31.1	14.44	2.77	4.35	6.70	0.26	-16.8	0.49
48	↓	3.55	8.50	735.3	-28.4	7.7		-28.4	-25.5	8.0		-25.5	14.16	2.95	3.18	2.83	0.14	-17.3	0.34
49	5VM	1.49	3.12	733.6	-20.4	25.1		-20.4	-26.2	42.4		-26.2	11.69	2.35	10.50	4.88	0.53	-34.0	1.10
50	↓	1.57	3.29	734.8									11.58	2.27	9.66	6.18	0.12		
51	↓	1.58	3.20	731.6									11.04	2.68	1.77	2.60	0.12		
52	↓	1.59	3.31	740.5									11.34	2.50	2.03	1.48	0.10		
53	5TS	2.56	5.33	731.9	-13.9	102.6		-13.9	-41.9	122.6		-41.9	11.10	3.48	8.50	9.83	0.01	-22.4	0.77
54	5VM	2.57	5.42	735.2	-9.3	48.0		-9.3	-18.5	53.8		-18.5	11.96	1.95	5.52	5.74	0.16	-16.7	0.56
55	↓	2.60	5.49	736.5	-12.1	37.8		-12.1	-21.4	44.2		-21.4	11.90	1.96	5.69	5.76	0.19	-22.3	0.75
56	↓	2.62	5.53	736.4	-11.3	131.0		-11.3	-22.6	129.4		-22.6	12.13	1.81	7.72	0.30	0.12	-22.2	0.81
57	5TS	3.51	7.24	727.3	-20.6	10.7		-20.6	-27.9	18.3		-27.9	10.04	3.63	5.47	7.48	0.08	-18.6	0.42
58	↓	3.56	7.35	727.9									10.60	3.76	2.03	0.39	0.05		
59	↓	3.62	7.52	727.4	-20.6	15.0		-20.6	-28.2	9.2		-28.2	10.22	3.78	1.66	4.76	0.13	-18.9	0.44
60	8VM	1.50	3.04	736.5	-17.4	34.0		-17.4	-25.0	48.3		-25.0	12.12	2.39	0.49	7.31	0.15	-30.2	1.05
61	↓	1.54	3.10	731.6	-22.7	17.2		-22.7	-13.5	15.9		-13.5	11.64	2.49	5.70	4.40	0.39	-25.5	0.54
62	↓	1.57	3.16	733.9	-8.8	10.9		-8.8	-29.1	12.0		-29.1	11.35	2.68	2.39	2.64	0.13	-26.3	1.14
63	↓	1.50	3.19	731.2									11.35	2.61	2.45	2.40	0.02		
64	↓	2.53	5.10	730.8	-11.1	2.8		-11.1	-18.4	3.8		-19.4	11.05	1.97	1.97	1.78	0.12	-19.5	0.65
65	↓	2.54	5.18	737.0	-10.8	65.7		-10.6	-19.8	73.1		-19.8	12.40	1.80	6.75	7.23	0.04	-18.8	0.64
66	↓	2.54	5.17	737.4	-13.2	28.5		-13.2	-19.5	31.4		-19.5	12.16	1.91	4.91	5.03	0.11	-21.3	0.66
67	↓	2.60	5.28	737.3	-11.7	147.0		-11.7	-17.1	122.2		-17.1	12.57	1.70	6.33	8.82	0.09	-17.6	0.52
68	6TS	3.53	7.04	728.5	17.2	25.5		-17.2	-31.8	30.9		-31.8	11.53	3.10	8.02	7.16	0.14	-19.0	0.53

TABLE II—PART II (Continued)

Shot No.	Model Nomenclature	M	Reg $\times 10^{-6}$	Range Pressure, mm Hg	$\mu_N \times 10^4$, 1/ft	δe_2^2 , deg ²	$C_5 \times 10^6$, 1/deg ² ft	$\mu_{N_0} \times 10^4$, 1/ft	$\mu_P \times 10^4$, 1/ft	δe_1^2 , deg ²	$C_4 \times 10^6$, 1/deg ² ft	$\mu_{P_0} \times 10^4$, 1/ft	ϕ_N , deg/ft	ϕ_P , deg/ft	K_N , deg	K_P , deg	K_T , deg	$(C_{mq} + C_{m\dot{q}})_0$	$C_{mp\beta_0}$
68	6TS	3.54	7.05	727.2	-17.5	0.7	0	-17.5	-22.7	1.0	↓	-22.7	11.27	3.22	1.43	1.09	0.10	-15.7	0.35
70	6TS	3.69	7.38	734.0	-18.3	27.6	↓	-18.3	-25.5	31.6	↓	-18.3	11.26	3.22	4.80	4.43	0.06	-16.6	0.38
71	7VM	1.50	2.98	741.2	-23.5	18.4	↓	-23.5	-29.4	19.7	↓	-23.5	12.11	2.54	7.11	7.23	0.26	-34.8	1.18
72	↓	1.52	2.86	731.2	-23.8	18.1	↓	-23.9	-22.6	17.5	↓	-23.8	12.19	2.54	6.82	5.74	0.22	-33.0	1.01
73	↓	1.50	3.13	742.4	-34.6	6.8	↓	-34.6	-9.2	5.6	↓	-34.6	11.55	2.77	2.08	1.86	0.20	-29.4	0.37
74	↓	1.59	3.14	742.4	↓	↓	↓	↓	↓	↓	↓	↓	11.66	2.73	1.92	2.18	0.24	↓	↓
75	↓	2.22	4.34	733.8	-13.0	5.3	5.3	-13.3	-19.1	5.5	-2.7	-19.0	12.40	2.09	2.37	2.93	0.08	-21.3	0.70
76	↓	2.42	4.74	731.0	-15.8	27.0	↓	-15.8	-17.5	25.2	↓	-16.8	12.76	1.98	4.72	5.71	0.17	-21.5	0.55
77	↓	2.50	4.99	735.9	-12.8	35.2	↓	-13.9	-16.9	37.2	↓	-15.9	12.91	1.78	5.43	5.91	0.16	-19.4	0.47
78	↓	2.51	4.00	731.9	↓	↓	↓	↓	↓	↓	↓	↓	12.63	1.92	3.54	3.21	0.08	↓	↓
79	↓	2.53	4.94	731.6	-7.9	127.2	↓	-14.5	-21.6	126.1	↓	-10.2	12.90	1.62	7.23	8.85	0.09	-21.4	0.64
80	7TS	3.50	6.74	727.1	-24.3	2.8	5.8	-24.5	-16.1	2.7	-14.4	-15.6	11.91	2.92	2.63	1.98	0.17	-15.1	0.17
81	↓	3.52	6.75	727.5	↓	↓	↓	↓	↓	↓	↓	↓	12.01	2.95	1.77	1.44	0.83	↓	↓
82	↓	3.92	6.05	727.2	-15.9	154.1	↓	-24.7	-33.3	88.2	↓	-16.2	12.37	2.62	3.20	11.94	0.16	-16.0	0.22
93	GVF	1.38	2.96	740.9	-9.2	70.3	14.2	-19.2	-29.5	81.6	-7.2	-22.8	10.39	2.94	7.04	7.59	0.19	-38.8	1.20
94	↓	1.54	3.23	732.0	-19.3	10.5	↓	-20.9	-21.3	21.4	↓	-19.8	10.22	2.91	5.78	5.28	0.89	-38.0	0.89
95	↓	1.57	3.33	740.6	5.1	167.3	↓	-18.6	-28.8	182.5	↓	-16.7	10.93	2.33	7.48	11.48	0.14	-30.7	0.70
96	↓	1.59	3.37	740.8	-7.5	67.6	↓	-17.1	-31.6	109.6	↓	-23.7	10.82	2.55	9.11	8.27	0.19	-36.9	1.18
97	↓	2.44	5.19	738.3	-9.1	44.9	8.2	-11.9	-23.8	54.3	-15.0	-15.6	10.56	2.19	3.29	5.15	0.07	-19.4	0.41
98	↓	2.46	5.24	739.4	-13.4	12.6	↓	-14.4	-16.8	12.7	↓	-14.9	10.77	2.34	3.66	4.20	0.04	-21.6	0.42
99	↓	2.48	5.19	729.9	-12.5	2.2	↓	-12.7	-17.0	2.3	↓	-19.9	10.45	2.33	1.56	1.89	0.05	-22.1	0.52
90	↓	2.49	5.18	729.5	-11.0	9.7	↓	-11.5	-17.5	7.7	↓	-16.3	10.75	2.31	2.91	2.74	0.04	-18.7	0.45
91	↓	2.52	5.36	737.7	-9.0	32.7	↓	-11.7	-22.5	28.7	↓	-19.2	10.74	2.28	3.72	6.72	0.86	-22.0	0.57
92	↓	3.35	7.28	739.1	↓	↓	↓	↓	↓	↓	↓	↓	0.42	4.98	1.42	1.14	0.10	↓	↓
93	8TV	3.37	7.19	741.8	-16.4	7.4	32.5	-18.8	-43.8	13.9	-14.2	-42.0	9.92	4.27	5.21	4.19	0.12	-28.0	0.95
94	↓	3.39	7.40	741.8	-4.3	27.5	↓	-13.2	-48.1	52.2	↓	-40.7	9.07	3.73	5.86	4.95	0.17	-21.9	0.72
95	↓	3.39	7.19	740.0	-22.8	1.0	↓	-23.1	-39.7	1.5	↓	-39.5	8.39	4.80	2.17	2.16	0.0008	-29.1	0.85
96	GVF	1.51	3.11	730.9	-18.0	1.0	16.4	-18.2	-15.4	1.2	-13.5	-15.2	9.79	3.09	1.44	0.92	0.09	-28.7	0.99
97	↓	1.59	3.31	744.0	-5.9	81.2	↓	-18.2	-26.1	80.2	↓	-15.3	10.57	2.87	5.95	9.30	0.15	-20.8	0.70
98	↓	1.65	3.41	740.5	-5.6	63.3	↓	-16.0	-32.4	97.0	↓	-19.3	10.79	2.64	7.72	7.78	0.17	-29.8	0.85
99	↓	1.84	3.92	741.4	-1.5	185.8	9.9	-18.0	-30.7	225.4	-6.3	-16.5	11.33	1.87	9.62	11.08	0.27	-28.6	0.70
100	↓	2.32	4.80	738.1	-3.7	128.9	↓	-15.3	-29.4	120.3	↓	-10.8	11.18	1.91	6.38	9.72	0.04	-28.2	0.76
101	↓	2.46	5.07	731.6	-15.4	6.4	↓	-16.0	-18.8	6.7	↓	-19.5	10.66	2.25	2.94	3.12	0.07	-28.7	8.78
102	↓	2.49	5.09	730.0	-8.8	30.3	↓	-11.6	-20.8	36.3	↓	-18.5	10.72	2.13	4.69	4.78	0.16	-23.4	0.68

TABLE II-PART II (Continued)

Shot No.	Model Nomenclature	M	$Re_f \times 10^{-6}$	Range Pressure, mm Hg	$\mu_N \times 10^4$, 1/ft	δe_2^2 , deg ²	$C_5 \times 10^6$, 1/deg ² ft	$\mu_{N_0} \times 10^4$, 1/ft	$\mu_P \times 10^4$, 1/ft	δe_1^2 , deg ²	$C_4 \times 10^6$, 1/deg ² ft	$\mu_{P_0} \times 10^4$, 1/ft	ϕ_N' , deg/ft	ϕ_P' , deg/ft	K_N , deg	K_P , deg	K_T , deg	$(C_{mq} + C_{md})_0$	$C_{mp\beta_0}$
103	9VF	2.50	5.20	738.7	-3.9	139.4	9.9	-16.3	-26.3	179.9	-6.3	-15.0	11.50	1.62	9.15	0.26	0.19	-25.0	0.57
104	9TV	3.39	9.97	740.9	-12.5	5.0	15.0	-13.2	-37.6	6.5	-5.5	-37.2	9.44	3.92	2.70	5.40	0.01	-22.3	0.71
105	↓	3.41	7.08	741.3									9.41	3.93	1.18	1.65	0.06		
106	↓	3.42	7.06	740.3	0.1	70.1	↓	-10.4	-46.9	116.3	↓	-40.5	9.97	2.93	7.34	7.21	0.15	-22.9	0.79
107	↓	3.53	7.31	740.0	-9.5	10.4	↓	-10.1	-30.9	10.1	↓	-37.9	9.18	3.90	3.72	3.40	0.09	-20.7	0.99
108	10VM	1.43	2.96	745.0	-9.8	60.3	4.0	-12.2	-20.9	70.9	-3.0	-19.9	12.72	1.60	8.37	9.33	0.09	-20.9	0.73
109	↓	1.61	3.32	741.3	-10.2	53.9	↓	-12.3	-19.6	53.6	↓	-18.0	12.75	1.49	5.29	6.51	0.03	-10.5	0.64
110	↓	1.62	3.35	742.1	-6.2	159.7	↓	-12.5	-27.7	163.1	↓	-22.8	13.02	1.28	8.01	9.78	0.15	-24.1	0.94
111	↓	1.64	3.41	744.0	-12.6	7.1	↓	-12.9	-22.5	9.5	↓	-22.2	12.65	1.59	2.90	2.40	0.19	-23.5	0.99
112	10VF	2.19	4.49	734.1	-0.5	72.1	0	-9.5	-17.6	74.2	-4.6	-14.2	13.01	1.17	5.98	6.63	0.13	-12.9	0.33
113	↓	2.40	4.93	735.0	-5.3	1.7	↓	-5.3	-15.1	3.1	↓	-15.0	12.79	1.19	1.50	0.54	0.07	-9.9	0.32
114	↓	2.45	5.02	735.2	-10.9	3.5	↓	-10.9	-11.6	3.9	↓	-11.4	12.87	1.23	1.74	1.55	0.11	-11.6	0.17
115	↓	2.46	5.05	733.9	-6.3	70.1	↓	-6.3	-16.1	66.0	↓	-13.1	13.02	1.13	5.08	6.65	0.19	-9.1	0.22
116	↓	2.57	5.31	736.0			↓				↓		13.06	1.06	9.13	8.36	0.46		
117	10VF	3.34	6.90	741.4	-7.1	2.2	↓	-7.1	-31.2	3.6	0	-31.2	9.94	2.09	1.73	2.12	0.09	-13.2	0.44
118	↓	3.41	7.04	739.2			↓				↓		9.84	2.06	0.65	1.27	0.07		
119	↓	3.46	7.12	740.3	-9.9	23.5	↓	-9.8	-29.0	29.4	↓	-29.0	9.72	2.01	4.22	4.44	0.13	-14.1	0.42
120	↓	3.49	7.21	742.8	-5.9	67.9	↓	-5.9	-29.2	79.9	↓	-29.2	10.08	1.90	5.92	5.98	0.08	-11.8	0.40
121	11VM	1.59	3.13	742.1	-5.6	49.3	3.2	-7.2	-22.5	65.5	-4.2	-19.7	13.08	1.51	6.21	6.66	0.07	-16.4	0.71
122	↓	1.62	3.16	740.1	-4.2	199.5	↓	-10.6	-32.0	287.6	↓	-19.9	13.41	1.01	11.70	8.58	0.27	-19.0	0.72
123	↓	1.62	3.20	740.6	-7.4	77.5	↓	-9.9	-20.2	73.1	↓	-17.1	13.09	1.46	5.43	7.39	0.10	-18.3	0.56
124	↓	1.63	3.22	743.6	-9.9	111.4	↓	-12.4	-21.8	103.9	↓	-17.4	13.12	1.40	6.29	8.19	0.11	-19.7	0.60
125	11VF	2.42	4.73	734.4			↓				↓		13.13	1.21	0.99	1.30	0.05		
126	↓	2.44	4.76	737.2			↓				↓		13.20	1.20	1.28	1.37	0.06		
127	↓	2.49	4.92	738.2	-12.8	10.0	6.5	-14.0	-13.7	21.5	-5.1	-12.6	13.24	1.15	4.79	4.11	0.19	-15.5	0.28
128	↓	2.49	4.92	737.6	-10.9	46.4	6.5	-13.9	-18.1	51.4	-5.1	-15.4	13.13	1.11	5.52	5.52	0.09	-17.6	0.44
129	11VF	3.36	6.63	741.6	-15.5	4.2	19.0	-16.3	-30.8	5.6	-24.5	-29.4	10.38	1.86	2.99	3.58	0.03	-16.7	0.45
130	↓	3.41	6.73	742.5	-2.2	75.3	↓	-19.5	-46.4	91.2	↓	-24.1	10.43	1.99	2.87	2.57	0.09	-13.9	0.29
131	↓	3.45	6.91	743.7	-10.3	6.8	↓	-11.6	-25.6	9.8	↓	-23.2	10.45	1.59	6.12	7.27	0.16	-11.1	0.25
132	↓	3.47	6.80	737.9	-6.2	21.6	↓	-10.3	-33.4	26.7	↓	-27.0	10.30	1.79	3.56	4.19	0.10	-12.2	0.34
133	12VF	2.01	4.16	724.5	-15.3	20.0	21.0	-19.6	-20.4	21.6	-12.0	-17.8	13.35	2.96	4.02	4.26	0.01	-23.6	0.700
134	↓	1.97	4.13	743.7	-21.0	15.0	↓	-24.2	-22.6	17.7	↓	-20.5	13.43	2.99	9.50	5.50	0.17	-29.0	0.942
135	↓	2.05	4.34	734.9	-23.7	0.0	↓	-23.9	-19.7	0.1	↓	-19.7	13.09	3.10	0.14	0.97	0.02	-27.0	0.793
136	↓	1.98	4.14	731.2	-18.9	23.4	↓	-21.7	-27.4	33.5	↓	-23.4	13.60	2.93	6.99	5.66	0.12	-29.0	0.894

TABLE II—PART II (Concluded)

Shot No.	Model Nomenclature	M	$R_{eg} \times 10^{-6}$	Range Pressure, mm Hg	$\mu_N \times 10^4$, 1/ft	δe_2^2 , deg ²	$C_5 \times 10^9$, 1/deg ² ft	$\mu_{N_0} \times 10^4$, 1/ft	$\mu_P \times 10^4$, 1/ft	δe_1^2 , deg ²	$C_4 \times 10^6$, 1/deg ² ft	$\mu_{P_0} \times 10^4$, 1/ft	ϕ_N' , deg/ft	ϕ_P' , deg/ft	K_N , deg	K_P , deg	K_T , deg	$(C_{mq} + C_{m_0})_0$	C_{mpBo}
137	13V	1.97	3.97	724.3	-24.6	12.0	25.0	-27.6	-21.3	13.4	-3.0	-20.8	13.69	2.86	6.79	4.69	0.07	-32.7	1.010
139	↓	2.00	4.08	732.7	-15.3	40.0	↓	-25.3	-20.3	45.0	↓	-18.0	13.88	2.78	6.37	6.14	0.06	-28.4	0.830
138	↓	1.99	4.03	723.9									13.41	2.93	3.08	3.01	0.04		
140	↓	1.97	3.99	730.1	-25.9	4.0	↓	-26.9	-20.2	3.7	↓	-20.1	13.58	2.89	2.96	2.70	0.14	-31.2	0.938
141	14VA	2.00	3.02	724.2									14.75	3.05	0.88	0.002	0.83		
142	↓	1.99	3.93	732.1									14.53	3.06	0.09	0.55	0.03		
143	↓	1.99	3.87	722.8									15.29	3.00	0.37	1.89	0.05		
144	↓	1.98	3.99	723.7	-22.3	18.8	0	-22.3	-15.0	23.7	0	-15.0	15.33	3.01	5.05	3.02	0.09	-20.4	0.519
145	12V	2.03	1.96	336.7	-10.4	13.3	↓	-10.4	-7.7	11.2	↓	-7.7	15.00	1.18	2.51	2.96	0.11	-24.2	0.571
146	↓	2.07	2.03	342.6	-9.7	8.4	↓	-8.7	-6.9	8.5	↓	-6.9	15.02	1.21	1.44	2.05	0.08	-19.2	0.381
147	↓	2.06	2.02	342.2									15.13	1.21	0.51	1.11	0.09		
148	13V	2.04	1.93	338.9	-11.3	10.9	↓	-11.3	-3.2	6.4	↓	-3.2	15.24	1.19	1.29	2.57	0.06	18.2	-0.025
149	↓	2.08	2.00	344.6									15.04	1.22	1.28	1.34	0.14		
150	↓	2.04	1.86	343.9	-8.8	17.0	↓	-8.8	-6.4	13.6	↓	-6.4	15.17	1.18	2.31	4.01	0.09	-20.8	0.414
151	↓	2.02	1.93	345.2	-8.2	13.7	↓	-8.2	-5.3	9.0	↓	-5.3	15.24	1.22	1.64	3.02	0.16	-16.6	0.246
152	14VA	2.05	1.92	344.0	-13.1	5.8	↓	-13.1	-3.7	4.0	↓	-3.7	17.06	1.24	1.43	1.04	0.07	-19.0	0.051
153	↓	2.07	1.84	344.8															
154	↓	2.04	1.90	343.9	-13.1	45.9	↓	-13.1	-4.8	30.4	↓	-4.8	16.94	1.28	2.55	4.75	0.01	-20.5	0.198
155	↓	2.03	1.90	341.1	-7.6	13.6	↓	-7.6	-5.4	14.0	↓	-5.4	16.95	1.25	2.88	2.36	0.21	-13.3	0.221
156	12V	2.02	0.83	143.9			↓				↓		15.60	0.43	0.72	0.70	0.10		
157	↓	2.04	0.84	143.5	-4.9	16.0	↓	-4.9	-2.2	15.4	↓	-2.2	15.72	0.47	2.75	2.50	0.04	-24.5	0.237
158	↓	2.00	0.78	136.8									15.65	0.44	2.30	0.32	0.09		
159	↓	2.04	0.03	142.6	-9.7	17.8	↓	-9.7	-1.8	10.0	↓	-1.8	15.49	0.49	0.93	3.09	0.05	-37.5	0.090
160	13V	2.04	0.83	146.1	-5.5	5.9	↓	-5.5	-7.2	4.4	↓	-7.2	15.67	0.48	1.21	1.97	0.09	-47.3	2.079
161	↓	2.04	0.81	141.9	-1.2	32.9	↓	-1.2	-2.3	18.0	↓	-2.3	15.65	0.49	1.02	4.16	0.21	-8.8	0.263
162	↓	2.03	0.82	144.9	-1.7	2.6	↓	-1.7	-8.0	3.2	↓	-8.0	15.67	0.48	0.98	1.26	0.07	-26.8	1.653
163	↓	2.04	0.79	139.2	-3.0	74.6	↓	-3.0	-3.6	63.3	↓	-3.6	15.72	0.43	4.35	3.65	0.04	-21.7	0.757
164	14VA	2.03	0.78	142.0	-6.4	37.2	↓	-6.4	-5.1	30.5	↓	-5.1	17.61	0.50	3.49	4.52	0.19	-38.4	1.359
165	↓	2.05	0.70	139.4	-6.7	14.7	↓	-6.7	-2.5	10.8	↓	-2.5	17.69	0.50	1.03	2.71	0.11	-20.5	0.383
166	↓	2.05	0.77	139.6	-5.3	5.9	↓	-5.3	-4.1	4.8	↓	-4.1	17.39	0.49	1.29	1.70	0.04	-30.4	1.003
167	↓	2.03	0.78	141.8	-5.9	43.2	↓	-5.9	-5.0	40.7	↓	-5.0	17.78	0.48	4.36	4.63	0.04	-36.0	1.320
168	12V	1.89	0.31	54.4	-1.6	26.2	↓	-1.6	2.3	37.1	↓	2.3	15.97	0.17	4.12	2.18	0.05	15.5	-3.163
169	↓	1.98	0.30	53.0	-3.7	10.4	↓	-3.7	-2.0	10.6	↓	-2.0	15.95	0.18	2.08	1.92	0.02	-64.6	1.602
170	↓	1.99	0.29	51.5	-1.5	11.0	↓	-1.5	-1.8	19.6	↓	-1.8	15.93	0.18	2.60	2.71	0.07	-34.6	1.360
171	↓	2.00	0.30	53.0	1.6	19.0	↓	1.0	-2.2	5.2	↓	-2.2	16.07	0.18	1.21	1.55	0.03	-8.3	1.770
172	13V	2.00	0.30	54.4	-1.6	47.3	↓	-1.6	-2.8	30.3	↓	-2.8	15.90	0.18	2.19	4.90	0.04	-48.6	2.470
173	↓	1.99	0.29	52.1	-4.6	84.7	↓	-4.6	-1.6	58.6	↓	-1.6	15.90	0.19	3.57	9.25	0.14	-71.0	1.186
174	↓	1.99	0.30	54.7	-2.1	40.6	↓	-2.1	-0.5	27.4	↓	-0.5	15.78	0.18	2.31	4.29	0.04	-26.1	-0.076
175	↓	1.99	0.30	53.9	-1.4	50.8	↓	-1.4	-1.3	73.2	↓	-1.3	16.06	0.18	5.98	3.25	0.06	-26.0	0.704
176	↓	1.99	0.28	52.3	-1.2	70.4	↓	-1.2	1.9	91.5	↓	1.6	17.88	0.18	5.84	4.16	0.12	-10.5	-2.447
177	14VA	2.02	0.31	56.2			↓				↓								
178	↓	2.02	0.30	54.9	-1.6	31.4	↓	-1.6	-0.7	44.6	↓	-0.7	17.87	0.21	4.61	2.52	0.11	-15.1	-0.005

DOCUMENT CONTROL DATA - R & D

(Security classification of title, body of abstract and indexing annotation must be entered when the overall report is classified)

1. ORIGINATING ACTIVITY (Corporate author) Arnold Engineering Development Center Arnold Air Force Station, Tennessee 37389		2a. REPORT SECURITY CLASSIFICATION UNCLASSIFIED
		2b. GROUP N/A
3. REPORT TITLE FREE-FLIGHT RANGE TESTS OF BLUNTED 4-, 4.5- AND 5-CALIBER BODIES OF REVOLUTION WITH SECANT-OGIVE, TANGENT-OGIVE, AND CONICAL NOSE SHAPES		
4. DESCRIPTIVE NOTES (Type of report and inclusive dates) Final Report - December 10, 1970, to March 4, 1971		
5. AUTHOR(S) (First name, middle initial, last name) R. M. Watt and G. L. Winchenbach, ARO, Inc.		
This document has been approved for public release		
6. REPORT DATE December 1971	7a. TOTAL NO. OF PAGES 80	7b. NO. OF REFS 11
8a. CONTRACT OR GRANT NO.	9a. ORIGINATOR'S REPORT NUMBER(S) AEDC-TR-71-166 AFATL-TR-71-111	
b. PROJECT NO.		
c. Program Element 63716F	9b. OTHER REPORT NO(S) (Any other numbers that may be assigned this report) ARO-VKF-TR-71-105	
d. System 670A		
10. DISTRIBUTION STATEMENT Distribution limited to U.S. Government agencies only; this report contains information on test and evaluation of military hardware; December 1971; other requests for this document must be referred to Air Force Armament Laboratory (DLRA), Eglin AFB, FL 32542.		
11. SUPPLEMENTARY NOTES Available in DDC.	12. SPONSORING MILITARY ACTIVITY Air Force Armament Laboratory (DLRA), Eglin AFB, FL 32542	

13. ABSTRACT

Results of free-flight range tests of spin stabilized, blunted 4-, 4.5-, and 5-cal bodies of revolution with secant-ogive, tangent-ogive, and conical nose shapes, and cylindrical afterbodies with and without boattails are presented. The tests were conducted over a Mach number range from approximately 1.5 to 3.5 and at simulated altitudes up to 60,000 ft. Measurements indicate that the drag coefficient decreased with increasing nose length and that the secant-ogive nose shape had the minimum drag coefficient. The drag coefficient could be further reduced by the addition of a boattail. Measurements also indicate that the static instability decreased significantly with an increase in the ogive radius of the nose. Nonlinear variations of force and moment coefficients with yaw angle were observed and treated using a cubic analysis.

Distribution limited to U.S. Government agencies only; this report contains information on test and evaluation of military hardware; December 1971; other requests for this document must be referred to Air Force Armament Laboratory (DLRA), Eglin AFB, FL 32542.

This document has been approved for public release
its distribution is unlimited. *Page 16 Aug 74*

14.

KEY WORDS

LINK A

LINK B

LINK C

ROLE

WT

ROLE

WT

	ROLE
Chairman	Mr. J. Edgar Hoover
Vice Chairman	Mr. Clegg
Members	Mr. Glavin Mr. Ladd Mr. Nichols Mr. Rosen Mr. Tracy Mr. Carson Mr. Egan Mr. Gurnea Mr. Hendon Mr. Pennington Mr. Quinn Tamm Mr. Nease Mr. Harbo Mr. Mohr Mr. Winterrowd Miss Gandy

WT

projectiles

spin stabilized ammunition

altitude simulation

ballistic ranges

supersonic flow